NASA Technical Memorandum 102612

EVALUATION OF WATER COOLED SUPERSONIC TEMPERATURE AND PRESSURE PROBES FOR APPLICATION TO 2000°F FLOWS

NICHOLAS T. LAGEN
JOHN M. SEINER

JUNE 1990

National Aeronautics and Space Administration

Langley Research Center
Hampton, Virginia 23665-5225

ABSTRACT

This work addresses the development of water cooled supersonic probes used to study high temperature jet plumes. These probes are: total pressure, static pressure, and total temperature. The motivation for these experiments is the determination of high temperature supersonic jet mean flow properties.

A 3.54 in. exit diameter water cooled nozzle was used in the tests. It is designed for exit Mach 2 at 2000°F exit total temperature. Tests were conducted using water cooled probes capable of operating in Mach 2 flow, up to 2000°F total temperature. Of the two designs tested, an annular cooling method was chosen as superior.

Data at the jet exit planes, and along the jet centerline, were obtained for total temperatures of 900°F, 1500°F, and 2000°F, for each of the probes. The data obtained from the total and static pressure probes are consistent with prior low temperature results. However, the data obtained from the total temperature probe was affected by the water coolant. The total temperature probe was tested up to 2000°F with, and without, the cooling system turned on to better understand the heat transfer process at the thermocouple bead. The rate of heat transfer across the thermocouple bead was greater when the coolant was turned on than when the coolant was turned off. This accounted for the lower temperature measurement by the cooled probe. The analysis is presented in this paper. The velocity and Mach number at the exit plane and centerline locations were determined from the Rayleigh-Pitot Tube formula.

INTRODUCTION

Interest in the flow properties of high temperature supersonic jet plumes has increased over the years, and serves as the motivation for measuring hot jet mean flow properties in these experiments. A knowledge of these mean flow properties aids the prediction of jet noise and may guide concepts for reduction of the jet noise. Instability waves are the primary noise generators for perfectly expanded supersonic jets[1, 2, 3, 4]. Theoretical

models that are used to predict amplitudes for Kelvin-Helmholtz instability waves thus far require empirical input for mean jet flow properties.

Extensive mean flow measurements have been acquired in the NASA/LaRC Jet Noise Laboratory (JNL) using specially designed pressure and temperature probes for measurement with unheated supersonic jets with exit Mach numbers to 2.5. Seiner, Dash, and Wolf[5] have shown that good agreement exists between measured unheated jet flow properties and those predicted numerically. Hot, supersonic jet data has also been acquired in the JNL. In these studies jet temperatures to 900°F have been measured using uncooled probes and support wings. At the time, the 900°F jet total temperature represented the maximum attainable with the electric heat supply in the JNL. This temperature also corresponds to an upper practical limit for uncooled probes and support wings made from common and readily available materials. The maximum available temperature range has recently, however, been extended to 3000°F with the installation of a SUE propane burner in the JNL.

This research effort was initiated to determine if a satisfactory design could be found to extend the present uncooled probe measurement technology into the elevated temperature range by utilizing water cooling techniques and high temperature materials technology. This paper describes a research effort to develop such technology for measurement of static and total pressures, and total temperature in supersonic Mach 2 flows heated to 2000°F. Throughout this paper, the total temperature at the nozzle exit is refered to as the jet temperature, and the Mach number at the exit as the jet Mach number.

The experiments were conducted in three phases. Phase 1 was to develop and test the water cooled probe concept. The total pressure probe was used in this phase because it has the simplest internal geometry of the three probes. Two total pressure probes were built and tested to determine which of the two designs best cools the probes. The two designs are: the unsymmetric four tube cooling design, illustrated in figure 1, and the symmetric annular cooling design, illustrated in figure 2. Phase 2 utilized the most efficient cooling

design, determined from phase 1, in the production and testing of all the probes. Total pressure, static pressure, and total temperature data were taken along the jet centerline, and along the exit planes. The centerline readings begin at 0.051 nozzle diameters and extend to 23.4 nozzle diameters from the jet exit. The exit plane data extend radially from the jet centerline out to 0.56 nozzle diameters. A full set of data was collected for jet temperatures of 900°F, 1500°F, and 2000°F. Phase 3 was devoted to observing the temperature distribution along the total temperature probe surface. A high resolution infrared system was used to accomplish this.

PROBE ANALYSIS

Probe Structural Analysis

The probes are supported in the flow by a supersonic wing. Figure 3 shows the overall wing set-up near the nozzle, where the static pressure probe is shown in its testing configuration. The forces on the probes are illustrated in figure 4. The dominant load the probes experience is the fluctuating lift force due to the turbulence of the jet flow. This lift force is considered to be the cause of previous probe failures. The probes are sufficiently supported by the wing and the longitudinal loading is therefore neglected in the calculation. The probe is modeled as a simply supported cantilever beam for the analysis. The perturbation velocity is estimated to be 15 percent of the mean jet velocity when the probe is placed in the jet shear layer. When the probe is placed along the jet centerline, near the nozzle exit, a value of 1 percent or less is typical. This perturbation velocity establishes the maximum lift force on the probe surface, determined from:[6]

$$F_{pr} = \rho A_{pr} V^2/2 \tag{1}$$

where A_{pr} is the normal area of the probe the perturbation velocity impinges upon. The maximum stress a probe experiences is determined from:

$$\sigma_{max} = y M_{max}/I_{tot} \tag{2}$$

where M_{max} is the maximum bending moment the probe experiences due to the applied force, F_{pr}. The total moment of inertia of the cross-sectional area of the probe is I_{tot}, and y is the distance from the probe neutral axis, which in this case is the probe centerline. The calculated maximum stress is compared to the allowable bending stresses of the probes at the temperatures expected. This analysis provides an indication of a specific probe design's structural integrity under the expected test conditions.

Total Temperature Probe Heat Transfer Analysis

A heat transfer analysis of the total temperature probe is performed to explain the effect of the cooling system on thermal response. The total temperature probe is illustrated in figure 5, and the probe tip is illustrated in figure 6. Note that the thermocouple leads inside the sheath are surrounded by a powdered magnesium oxide core. Figure 7 defines the relevant temperatures and pressures in the analysis, and also a possible temperature distribution along the centerline when the coolant is turned on. The extent of the water coolant's reach is evident from this temperature distribution. The probe face temperature is T_F and the probe exterior temperature is T_{surf}. The temperatures of the chamber (interior) foward wall, rear wall, and cylindrical sidewall are T_1, T_3, and T_4, respectively. The bead temperature is T_2. The temperature of the thermocouple leads where the coolant impinges the backside of the rear wall is T_5. The water coolant temperature is T_6. Three openings in the probe expose the thermocouple bead to the jet: the foward opening allows flow to impinge upon the bead, and the two vent holes control the mass flow through the probe. The local static pressure inside the chamber, P_c, and outside the vent holes, P_v, is less than the probe face pressure, P_F, which is assumed to be the stagnation pressure of the flow behind the shock. The resulting pressure difference drives the low Mach number flow through the chamber as shown in figure 7.

The heat transfer analysis is based upon placing a control volume around the thermocouple bead of the probe, shown in figure 8. For an isentropic process it is known that

the total temperature across a shock does not change. By neglecting the convective heat transfer to the probe interior walls it is assumed the stagnation streamline impinging upon the bead will have the desired freestream total temperature. The key assumption is that the chamber in which the thermocouple bead is placed can be treated as a blackbody.

The conductive heat transfer takes place between the two chromel-alumel leads and the thermocouple bead. The analysis assumed that 1-D conduction exists and neglected any convection that was occuring across the leads while in the probe chamber. The conductive heat transfer is determined from:[7]

$$q_{cond} = \frac{Ak_5(T_2 - T_5)}{L} \tag{3}$$

where k_5 is the conductive heat transfer coefficient of the thermocouple lead being analyzed. The cross-sectional area, A, of the lead is 0.000078 in^2, and the length, L, of the lead from the thermocouple bead to location 5 is 0.1507 in. T_5 is dependent on whether the probe coolant is turned on or off. If the coolant is turned on, then T_5 is assumed to be equal to T_6, which is 80°F. This assumption was based upon the ability of the magnesium oxide core, at location 5, to adequately insulate the leads from the high temperatures. If the coolant is turned off, then T_5 was assumed to be equal to T_{surf}, determined from the infrared system.

The radiative heat transfer is calculated by using shape factors, F_{ij}, where the i^{th} subscript represents the component from which radiation is leaving, and the j^{th} subscript represents the component on which radiation is incident. The analysis assumes the geometry of the probe can be treated as four simplified components, shown in figure 9. The analysis considers the radiation between the bead and the chamber consisting of interior foward wall, rear wall, and cylindrical sidewall. The three openings are treated as part of the respective walls (i.e. not included), and it is assumed that the local flow temperature is equal to the wall surface temperature. The shape factor analysis for the foward and rear wall with the thermocouple bead is modeled by coaxial parallel disks.[7] The reciprocity

equation is:

$$A_i F_{ij} = A_j F_{ji} \tag{4}$$

where A is the area of the component being analyzed. From the summation rule, the following equation is obtained:

$$F_{21} + F_{23} + F_{24} = 1 \tag{5}$$

These relationships are used to determine the shape factors presented in figure 9.

The heat transfer of the thermocouple bead due to the radiation affects from each component is determined from:[7]

$$q_{ij} = A_i F_{ij} \sigma (T_i^4 - T_j^4) \tag{6}$$

where σ is the Stefan-Boltzmann constant. To simplify the analysis T_{surf} was assumed constant along the uncooled portion of the probe, regardless of whether the coolant was turned on or off. Neglecting conduction between the exterior and interior walls, T_{surf} was assumed equal to T_4, and T_F was assumed equal to T_1. The infrared system however did not detect T_F. The flow is assumed to be stagnant in the region ahead of the probe face, which is modeled as a solid disk for the radiative analysis. It is assumed there is no convective heat transfer in this region. The recovery temperature, T_{rec}, was equal to T_F and is calculated from:[8]

$$r = \frac{(T_{rec} - T_y)}{(T_{oy} - T_y)} \tag{7}$$

where T_y and T_{oy} are the local static temperature, and the local stagnation temperature of the flow behind the shock, respectively. The recovery factor, r, is taken as the cube-root of the Prandtl number, since the flow is considered to be turbulent. The temperature of all the components, except that for the interior rear wall, T_3, are known. It was assumed that the magnesium oxide core does not allow for significant heat transfer between locations 3 and 5. Therefore, T_3 was assumed equal to T_4.

The convective heat transfer to the bead is determined from the energy equation, where the energy entering the control volume equals the energy leaving the control volume such that:

$$q_{cv} = q_{Acd} + q_{Ccd} + q_r \tag{8}$$

where q_{cv} is the convective heat transfer into the bead, and q_r is the net radiative heat transfer leaving the bead. The conductive heat transfer leaving the bead through the alumel and chromel leads is denoted by q_{Acd} and q_{Ccd}, respectively.

The overall heat transfer analysis at the thermocouple bead has been simplified considerably in an attempt to determine the conductive and radiative effects of the coolant contributing to the lower temperature measurements. The assumptions pertaining to low thermal conductivity of the magnesium oxide core is one such simplification. The convective heat transfer is considered the least accurate since it is affected by the errors in simplification of both the conductive and radiative modes. A more detailed heat transfer analysis is difficult since the temperature and velocity of the flow inside the chamber cannot be accurately determined. The error between the jet temperature and the temperature measured at the nozzle exit is determined from:

$$Error = \frac{(T_{jet} - T_{meas})100}{T_{jet}} \tag{9}$$

and the error between the uncooled measurements and the cooled measurements is determined from:

$$Error = \frac{(T_{uncool} - T_{cool})100}{T_{uncool}} \tag{10}$$

Determination of Local Jet Flow Velocity

The measured data must be reduced due to the presence of the bow shock upstream of the total pressure probe tip. The total pressure probe reads the pressure behind the

a.) The shock wave is locally normal to the stagnation streamline at the point where the streamline crosses the bow shock. The probe is parallel to the flow.

b.) The particles following the stagnation streamline are brought to rest isentropically in the subsonic region behind the shock.

bow shock, not the desired freestream total pressure. The following assumptions are made in determining the Mach number of the undisturbed stream ahead of the shock:[9]

These assumptions serve as the basis for the isentropic and normal shock relationships that result in the supersonic Rayleigh Pitot-Tube formula:

$$\frac{P_{oy}}{P_x} = \frac{\left(\frac{\gamma+1}{2}M_x^2\right)^{\frac{\gamma}{\gamma-1}}}{\left(\frac{2\gamma}{\gamma+1}M_x^2 - \frac{\gamma-1}{\gamma+1}\right)^{\frac{1}{\gamma-1}}} \tag{11}$$

where P_{oy} is the stagnation pressure behind the normal shock, and P_x is the freestream static pressure. The freestream stagnation temperature is T_{ox}. P_{oy},P_x, and T_{ox} are determined experimentally. The local ratio of specific heats, γ, and the local speed of sound are determined from T_x. T_x and the local freestream Mach number are calculated through an iteration program which applies these known quantities to the Rayleigh Pitot-Tube formula to account for the variation of the specific heat ratio γ with temperature. The local velocity is determined as the local Mach number times the local speed of sound (a), determined from:

$$a = (\gamma R T_x)^{1/2} \tag{12}$$

. The error between the theoretical velocity and the calculated velocity is determined from:

$$Error = \frac{(V_{jet} - V_{calc})100}{V_{jet}} \tag{13}$$

and the error between the calculated velocities using the uncooled and cooled temperature data is determined from:

$$Error = \frac{(V_{uncool} - V_{cool})100}{V_{uncool}} \tag{14}$$

EXPERIMENTAL APPARATUS AND APPROACH

Test Facility

The experiments were conducted in the NASA-Langley Supersonic Jet Noise Facility. The floor plan of the test cell is shown in figure 10. The test cell is approximately 26 ft. wide by 100 ft. long by 23 ft. high. Air pressure and temperature can be independently controlled either manually or by computer. The air pressure was accurate to within 0.2 psi. The temperature was accurate to within 65°F at a jet temperature of 1100°F, and within 20°F at the design temperature of 2000°F. The working pressure in the burner, during fuel burning, is limited to 140 psig. The model air system can supply dry air at a maximum flow rate of 25 lbm/sec to the burner. The propane flow rate is controlled manually. The maximum propane mass flow rate is 0.45 lbm/sec.

The overall experimental setup is shown in figure 11. A convergent-divergent water cooled nozzle was used, as shown. The nozzle exit diameter is 3.54 inches. The nozzle is designed to produce an exit Mach of 2.0 at 2000°F exit total temperature. The axes of the nozzle are shown in figure 12. All thermocouples used in this experiment are type K chromel-alumel. Within the burner are two open bead thermocouples located 180 degrees apart from each other on the flange that connects the burner to the nozzle, shown in figure 11. These thermocouples provide the burner stagnation temperature readings. One burner thermocouple is obtained by the system computer, while the other is obtained by a digital display.

System Operations

A three dimensional traverse rig positions the probe anywhere in the jet plume. The placement of the probe can be controlled either manually or with a computer. The probe is moved by three 200 pulse/revolution stepping motors. Three bidirectional totalizers are used to read the location of the probe. A digital voltmeter is used in both the total and static pressure experiments to read the output from the transducers.

The pre-test preparation involved leveling and aligning the traverse with the nozzle

centerline axis using an alignment laser, placed within the nozzle. The laser light coincided with the centerline of the jet nozzle. A flat black dummy probe was located on the wing to align the traverse rig with the jet centerline. The laser light appears on the dummy probe whenever the probe is on the jet centerline. The traverse is aligned by moving the probe in the X2 minimum to X2 maximum centerline directions, and simultaneously adjusting the height of the rig until the laser light appears on the dummy probe throughout this X2 movement. The pressure probes were also calibrated every morning prior to testing.

Supersonic Probe Support

The wing support has a diamond shaped cross-section and is composed of stainless steel. The wing cross-section can be seen in figure 3. The wing is 27.500 in. long by 3.875 in. wide by 0.719 in. maximum thickness. The leading edge is sharp, so as to maintain minimum profile drag while in the jet. By minimizing the drag on the wing, the deflection of the wing is minimized, and the location error of the probe, inside the jet plume, is minimized. The wing was initially designed for cold flow testing[10]. Water coolant channels were built into the wing for the hot jet testing. The cooling system, shown in figure 13, provides water for the wing, wing tip, and probe. The portion of the wing leading edge exposed to the jet plume was modified prior to phase 2 of testing due to the severe heating it encountered. The upper surface of the wing exposed to the flow is shown in figure 14, the lower surface of the wing exposed to the flow is shown in figure 15. Both photographs were taken after the final test run. The affected leading edge area was removed after phase 1 and two water coolant tubes, copper tube as the leading edge and stainless steel tube between the wing and copper tube, were installed. The leading edge initially consisted of a copper strip welded to the front of the copper tube, machined to match the sharp leading edge of the wing. This copper strip failed to remain attached to the copper tube, resulting in the copper tube becoming the leading edge of the exposed wing. This had no apparent affect upon the results. A Zirconium flame spray was applied on the surface of the wing exposed to the flow.

The severe temperatures also affected the wingtip, making it necessary to determine an adequate wingtip design capable of sustaining the expected high temperatures. Three different wing tips were used in this experiment and are shown in figure 16. The original wing tip built with the wing (WNGTP1) is 3.875 in. long by 1.000 in. maximum width by 0.719 in. maximum thickness. It is composed of stainless steel with a Zirconium flame spray applied to its surface, and is not cooled. A thermocouple was installed approximately 0.0625 in. from the leading edge. WNGTP1 was tested during phase 1 of testing. The wing tip tested throughout phase 2 of testing (WNGTP2) is composed of stainless steel with a 0.125 in. O.D. (0.0625 in. I.D.) water coolant tube running into the back, going up to within 0.0625 in. the leading edge. WNGTP2 is 3.625 in. long by 1.000 in. maximum width by 0.719 in. maximum thickness. The third wing tip tested (WNGTP3) is composed of carbon-carbon with a silicon carbide coating, and is not cooled. WNGTP3 is 3.250 in. long by 1.000 in. maximum width by 0.719 in. maximum thickness. WNGTP3 was built to evaluate the feasibility of using carbon-carbon for future wings to be tested at, and above, 3000°F, and also as a backup to WNGTP2. The leading edge on WNGTP1 is sharp, while the leading edges on WNGTP2 and WNGTP3 are rounded. This rounding is due to manufacturing considerations and did not affect the results. The leading edge of WNGTP2 was rounded to accomodate the cooling tubes, yet provide coolant as close to the leading edge as possible. It is assumed that if a high enough mass flow rate is achieved through WNGTP2, the heat on the blunt leading edge will be adequately dissipated. WNGTP3 requires that no sharp edges are exposed to the flow, to prevent fracture of the coating and core.

SUPERSONIC PROBES

Were it is applicable, the mass flow rate of coolant water through the probes was determined using a stop watch and a measuring glass, see Table 1. All the probes are manufactured from AISI Type-347 Stainless Steel tubing. The four water cooled supersonic

probes tested in these experiments are shown in figure 17. The probes are, from left to right: CTP2, CTP3, CSP2, and CTT2. The designation of NCTT2 is the CTT2 probe with the coolant turned off. Uncooled probe diameters of 0.062 in. and 0.093 in. for pressure, and 0.125 in. for temperature were used in previous experiments up to 900°F. For the previous experiments the probe to nozzle diameter ratios were 0.035, and in the present experiment the probe diameters was increased such that this ratio is 0.053. The increase in this ratio is necessary to accomodate the cooling system incorporated into the probes. NCTP1 and NCSP1 were destroyed during the previous tests.

Total Pressure Probe

CTP2 and CTP3 are used in phase 1 of the experiment to determine which cooling system design is to be used in phase 2. Difficulty was encountered in the manufacturing of the probes. The 0.1175 in. I.D. of the outer tube for CTP2 provides a small volume, 0.397 $in.^3$ with which to install a cooling system. CTP2 utilized the unsymmetric cooling design which has a center pressure tube, surrounded by four water coolant tubes. CTP2 is illustrated in figures 1, and 18, and is shown in figure 17. Two inlet water tubes extend up to the tip of the probe, while two outlet water tubes are located in the rear of the probe. This is acknowledged to be the weaker of the two designs due to the unsymmetric cooling and smaller coolant volume resulting from the additional internal tubing. The five tubes in CTP2 are connected to tygon tubing halfway through the wing. The pressure transducer's linear range is 200 psia.

Even though the annular cooling design is assumed to be the better of the two designs, the interior dimensions are small enough to raise concerns as to whether sufficient water cooling could be supplied. Stock tubing with an initial wall thickness of 0.035 in. was bored until a wall thickness of approximately 0.015 in. was achieved. The divider tube was also bored, resulting in an average wall thickness of 0.0125 in. The internal volume of CTP3 is 0.935 $in.^3$, over twice that for CTP2. CTP3 is illustrated in figures 2, and 19, and is shown in figure 17 after testing. An X-ray of CTP3, shown in figure 20, provides

an indication of how thin the probe outer wall is, and also shows the position of the installed thermocouple in the reservoir used to measure the coolant temperature exiting the probe tip. This thin outer wall thickness raised concerns as to whether the structure could withstand the expected stresses.

The water coolant is delivered to the tip of the probe through a 0.1086 in. O.D. (0.0960 in. I.D.) divider tube. A 0.060 in. O.D. tube inside the divider tube serves to read the stagnation pressure of flow behind the bow shock. The backside of the cap serving as the probe tip was curved to turn the flow of coolant water towards the reservoir. The base of the 0.1875 in. probe outer tube is attached to a 0.500 in. tube that acts as a pressurized water reservoir. The reservoir concept contributes to the cooling of not only the probe, but also the surrounding wing and wingtip. Thermocouples located inside the reservoirs of all of the probes measure the probe exit water temperature. The reservoir design is incorporated into CSP2,CSP3, and CTT2.

Static Pressure Probe

The water cooled static pressure probe utilizes the annular cooling method. The findings of Pickney [11] were used for the design of the static pressure probe. The probe is illustrated in figures 21 and 22, and seen in figure 17 after the experiment was completed. The sloping of the probe tip to a point, along with the small diameter static pressure ports, posed a serious manufacturing problem to the annular design. A solid steel cylinder was drilled and lathed to serve as the tip, and was fit and brazed to the 0.1875 in. outer tube. The foward component of CSP2, shown in figure 23 prior to the attachment to the probe outer wall, has a 0.060 in. O.D. center inlet water tube and the four smaller 0.020 in. O.D. pressure tubes. The water sprays the back of the tip and proceeds towards the reservoir. The pressure tubes have been installed into the pressure ports, and the excess portion of the pressure tubes is visible in this photo. The pressure tubes are brazed to the center tube, and are connected to a single 0.1250 in. tube once inside the reservoir. Figure 24 shows a magnified photo of the pressure ports for CSP3, detailing the connection

of the pressure tubes and the probe tip. The joint between the two components of the probe is also visible in this figure. An X-ray of CSP2, shown in figure 25, shows the actual internal geometry of the probe. The thickness of the foward components is of interest from a structral point of view, especially since NCSP1 failed during one of the previous tests. The pressure transducer used for the static pressure probe has a linear range of 50 psia.

Total Temperature Probe

The NCTT1 and CTT2 thermocouple output is read by a digital thermometer. CTT2 incorporated the annular cooling method up to, but not beyond, the thermocouple bead inside the probe, and is illustrated in figures 6, 7, and 26. CTT2 is shown in figure 17 after the experiment was completed. The unassembled interior components of CTT2 are shown in figure 27. The placement of the thermocouple bead, sealed from the coolant water, was the most challenging manufacturing aspect of the total temperature probe, along with the drilling of the two vent holes. The outer tube consists of a solid cylindrical rod, 0.1875 in. O.D. bored, and counter bored, to hold both the annular coolant system and the thermocouple. The thermocouple location is such that the bead rests inside the 0.0625 in. diameter chamber while the thermocouple sheath is wedged tightly into the tapered section. The thermocouple sheath is vacuum brazed into place using a braze material composed of 82 percent Gold and 18 percent Nickel. This process involved first building several prototypes and determining whether the bead could be vacuum brazed. X-Rays of all the prototypes and the final product are full scale and were used in the manufacturing of the probes. The thermocouple bead could not have been properly located for the brazing to occur without the use of these X-rays. After the brazing was completed, X-rays were again used to locate the thermocouple for drilling the two vent holes. During the drilling of the vent holes the drill bit broke off in the second hole. This resulted in a tapered vent hole, with a minimum 0.010 in. (0.020 in. maximum) diameter. This is assumed to be insignificant since the minimum vent hole opening is still 0.010 in.

Infrared measurement

Phases 1 and 2 of testing utilized an infrared scanner, with an indium antimonide (InSb) photovoltaic detector, for thermal visualization. The detector has a spectral range of 2 - 5.6 micrometers and is cooled by liquid nitrogen. The detector, and display unit, is shown in figure 28. The images appeared on a display unit which operates at the same rate as the camera. The detector scan rate is converted to a TV scan rate, for viewing on a color monitor. This system served as a means of determining how the probes reacted to the elevated temperatures.

Phase 3 of testing utilized a high resolution infrared system that provided the probe surface temperature along the length of the probe. The amplitude resolution is capable of resolving 256 gray scale levels. The infrarerd system has two spectral ranges of 3-4 micrometers and 8-12 micrometers and was fitted with a 3X telescope. A 1 in. aperture blackbody was used as the temperature reference.

DATA COLLECTION

Data was collected by computer in an ensemble fashion for phase 1. This prevented the high temperatures from damaging the probes, wing, and WNGTP1. This also provided some insight into the affects of high temperatures on the wing and probes. An example of how the ensemble data method was performed is provided for a centerline run, using WNGTP1. A computer program moves the probe to a new location outside the flow, directly above a data point to be tested. The probe is then moved to a data point on the centerline. After allowing a specified amount of time for the probe to reach equilibrium, data is collected. The thermocouple located in the leading edge of WNGTP1 provides the critical temperature reading that initiates the movement of the probe out of the flow, to its previous location. This critical temperature is the temperature at the leading edge and is set for 1400°F, approximately 200°F below the temperature at which the wing surface will begin to sustain visible damage. If the required number of data readings is not collected,

the program will allow several seconds for the wing to cool, outside the flow. Once a cool temperature of 500°F is read by the leading edge thermocouple, the wing will move back to the previous data point and continue collecting data. This continues until once again the critical temperature is reached and the wing moves out of the flow. This process is repeated until all the specified data ensembles for that point are collected. The probe then moves to a new position outside of the flow, and repeats this data collection process for the new data point. The total amount of ensemble readings for a data point is equivalent to two seconds of continous data collection.

Data collection at 900°F and 1500°F were continous for phase 2. The cooling of the probe, and wing, eliminated the need to move the probe out of the flow as in phase 1. The probe remained in the flow until all the data readings, for all the data points, had been taken. However, the collection of data at 2000°F was not continous. The probe, from a position outside of the flow, moves to a data point and continously collects all the data readings for that point. The probe then moves to the previous position outside the flow to cool off before moving to the next data point, and continue the process.

RESULTS

A total of 26 test runs were conducted for phase 1. CTP2 was tested in three runs, on the jet centerline reaching a maximum temperature of 1200°F, shown in figure 29. In this infrared photo CTP2 is detected by the detector, and is cooler than the wing. The infrared scanner was set to cover a full scale range of 284°F to 1220°F; the lighter gray scale in figure 29 corresponds to hotter temperatures. The melting of the tygon tubing on the third run terminated the testing of CTP2. CTP3 was tested up to a temperature of 1600°F, where the limiting factor became the high temperatures on the wing and wingtip. Figure 30 shows the infrared results of CTP3 at 1600°F. Comparing figure 30 to 29, it is seen that CTP3 is cooled well enough such that it was not detected by the infrared camera. These results illustrate the superior cooling of the symmetric annular cooling design over

the unsymmetric four tube cooling design. Of even greater significance was the fact that CTP3 did not experience any structural damage. The 0.015 in. outer tube wall thickness was proven to be structurally sound in this respect. NCTT1 was also tested during this phase to determine the limit of the uncooled design. The result was that NCTT1 was tested up to 1600°F and suprisingly sustained these temperatures without incident. The method of collecting data for NCTT1 is the same as that used for phase 2 at 2000°F. Figures 29 and 30 also provide a good indication of the heating the wing and wingtip sustained. During this phase of testing the wingtip and the exposed portion of the wing experienced temperatures as high as 1450°F. Water cooling systems were incorporated into the wingtip and wing leading edge to counter these high temperatures in the remaining test runs.

A total of 109 test runs were conducted during the second phase of experimentation. The traverse was aligned once again and leveled using the same methods as in phase 1. The wing, nozzle, and probes were painted with a high temperature flat black spray paint to provide a uniform high emissivity of about 0.95. The use of the black paint appeared to have no affect on the images obtained from the low resolution infrared system. This is attributed to the poor resolution of the system in the 3-5 micrometer band when imaging surface temperatures. WNGTP2 was used throughout phase 2 of testing. Damage in the form of small cracks was occuring along the leading edge of WNGTP2, but to such a small degree as not to warrant concern.

Total Pressure Results

The CTP3 readings along the centerline at 900°F, 1500°F, and 2000°F are shown in figure 31. As the temperature increases the peaks in the pressure become less pronounced, indicating that the nozzle is approaching its design condition of 2000°F. The nozzle is designed to have a unique wall boundary, and a corresponding unique ratio of specific heats, γ, to yield a Mach 2 exit distribution at 2000°F jet temperature. Jet temperatures that are not 2000°F are considered to be off-design conditions, and Mach 2 at the exit

becomes an approximation. This is due to the variation in γ as the temperature varies. A value of γ that is not the same as that used in the design yields an off-design condition. The offset of as much as 2 psi in figure 31 is due to this off-design condition.

Several total pressure readings at 900°F are compared in figure 32. The NCTP1 data is from the old test runs and is used to check the data obtained using CTP3. The results obtained from the old tests closely match those obtained for these experiments and indicate that CTP3 was functioning properly. Any differences may be attributed to the affect of the coolant and/or the burner operation. The phase 1 and phase 2 total pressure readings at 1500°F are compared in figure 33. The results obtained from the phase 1 tests are equal to those obtained for the phase 2 tests. The repeatability of data in figure 33 indicated that the traverse rig was properly aligned along the jet centerline throughout the phase 1 and phase 2 testing.

The total pressure data at the nozzle exit planes are compared along each axis for all three temperatures tested in figures 34 and 35. The data indicates that little difference exists in the initial jet exit boundary layer thickness for a wide range of operating jet total temperatures. The +X3 exit plane shear layer data does show more dispersion than the +X1 data. A comparison of the +X1 and +X3 exit plane total pressure results at 900°F, 1500°F, and 2000°F, is shown in figures 36, 37, and 38, respectively. The readings in the +X3 exit plane are offset by approximately 0.070 in. in the jet shear layer at the temperature of 1500°F and 2000°F. The offset is less at 900°F.

The good repeatability of the centerline data of figures 32 and 33 clearly indicate that probe positioning with the remotely controlled digital traverse can be done with great precision. However, the radial data at the jet exit indicates a definite effect between the +X1 and +X3 coordinate directions. It is important to note that there is a large difference in the aerodynamic loading of the support wing as the probe approaches the shear layer along each respective coordinate direction. Along +X1 the wing loading remains symmetric, whereas along +X3 it is unsymmetric. The non-symmetric loading along +X3

could be a major factor producing the observed affect. Since the shear layer is relatively thin compared to the probe diameter, only small probe and wing deflections are required to produce such an effect. The +X3, -X3, and +X1 data comparisons at 1500°F in figure 39 do not entirely confirm that this is the only explanation since the +X3 and -X3 data are not equally offset from the +X1 data which is presumed to be unaffected.

Static Pressure Results

The phase 2 centerline data obtained for CSP2 is shown in figure 40. The minimum and maximum static pressure locations, within 7 diameters of the nozzle exit, match closely for the three temperatures tested. However, further downstream of the nozzle this is not the case. This is due to the differences in the shock cell length between the three cases resulting from the differences in jet temperature. The results show that as the nozzle approaches its 2000°F design point, the shock strength of the waves in the plume diminish. The 900°F results beyond $X/R = 20$ appear irregular. However, the data up to $X/R = 20$ from the jet exit is in good agreement with prior uncooled pressure measurements, as shown in figure 41. The +X1 and +X3 exit plane static pressure results at 900°F, 1500°F, and 2000°F, are shown in figures 42 and 43.

Total Temperature Results

The total temperature reading obtained by both the uncooled and cooled probes was less than the reading obtained from the burner thermocouples. The cooled probe data understandably was affected by the coolant, however, the uncooled probe data errors indicated that energy loss from the thermocouple bead also existed, though not as great. A total of four runs were performed with the probe coolant on (CTT2), and the probe coolant off (NCTT2), through a temperature range of 900°F to 2000°F. This was an attempt to better understand the heat transfer process contributing to the lower temperature measurements from the probe.

The centerline data obtained for the water cooled probe CTT2 at all three tempera-

tures tested are shown in figure 44. These results show that the measured temperatures are below the jet temperatures obtained from the burner thermocouples. The measured temperatures are approximately 60°F, 220°F, and 400°F below the assumed jet temperatures of 900°F, 1500°F, and 2000°F, respectively. The error is shown to increase with increasing jet total temperature. Such errors greatly effected the calculated ratio of specific heats and velocities, and slightly affected the calculated Mach numbers. The comparison of the 1500°F centerline data obtained by NCTT1 and CTT2 is shown in figure 45. The NCTT1 data is approximately 70°F below the jet temperature, and the CTT2 data is approximately 230°F below the jet temperature. This comparison clearly indicates that the use of cooling dramatically effects the accuracy of probe measurement. The difference between the uncooled probe data, at the nozzle exit, and the jet temperature is also evident.

The CTT2 total temperature exit plane data are compared in figure 46 along the +X3 axis for all three temperatures tested. A comparison of NCTT2 and CTT2 in the +X3 exit plane, at 900°F, is shown in figure 47. The use of coolant is again shown to produce significant deviation from expected jet total temperatures.

The third test was attempted using NCTT1 and WNGTP3. The starting temperature was 900°F and was increased at increments of 100°F. NCTT1 failed at 1600°F, and destroyed the wingtip in the process. The failure of WNGTP3 prevented assessing the capability of using Carbon-Carbon as a material for future wing and wingtip designs.

The fourth test (phase 3) was performed using the high resolution infrared system. CTT2 was tested at 900°F, 1500°F, and 2000°F with the coolant turned on, and the coolant turned off. The surface temperature of the probe was obtained for each of these cases and was used to determine the heat transfer process of the probe. The true effectiveness of the cooling system in each case is determined by this calibration.

The infrared result of NCTT2 at 900°F is shown in figure 48, and the surface temperature distribution is estimated as given in figure 49 assuming a surface emmissivity of 0.95 for the 8-12 micrometer range. The two lines along the centerline of the probe in all

the infrared photographs define the region from which the surface temperature distribution is obtained, not the actual temperature of the probe. The minimum probe surface temperature is approximately 350°F. The infrared result of CTT2 at 900°F is shown in figure 50, and the surface temperature distribution is given in figure 51. The minimum probe surface temperature is approximately 130°F. The constant surface temperature of the cylindrical sidewall, T_4, was estimated at 600°F. The difference between the NCTT2 and CTT2 measurements at the nozzle exit is approximately 18°F, which is an error of two percent.

The infrared result of NCTT2 at 1500°F is shown in figure 52, and the surface temperature distribution is given in figure 53. The minimum probe surface temperature is approximately 600°F. The infrared result of CTT2 at 1500°F is shown in figure 54, and the surface temperature distribution is given in figure 55. The minimum probe surface temperature is approximately 180°F. The constant surface temperature of the cylindrical sidewall, T_4, was estimated at 1005°F. The difference between the NCTT2 and CTT2 measurements at the nozzle exit is approximately 108°F, which is an error of eight percent.

The infrared result of NCTT2 at 2000°F is shown in figure 56, and the surface temperature distribution is given in figure 57. The minimum probe surface temperature is approximately 840°F. The infrared result of CTT2 at 2000°F is shown in figure 58, and the surface temperature distribution is given in figure 59. The minimum probe surface temperature is approximately 430°F. The constant surface temperature of the cylindrical sidewall, T_4, was estimated at 1350°F. The difference between the NCTT2 and CTT2 measurements at the nozzle exit is approximately 261°F, which is an error of fourteen percent. The infrared camera was checked against the blackbody set at a reference temperature of 532.4°F. The infrared system measured a temperature of 533.4°F for this condition, shown in figure 60, within 1°F of what the blackbody was set at, which is an error of a tenth of a percent.

The heat transfer analysis for the conductive, convective, and radiative modes of each

case tested is presented in Table 2, along with other relevant data used in the analysis. The conductive heat transfer was approximately three times as great with the coolant turned on than with the coolant turned off and is considered the major contributer to the lower temperature measurements. This result is heavily dependent upon the assumption that T_5 is equal to T_6 when the coolant is turned on. The radiative heat transfer leaving the bead, with the coolant turned on, is less than with the coolant turned off, assuming T_3 is equal to T_4. Therefore, the total heat transfer crossing the thermocouple bead control volume for the cooled case is significantly greater than the uncooled case. Applying conservation of energy to the bead, it is also seen that the convective heat transfer into the bead is greater for the cooled case than the uncooled case. Ideally, it is desired that little or no convective heat transfer exist with the bead, which requires that the chamber flow velocity is nearly zero. Any increase in the convective heat transfer indicates that the chamber flow velocity is increasing and the measured temperature is decreasing. Both the cooled and uncooled beads experience convective heat transfer, though not as great for the uncooled case. This may explain why the data obtained from the uncooled probes was also less than the jet temperature. Future experiments will require that any cooled total temperature probe used, is first calibrated through the range of temperatures it is to experience to accurately determine the flow total temperature. The analysis presented here is simplified considerably and serves only to define the major modes of heat transfer that result in lower temperature measurements by the probe when the coolant is turned on. Therefore, a more detailed model of the probe is recommended. The goal of this model would be to obtain a relationship between the measured temperature, by the thermocouple bead, and the jet temperature through a range of temperatures and pressures the probe is to experience.

Local Jet Flow Velocity and Mach No.

A comparison of the jet plume centerline velocity and Mach number at the temperatures tested is shown in figures 61 and 62, respectively, using the CTT2 temperature measurements. The 1500F centerline velocities and Mach numbers obtained using the

phase 1 NCTT1 data, and the phase 2 CTT2 data, are compared in figure 63 and figure 64. The CTT2 data tended to decrease the calculated velocity 150 ft/s below the calculated velocity using the NCTT1 data, or roughly a five percent error. In general, the coolant affected temperature reading tends to decrease the calculated velocity, but has no significant affect on the calculated Mach numbers. Future experiments will have to account for this affect by calibrating the cooled total temperature probe.

The +X3 exit plane velocity at 900°F, 1500°F, and 2000°F are shown in figure 65, using the CTT2 data. This figure allows the comparison of the calculated velocity with the theoretical velocity. From this the effect of the CTT2 data can be determined. Table 3 presents these calculations along with the corresponding errors. As the temperature increased so did the error in the calculated velocity. The velocities calculated using the CTT2 data had a larger error associated with them than those calculated using the NCTT2 data. A comparison of the +X3 exit plane NCTT2 and CTT2 calculations at 900°F, is shown in figure 66. Note that the calculated velocities using the NCTT2 data at 900°F is roughly the same as the theoretical velocity. The +X3 exit plane calculated Mach numbers for all three temperatures tested, shown in figure 67, indicates that the Mach number is insignificantly affected by these variations in temperature. This figure also shows that the nozzle was operating at Mach 2.0 at the exit.

System Considerations

The two burner thermocouples encountered difficulty in measuring the same temperature during phase 2. A test was performed to understand the differences between the two burner thermocouples and NCTT1. The results of this run are shown in figure 68. Five measurements were made at each jet temperature tested for all three thermocouples. The data presented in figure 68 represents the average measurement of these tests. The assumed jet temperature was read from the digital display. Experience had shown that this was more accurate than the computer at determining the actual jet temperature. The NCTT1 measurement was shown to be lower than the jet temperature due to energy leav-

ing the thermocouple bead. The reading from the computer is considerably less than that for the digital display. This was found to be attributed to the delicate positioning of the thermocouple bead in the burner. The burner thermocouple lead was shortened and the bead was moved slightly until the computer reading and the digital reading matched.

These experiments represent a research effort to develop and test water cooled probes that could accurately measure the pressures and temperatures in a high-temperature supersonic flow. Ideally, these experiments would be conducted with a nozzle and facility that produced a shock-free purely laminar jet flow. However, the jet flow in which the probes were tested contained shocks and was turbulent. Instead of being calibrated in a pure environment, the probes are calibrated in a facility that models actual flight conditions. The significance of this is not known and needs to be addressed.

The effects of the nozzle coolant on the jet exit temperature are not known. Some form of convective cooling may be occuring within the nozzle, thus decreasing the total temperature. The propane injectors were found to form clots that frequently discharged into the flow. This resulted in jet temperature variations beyond the control of the operators. These and other factors are accounted for in the temperature tolerances established for the burner operation.

CONCLUSION

The goal of successfully testing a water cooled supersonic total pressure probe, static pressure probe, and total temperature probe at 2000°F has been accomplished. The cooled total and static pressure readings agreed with previous uncooled results. The total temperature probe reading was found to be affected by the water coolant, and the extensive calibrations performed provided some insight into these effects. The cooled probe had a greater rate of heat transfer across the thermocouple bead control volume than the uncooled probe. This results in temperature measurements for the cooled probe that is considerably lower than the uncooled probe. The lower temperature measurements tended

to result in a calculated velocity that was significantly lower than theory. Further work needs to be done with the total temperature probe to fully understand the effects of the coolant system upon the temperature reading.

Bibliography

[1] C. K. W. Tam, P. J. Morris, "The Radiation of Sound by the Instability Waves of a Compressible Plane Turbulent Shear Layer", *J. Fluid Mech.*, vol. 98, pp. 349–381, 1980.

[2] P. J. Morris, "The Spatial Viscous Instability of Axisymmetric Jets", *J. Fluid Mech.*, vol. 77, pp. 511–529, 1976.

[3] J. E. Ffowcs Williams, A. J. Kempton, "The Noise from the Large Scale Structure of a Jet", *J. Fluid Mech.*, vol. 84, pp. 673–694, 1978.

[4] Crighton, "The Role of Coherent Structures in Modelling Turbulence and Mixing", Springen–Verlag, Ed. J. Ehfers, pp. 340–362, 1985.

[5] J. M. Seiner, S. M. Dash, D. R. Wolf, "Analysis of Turbulent Underexpanded Jets, Part II, Shock Noise Features Using SCIPVIS", *AIAA J.*, vol. 23, no. 5, pp. 669–677, April, 1985.

[6] J. M. Gere, S. P. Timoshenko, "Mechanics of Materials", 2nd ed., Brooks-Cole Engineering Division, 1984.

[7] F. P. Incropera, D. P. DeWitt, "Fundamentals of Heat and Mass Transfer", 2nd ed., John Wiley and Sons, 1985.

[8] E. R. G. Eckert, "Engineering Relations for Heat Transfer and Friction in High Velocity Laminar and Turbulent Boundary Layer Flow Over Surfaces With Constant Pressure and Temperture", *Transactions of the ASME*, vol. 78, no. 6, pp. 55–80, August 1956.

[9] A. H. Shapiro, "The Dynamics and Thermodynamics of Compressible Fluid Flow", vol. 1, Ronald Press Company, 1954.

[10] J. M. Seiner, T. D. Norum, "Experiments of Shock Associated Noise on Supersonic Jets", *AIAA Paper No. 79–1526*, 1979.

[11] S. Z. Pinckney, "A Short Static–Pressure Probe Design for Supersonic Flow", *NASA TN D–7978*, July 1975.

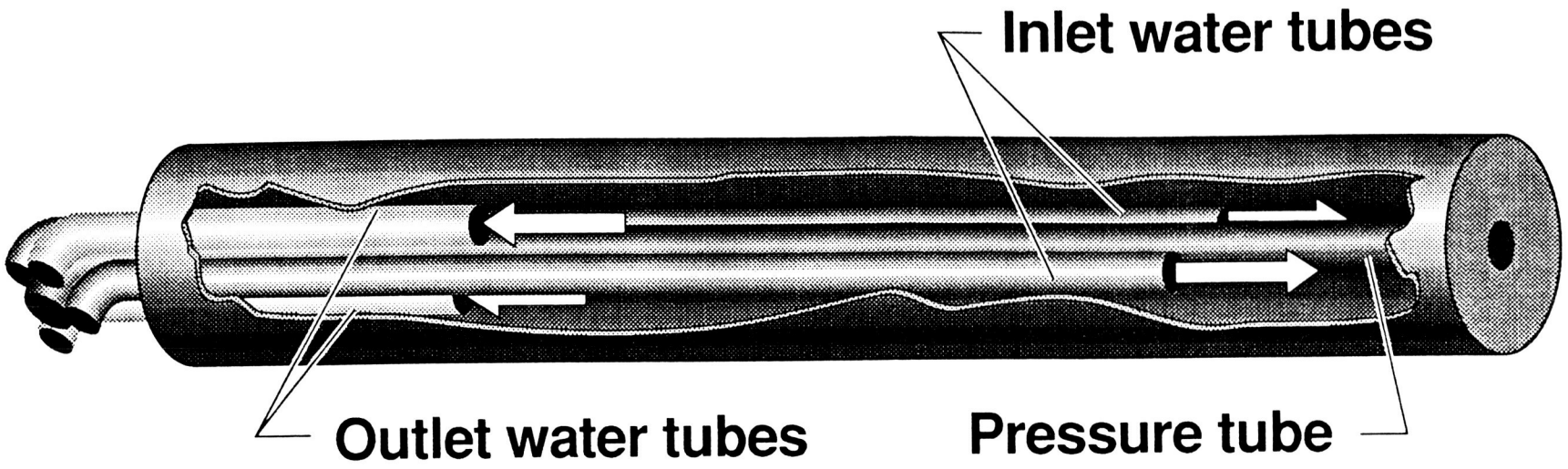

Figure 1. Illustrated total pressure probe with the unsymmetric four-tube cooling design.

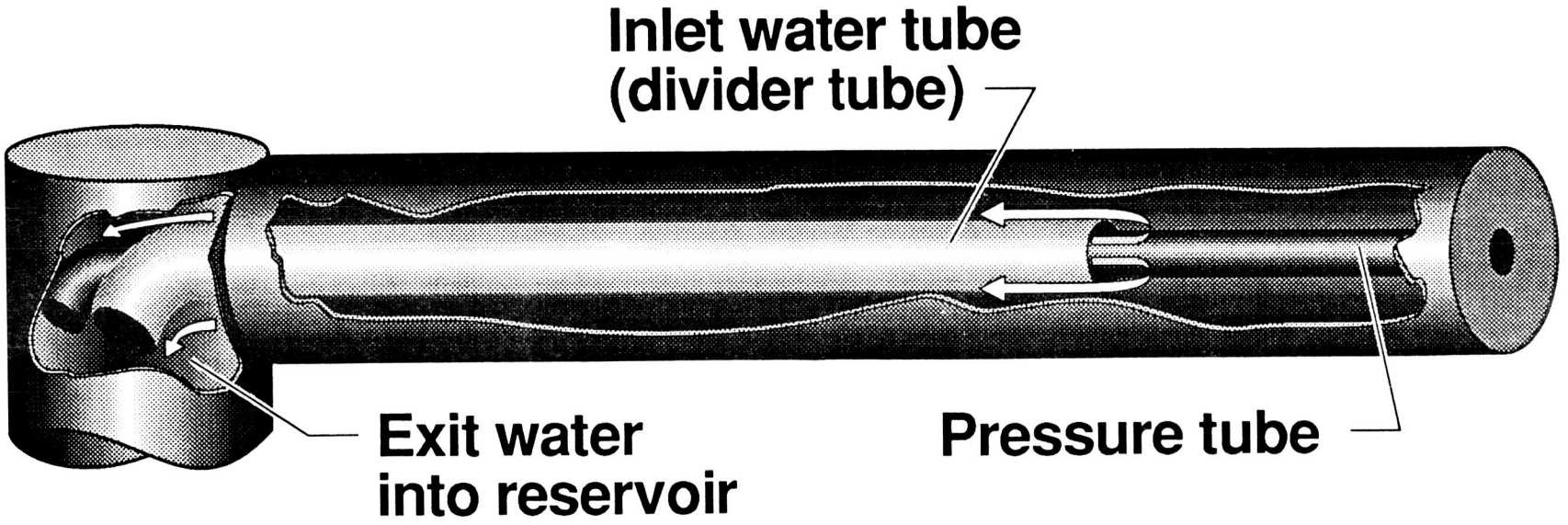

Figure 2. Illustrated total pressure probe with the symmetric annular cooling design.

ORIGINAL PAGE
BLACK AND WHITE PHOTOGRAPH

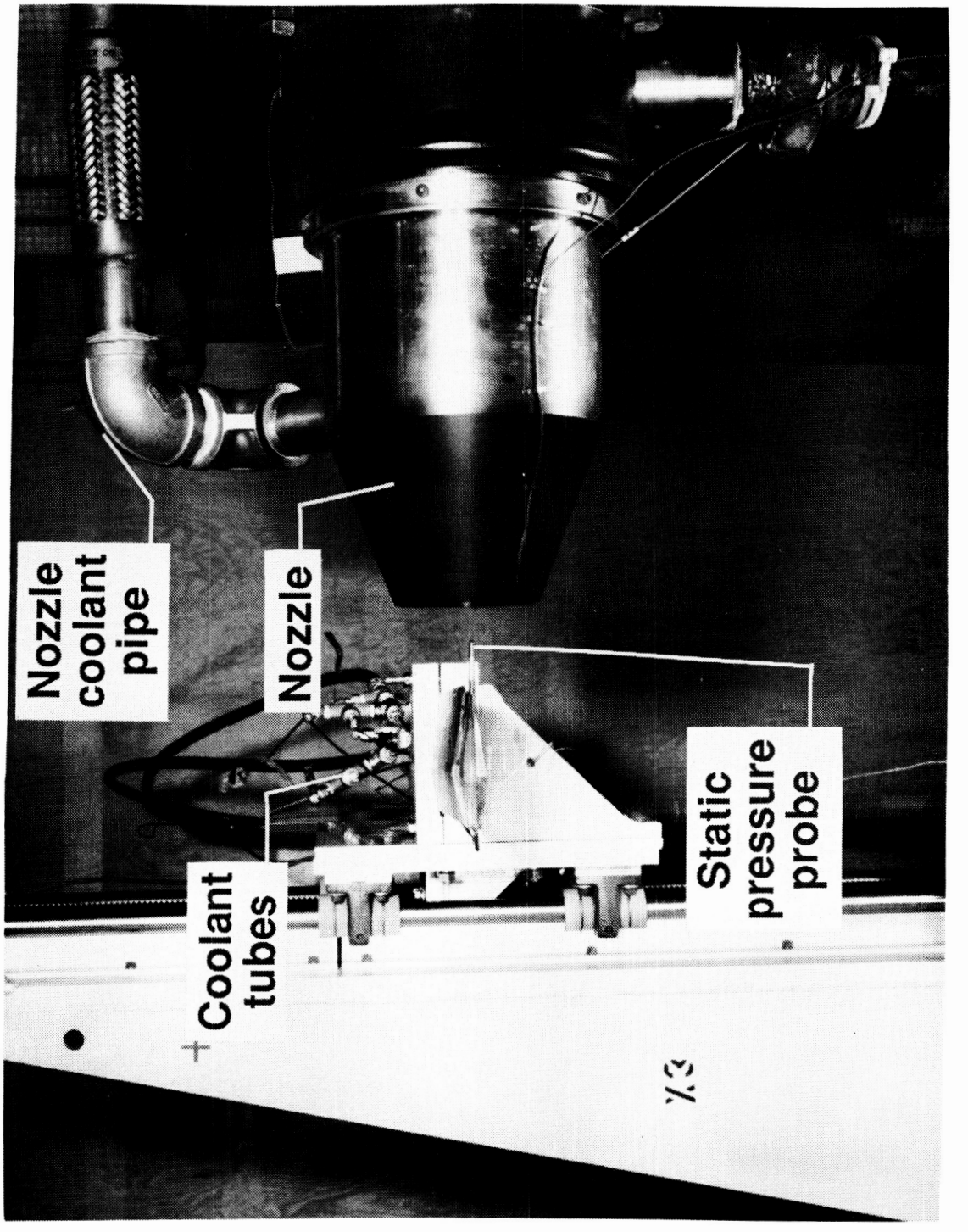

Figure 3. Probe and wing support assembly shown in test position.

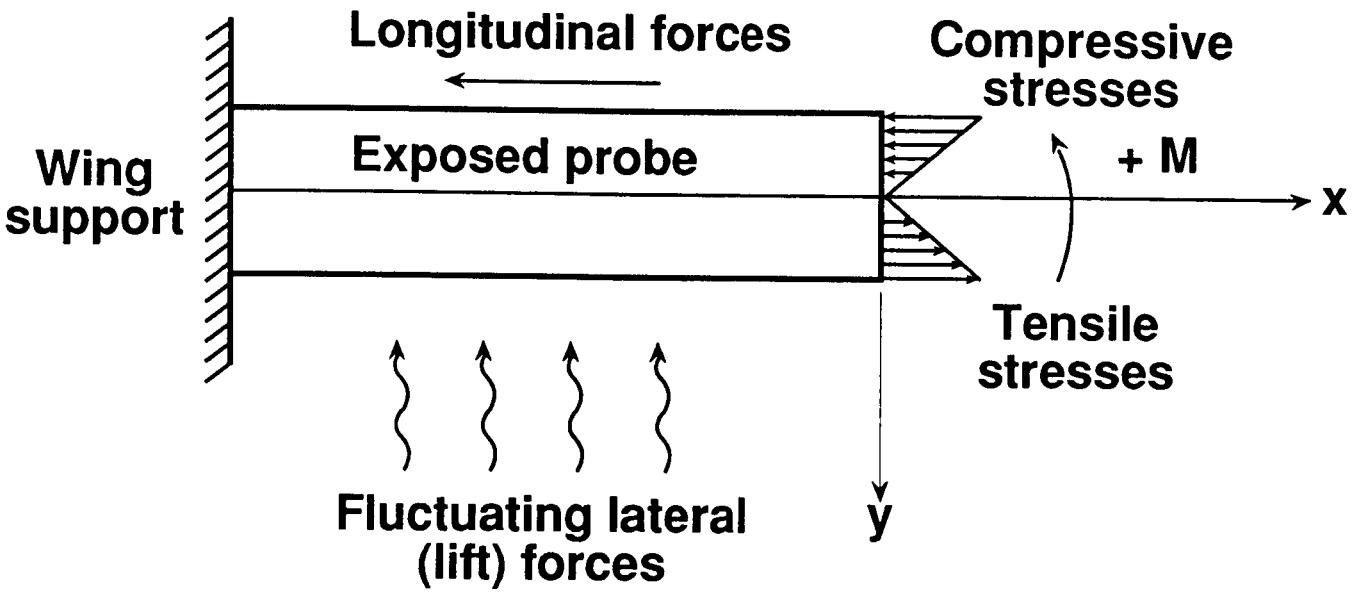

Figure 4. Probe stresses and moments encountered during testing.

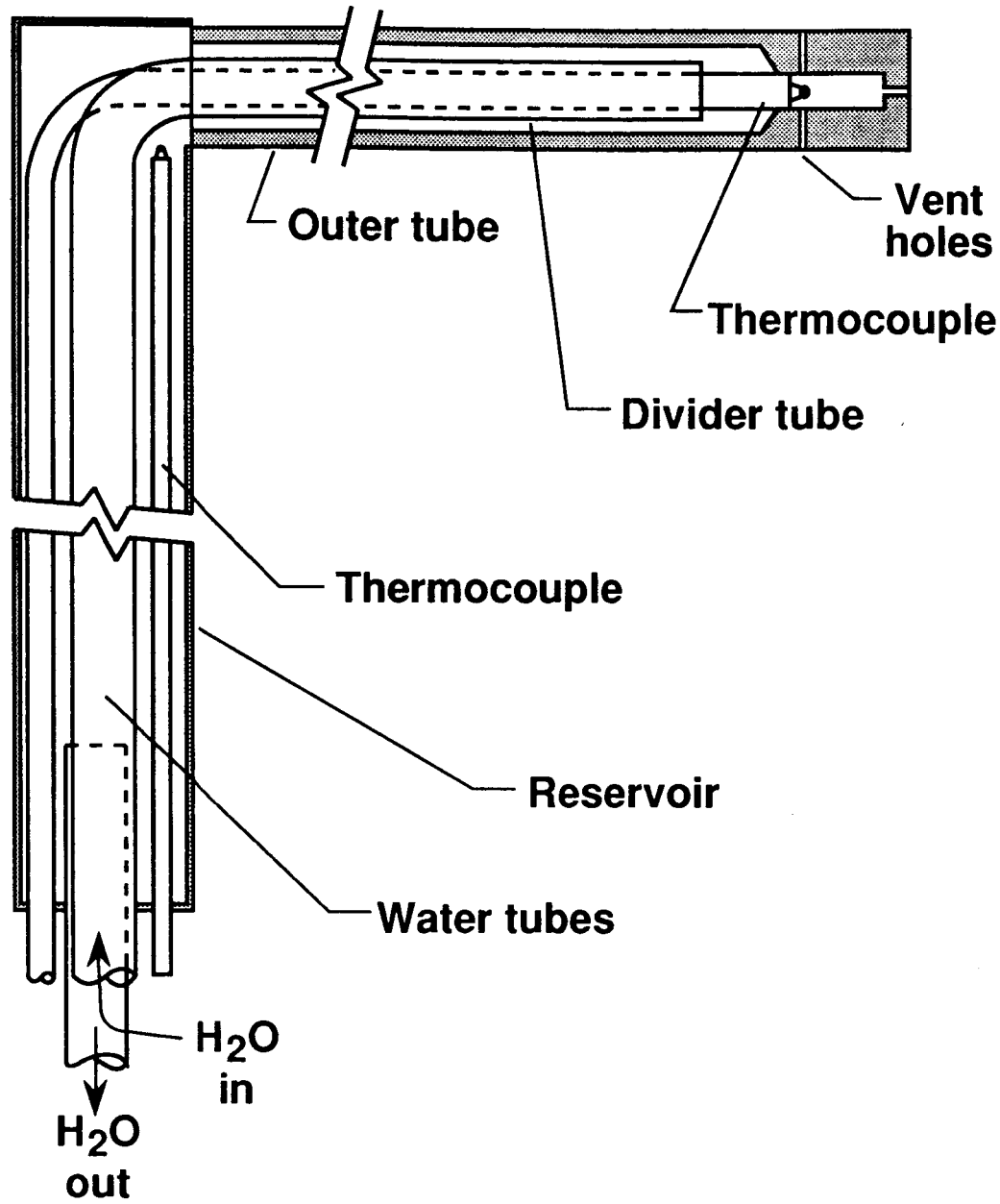

Figure 5. Water cooled total temperature probe.

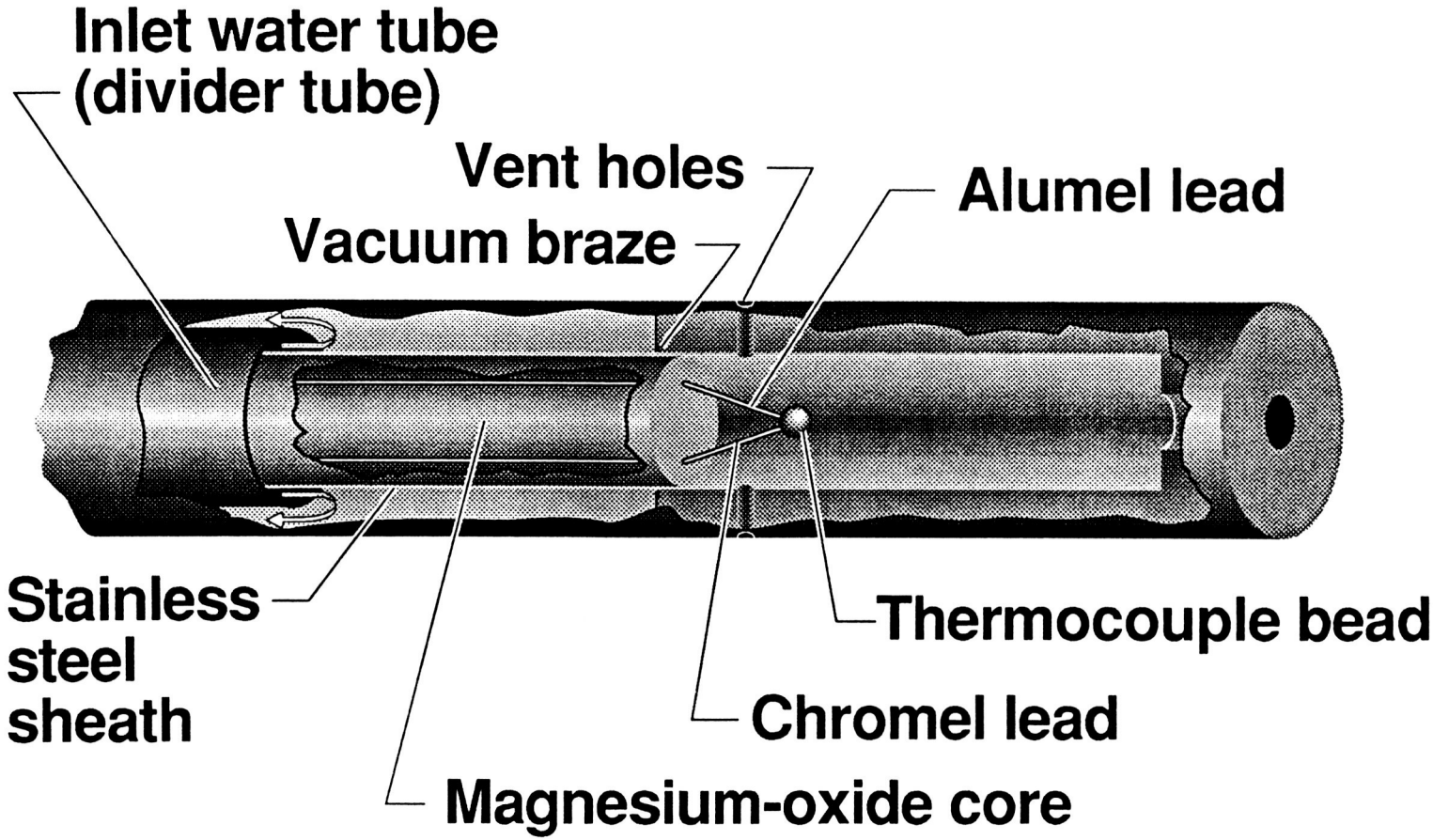

Figure 6. Illustrated cut-away view of the cooled total temperature probe tip.

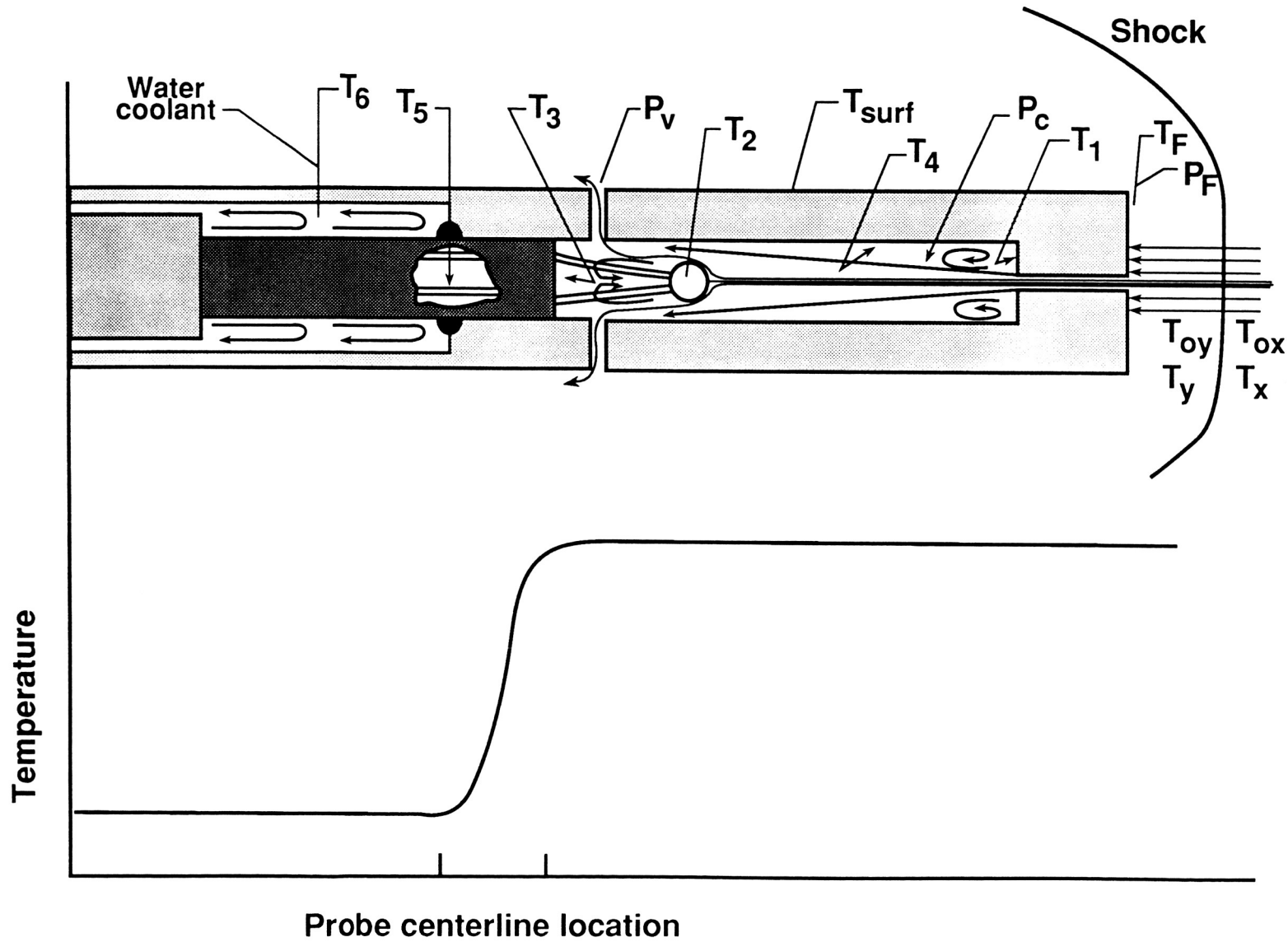

Figure 7. Cooled total temperature probe cross-section with a possible temperature distribution along the centerline.

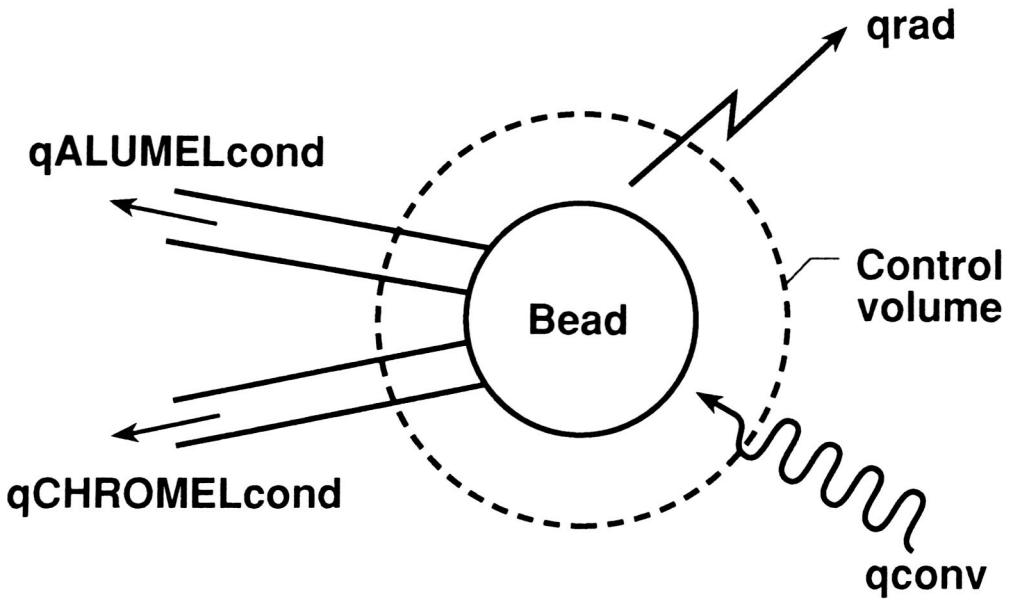

Figure 8. Thermocouple bead heat transfer analysis.

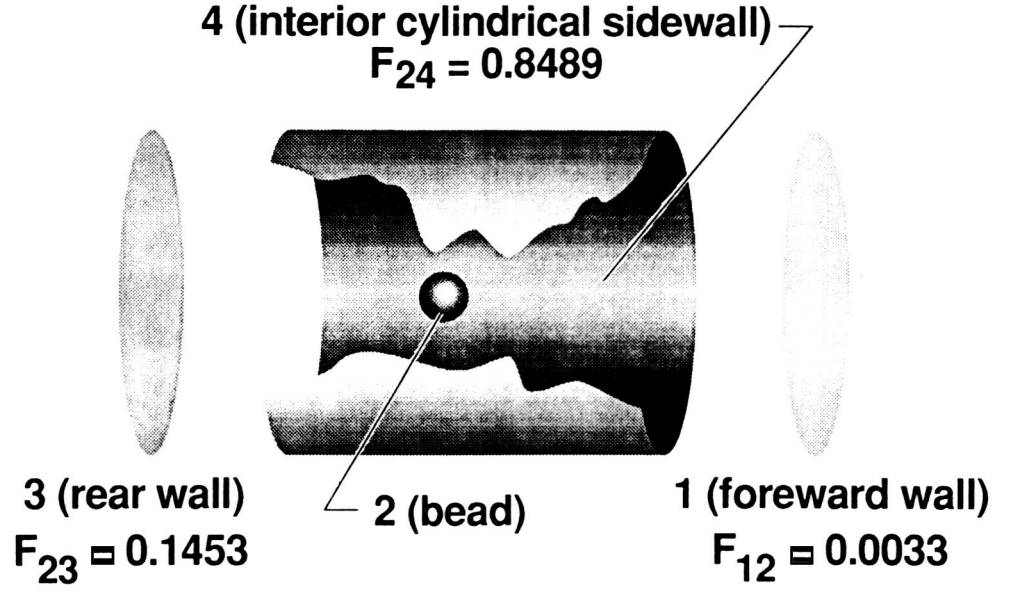

Figure 9. Thermocouple bead radiative heat transfer components and corresponding shape factors.

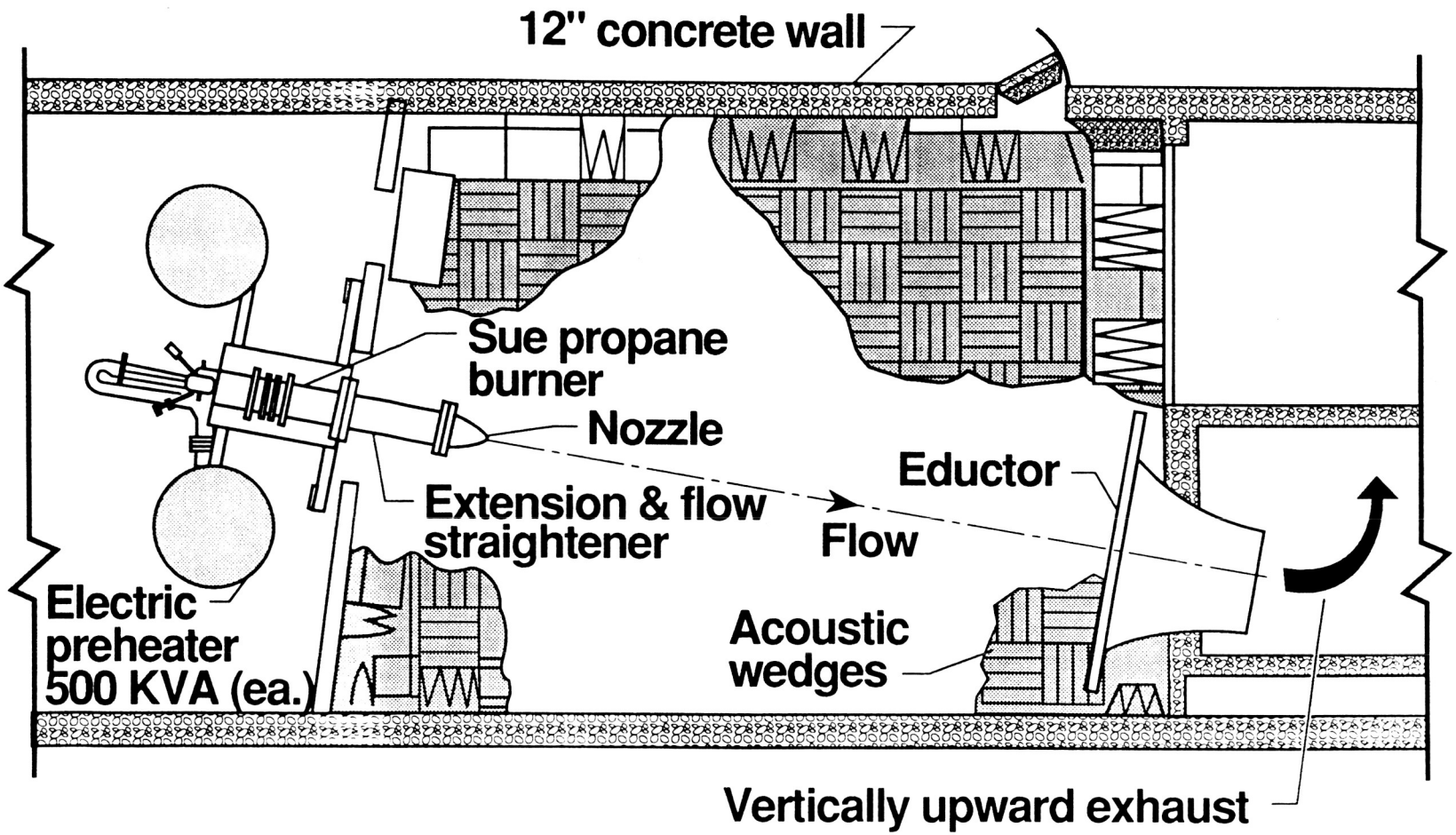

Figure 10. Jet Noise Laboratory Floor Plan.

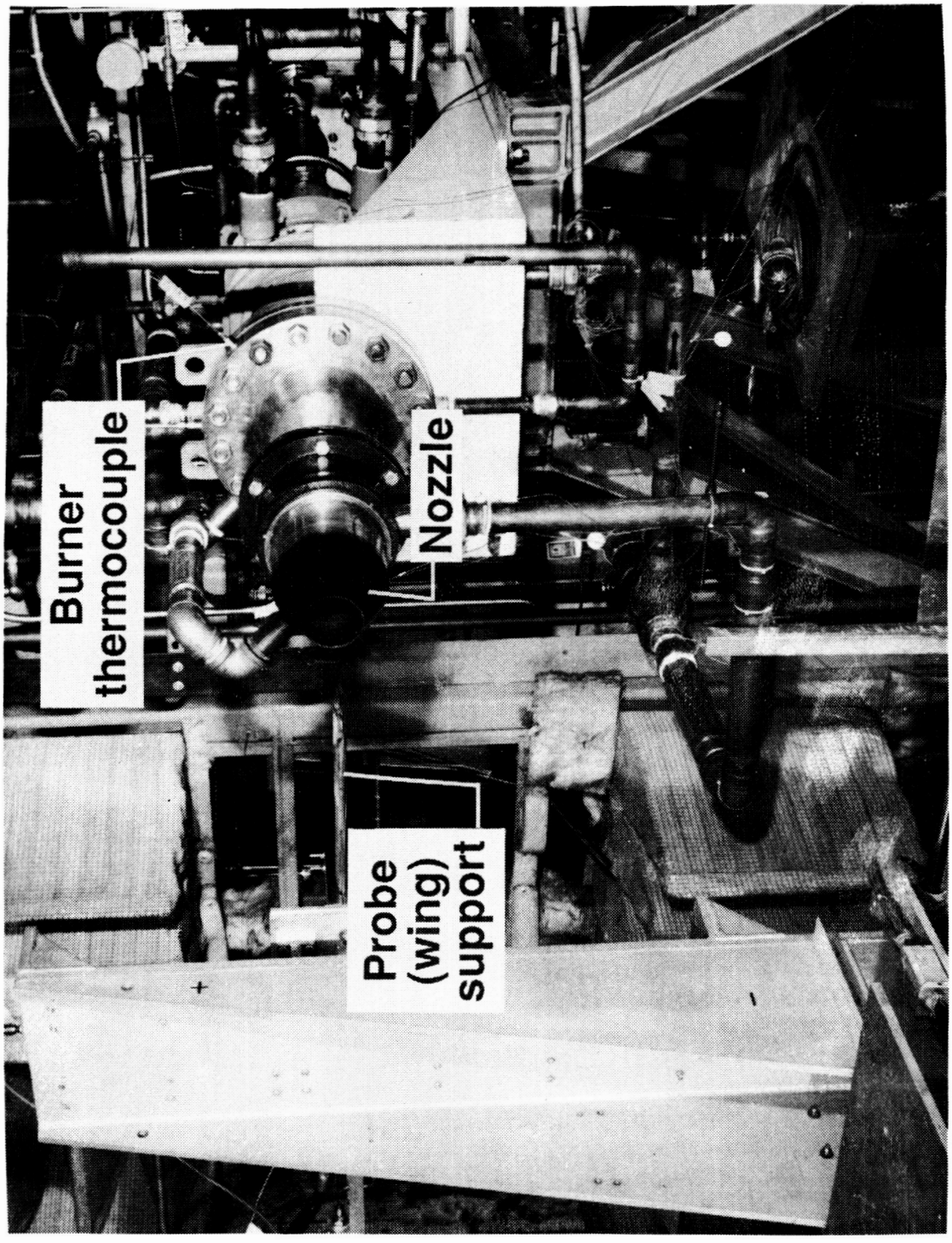

Figure 11. Overall experimental set-up.

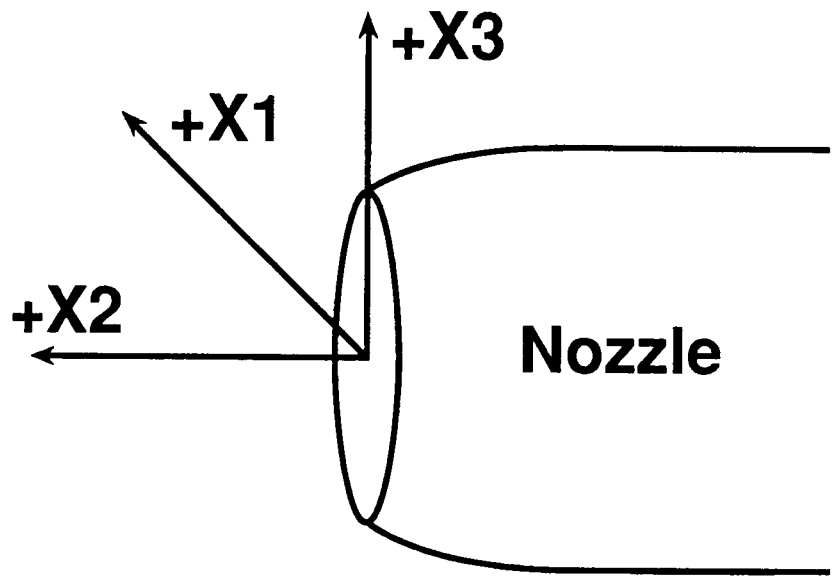

Figure 12. Nozzle axes.

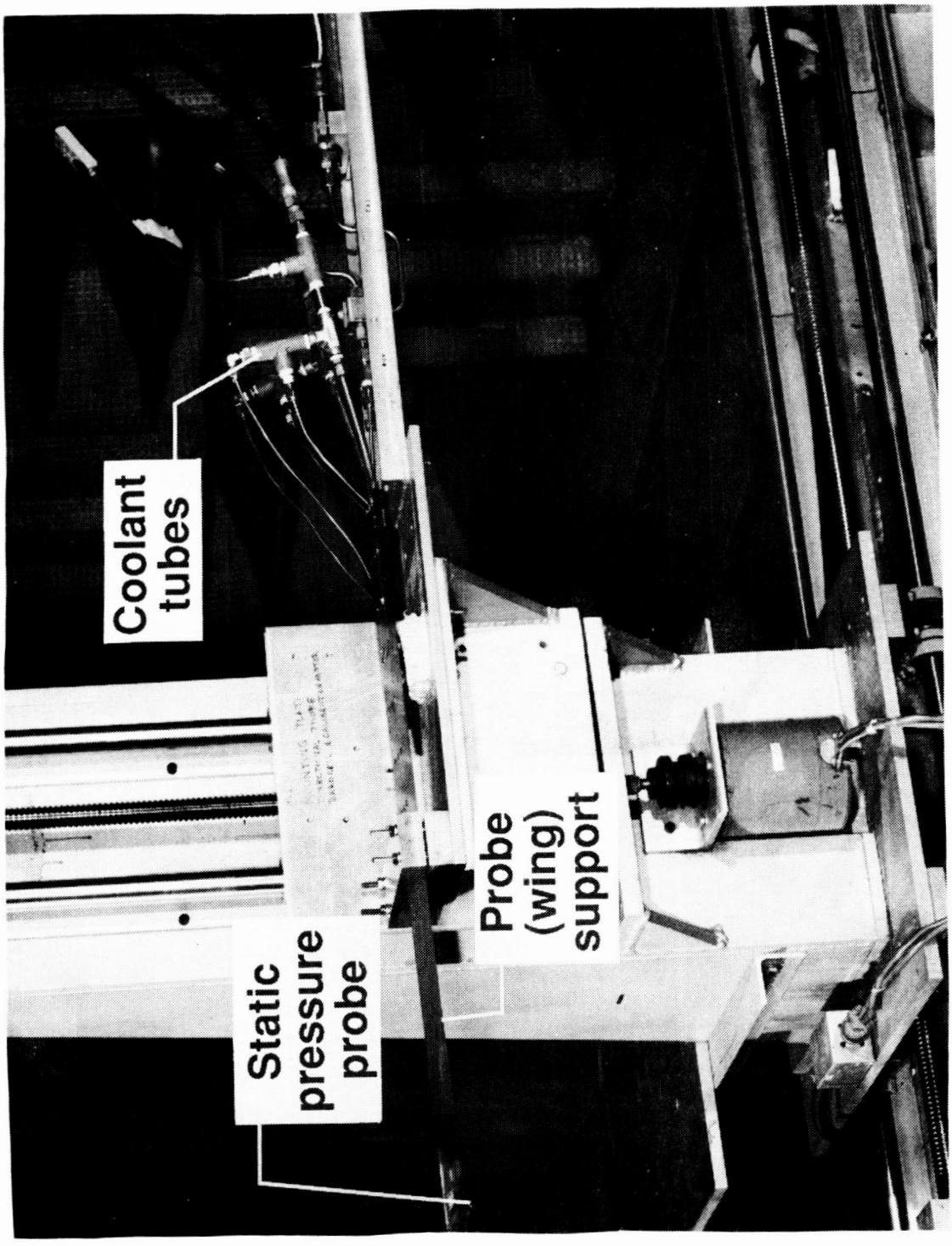

Figure 13. Wing support and coolant assembly.

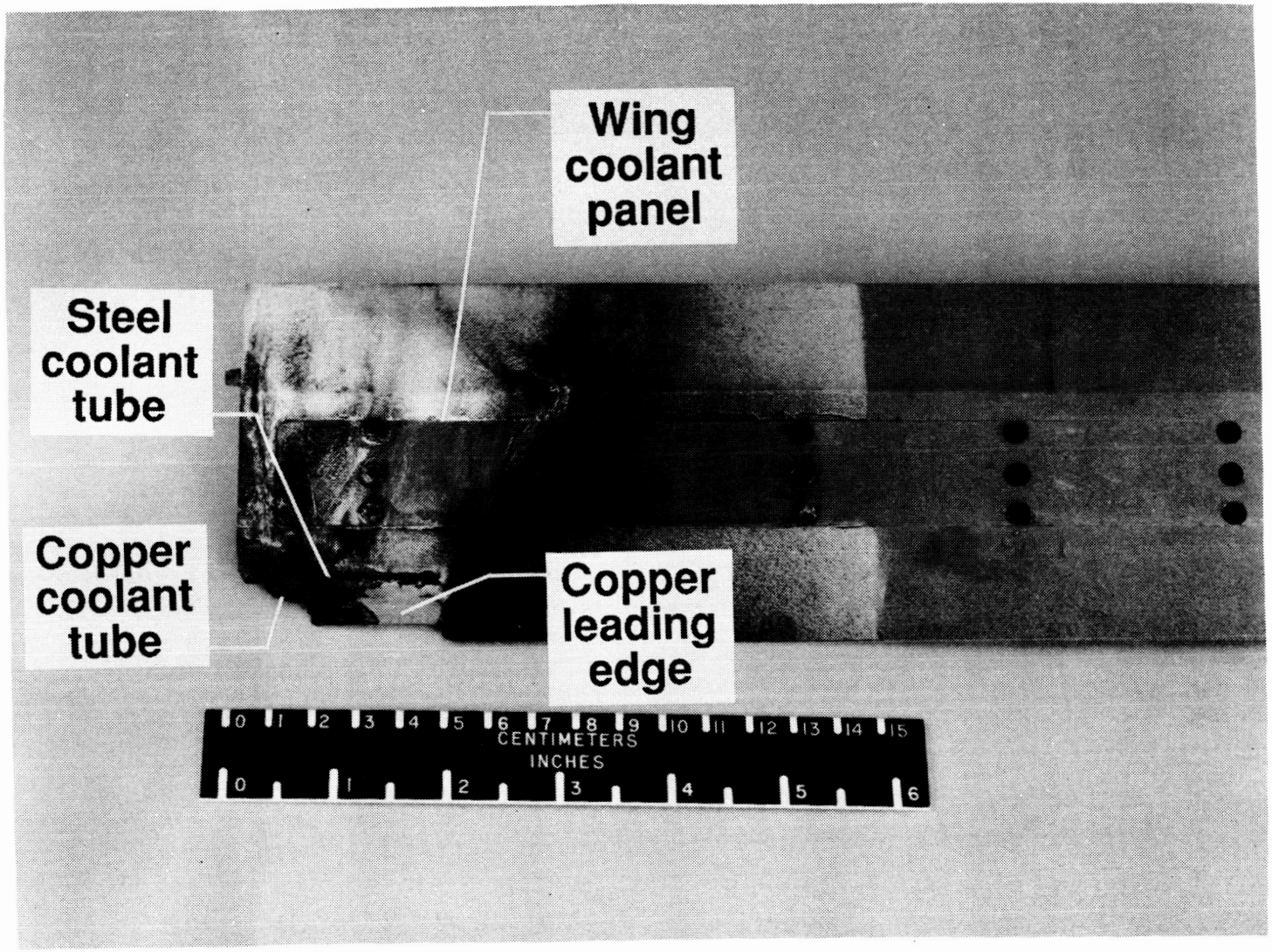

Figure 14. Upper surface of wing support after phase 2 of testing.

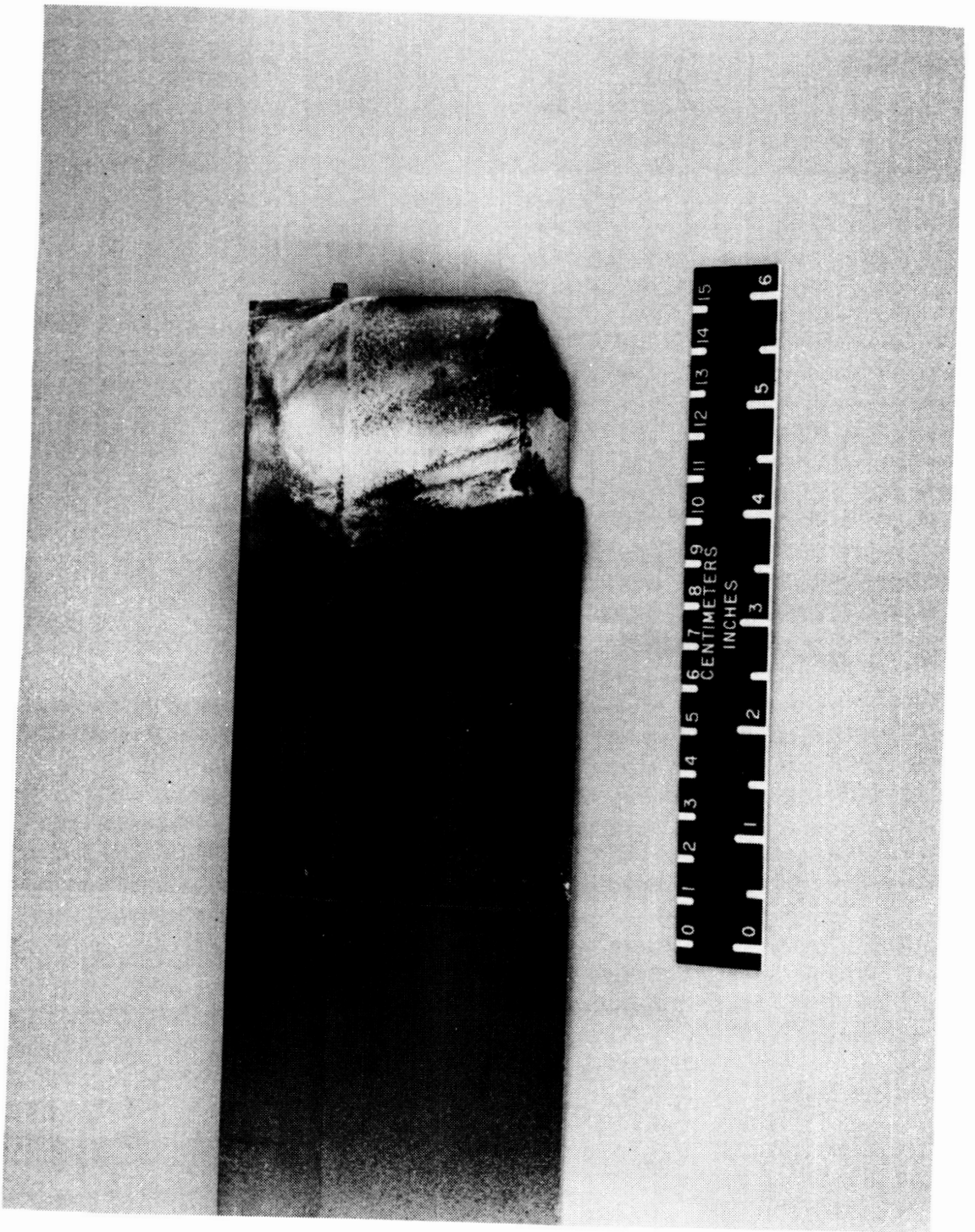

Figure 15. Lower surface of wing support after phase 2 of testing.

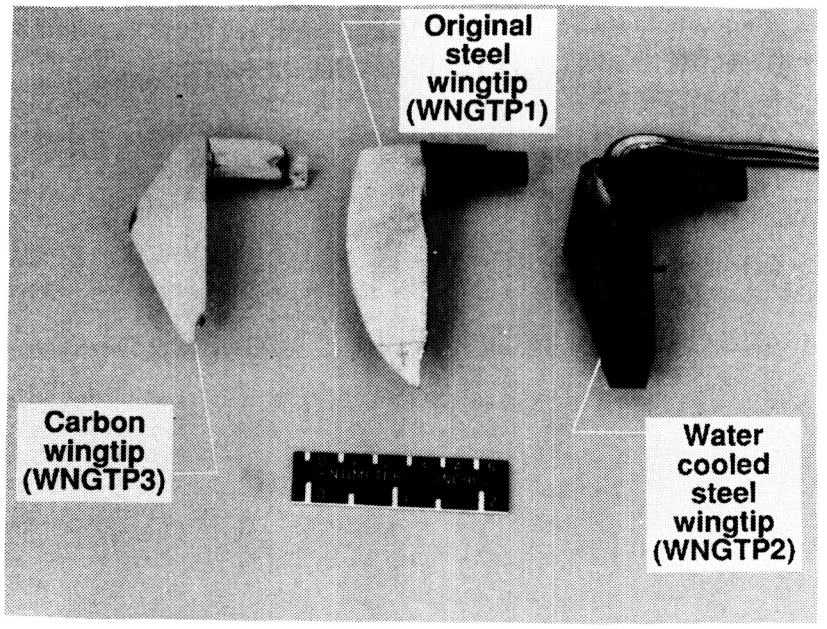

Figure 16. Wingtips utilized in experiment.

	Acronym	Mass flow (lbm/sec)	Comments
Total	NCTP1	-	Uncooled probe from previous tests
Press	CTP2	0.0026	Four tube water cooling up to tip
Probe	CTP3	0.0128	Annular flow cooling up to tip
Static	NCSP1	-	Uncooled probe from previous tests
Press	CSP2	0.0185	Annular flow cooling up to tip
Probe	CSP3	0.0185	Annular flow cooling up to tip
Total	NCTT1	-	Uncooled probe from previous tests
Temp	CTT2	0.0650	Annular flow cooling up to bead
Probe	-	-	-
	WNGTP2	0.0086	Water cooled wingtip

Table 1. Probe classifications and applicable mass flow rates.

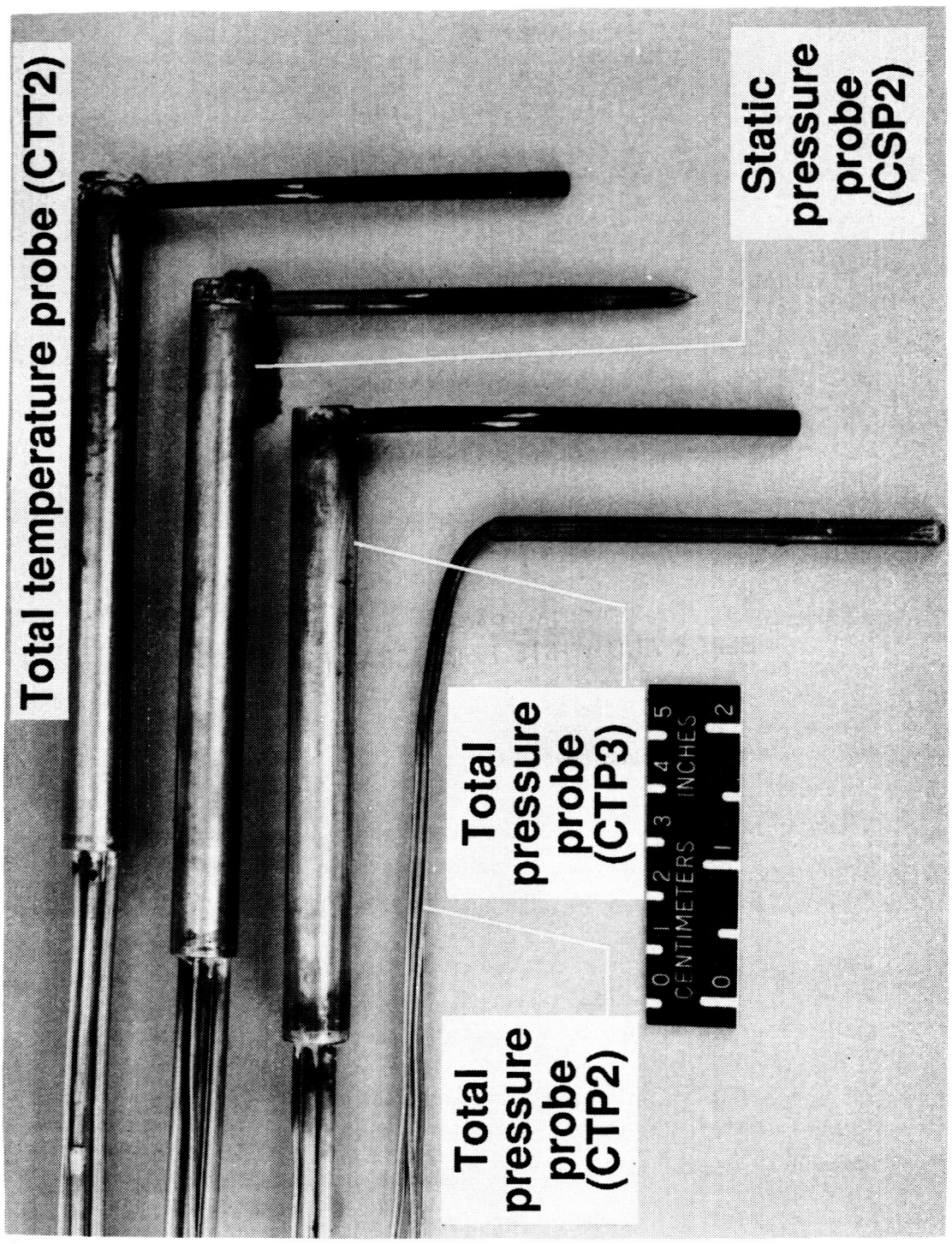

Figure 17. Water cooled probes utilized in experiment.

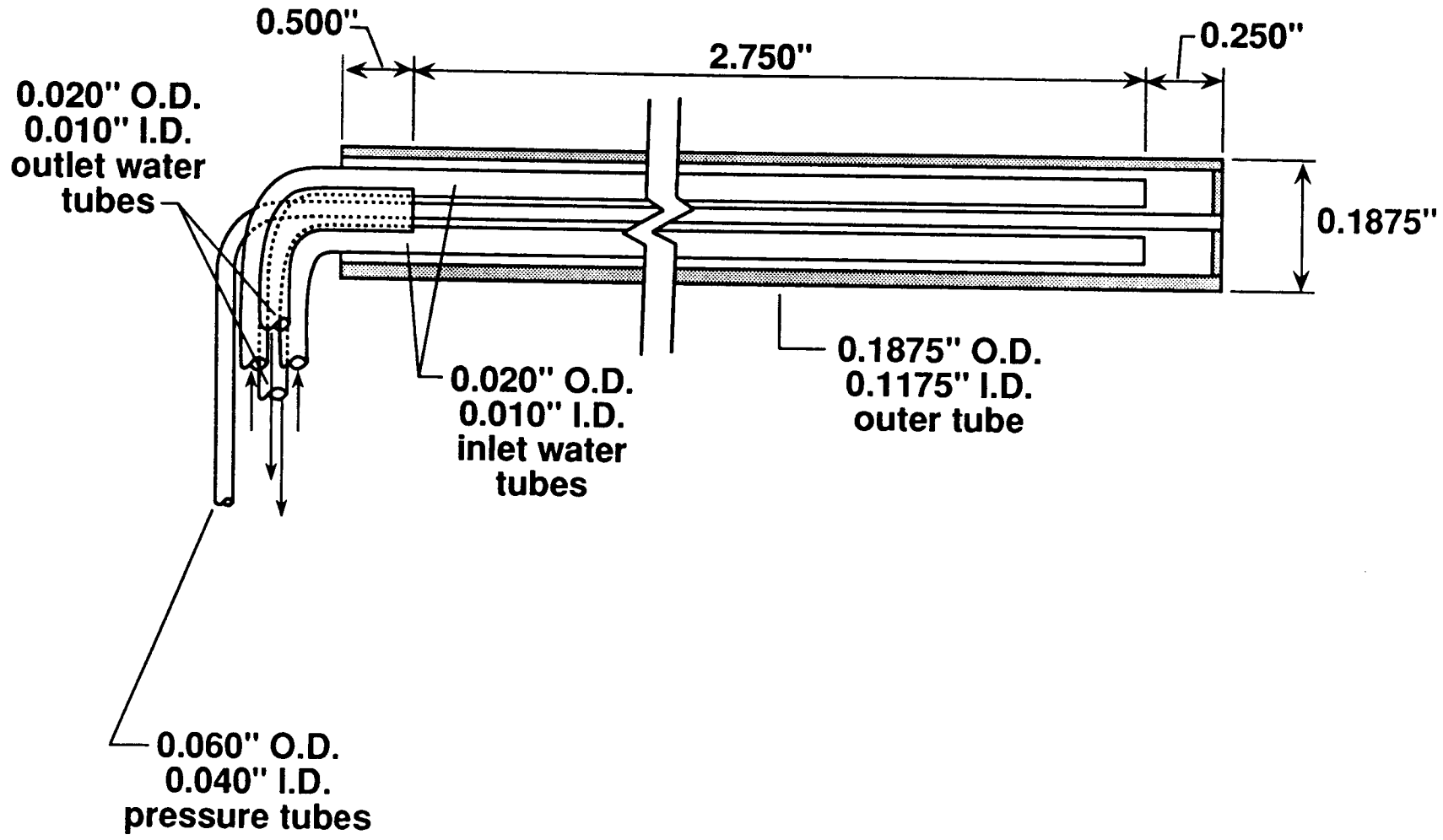

Figure 18. Total pressure probe with unsymmetric water cooling.

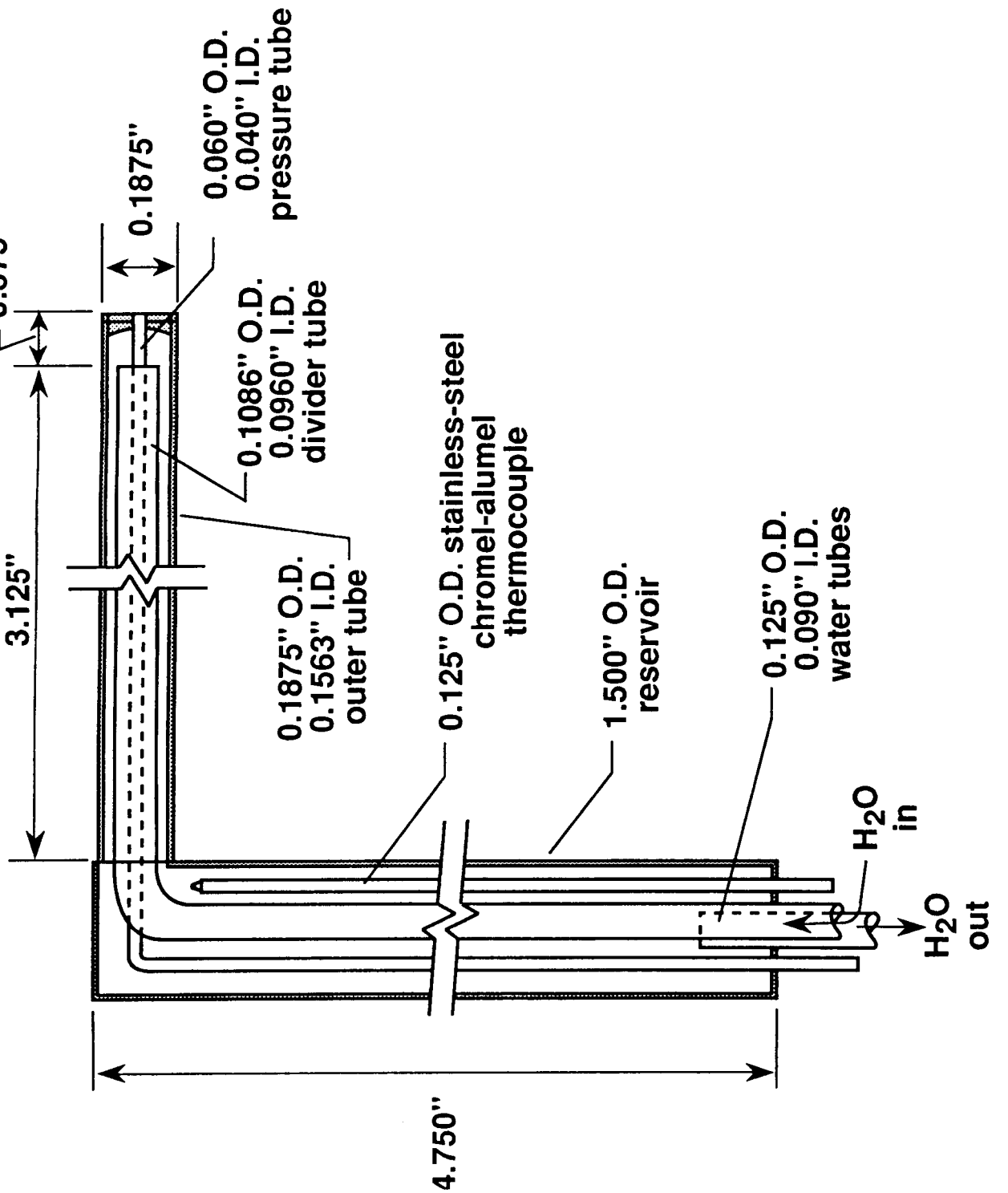

Figure 19. Total pressure probe with annular water cooling.

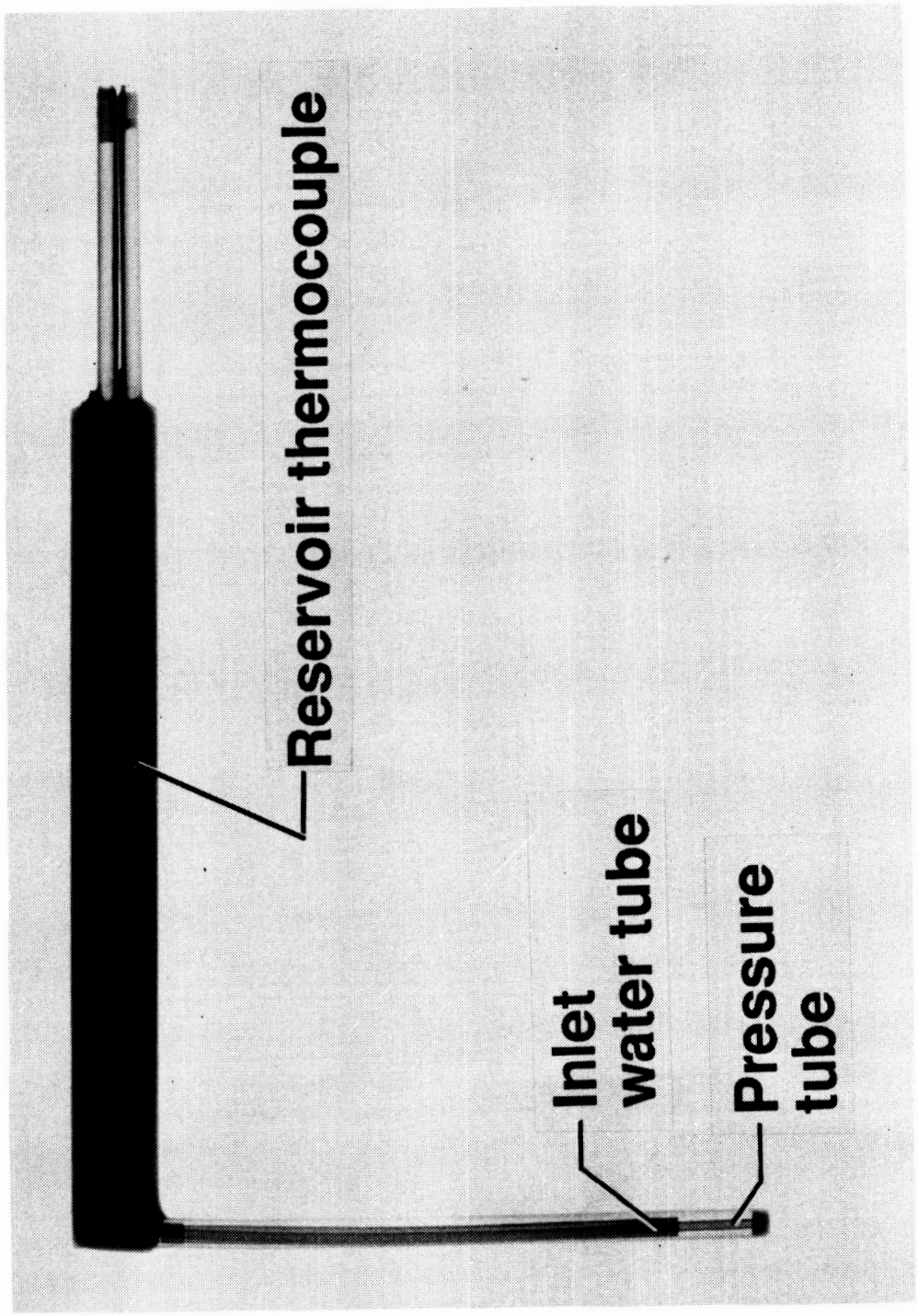

Figure 20. CTP3 X-ray.

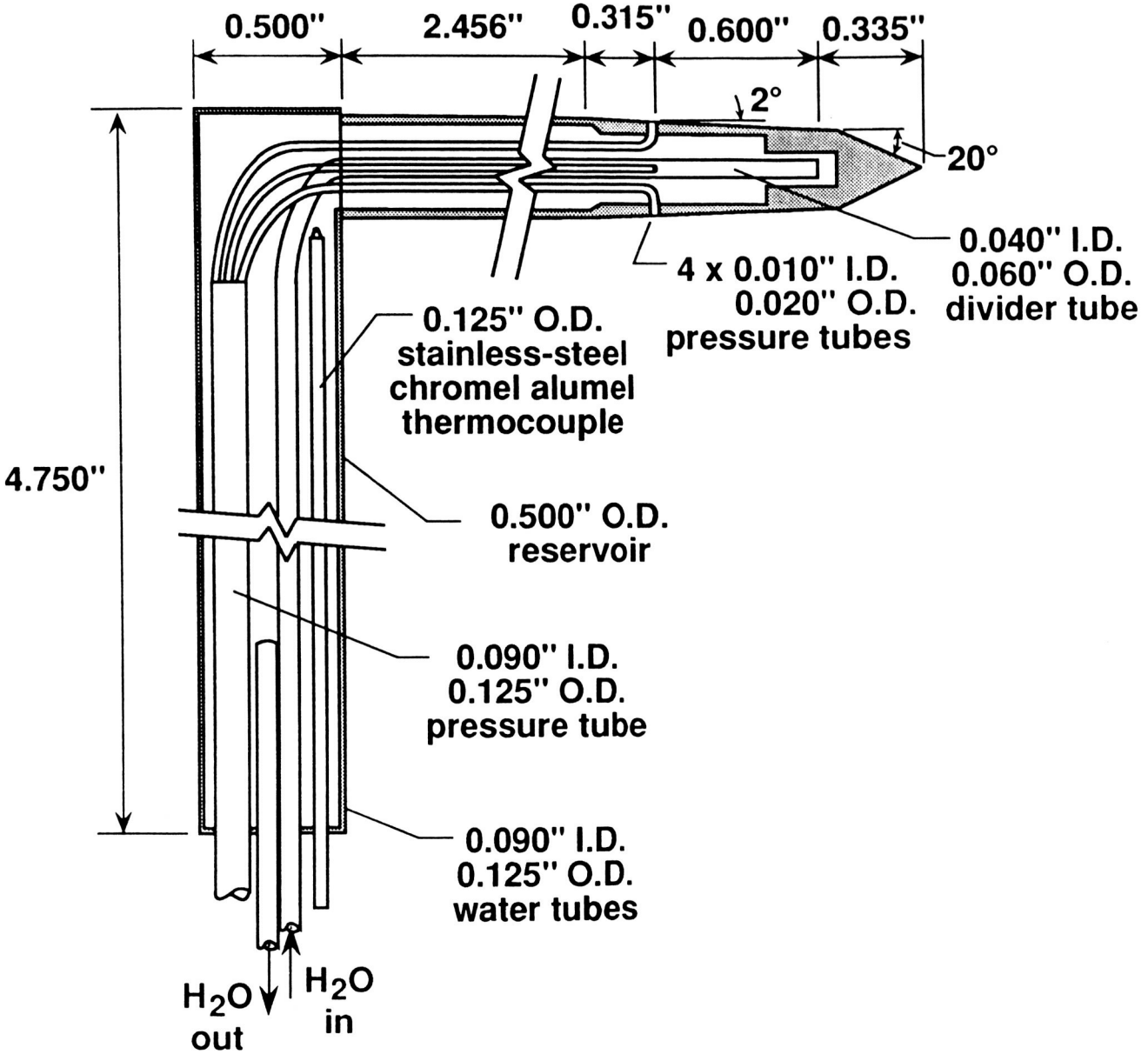

Figure 21. Water cooled static pressure probe.

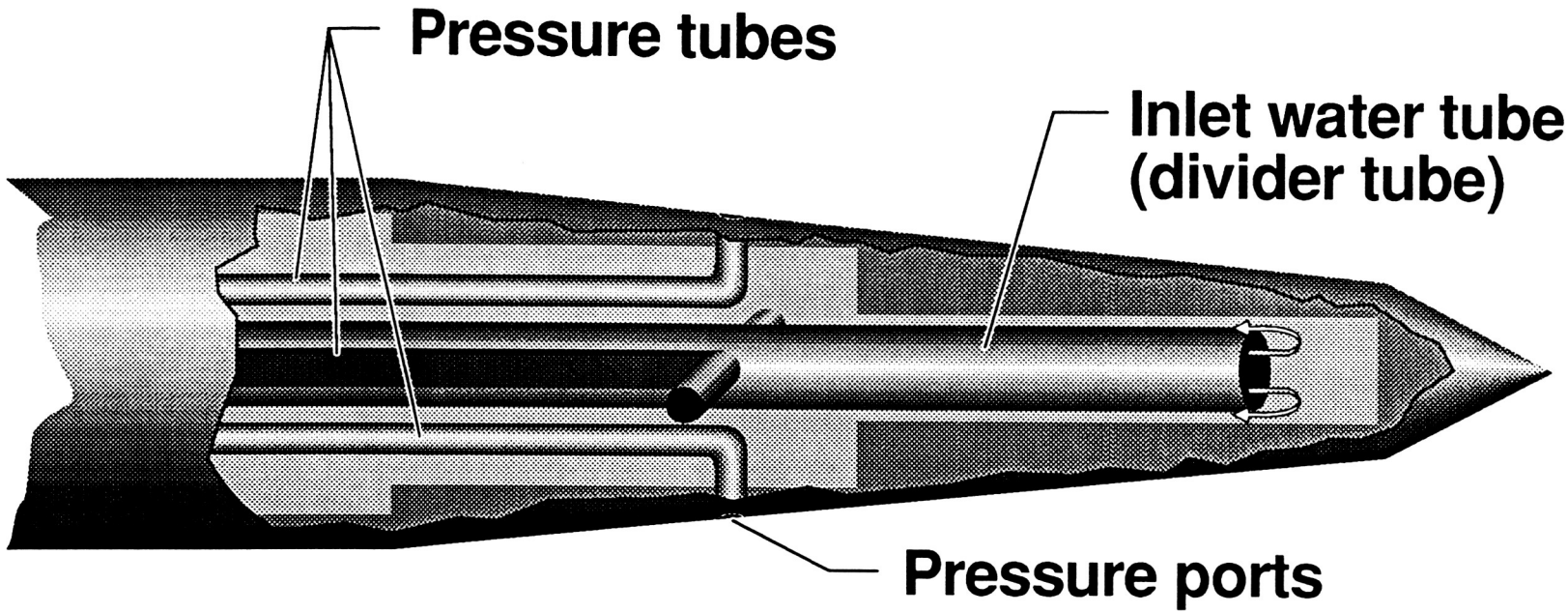

Figure 22. Illustrated cut-away view of cooled static pressure probe tip.

Figure 23. CSP2 partially assembled tip detailing coolant tube and pressure tubes.

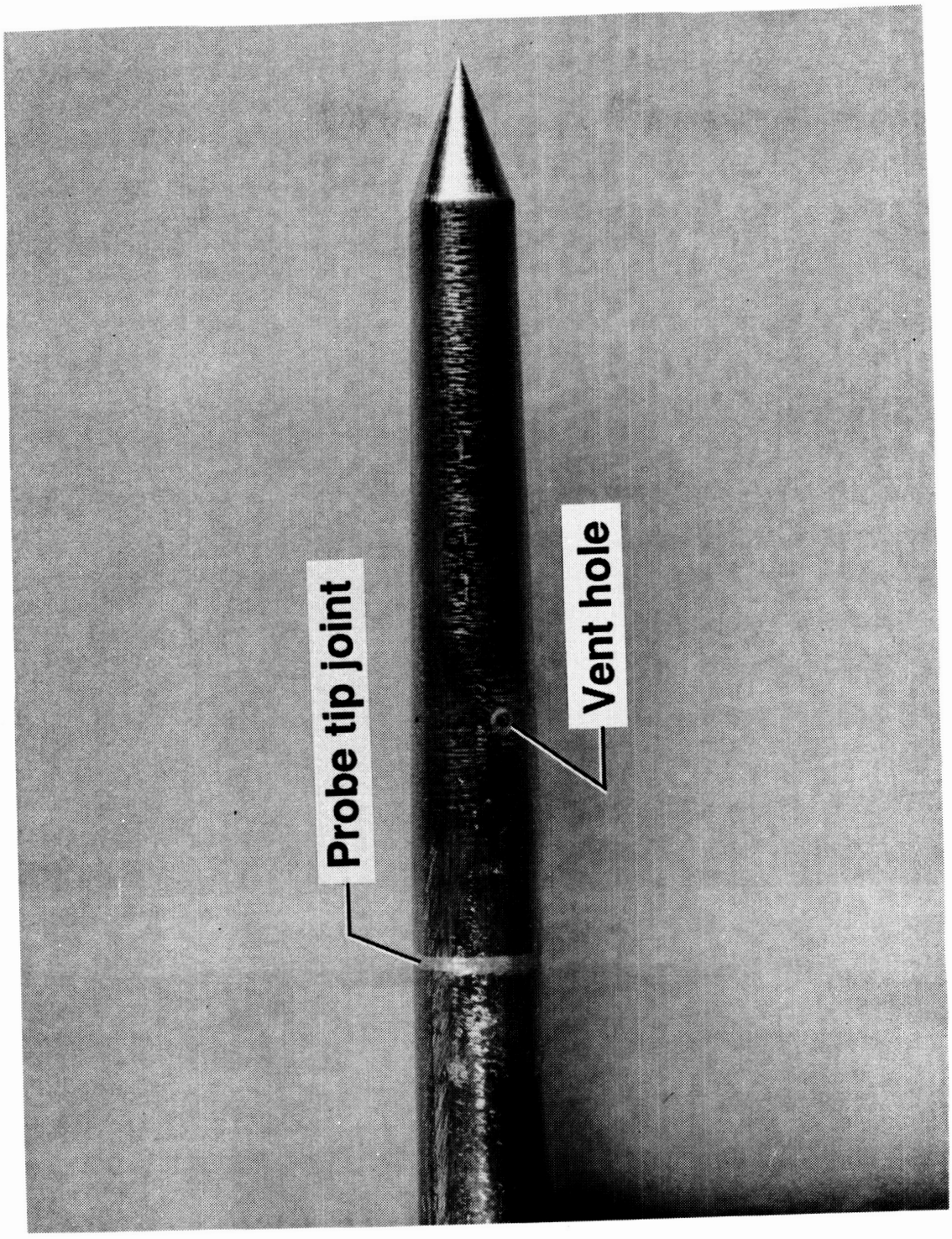

Figure 24. Magnified CSP2 highlighting the finished vent holes.

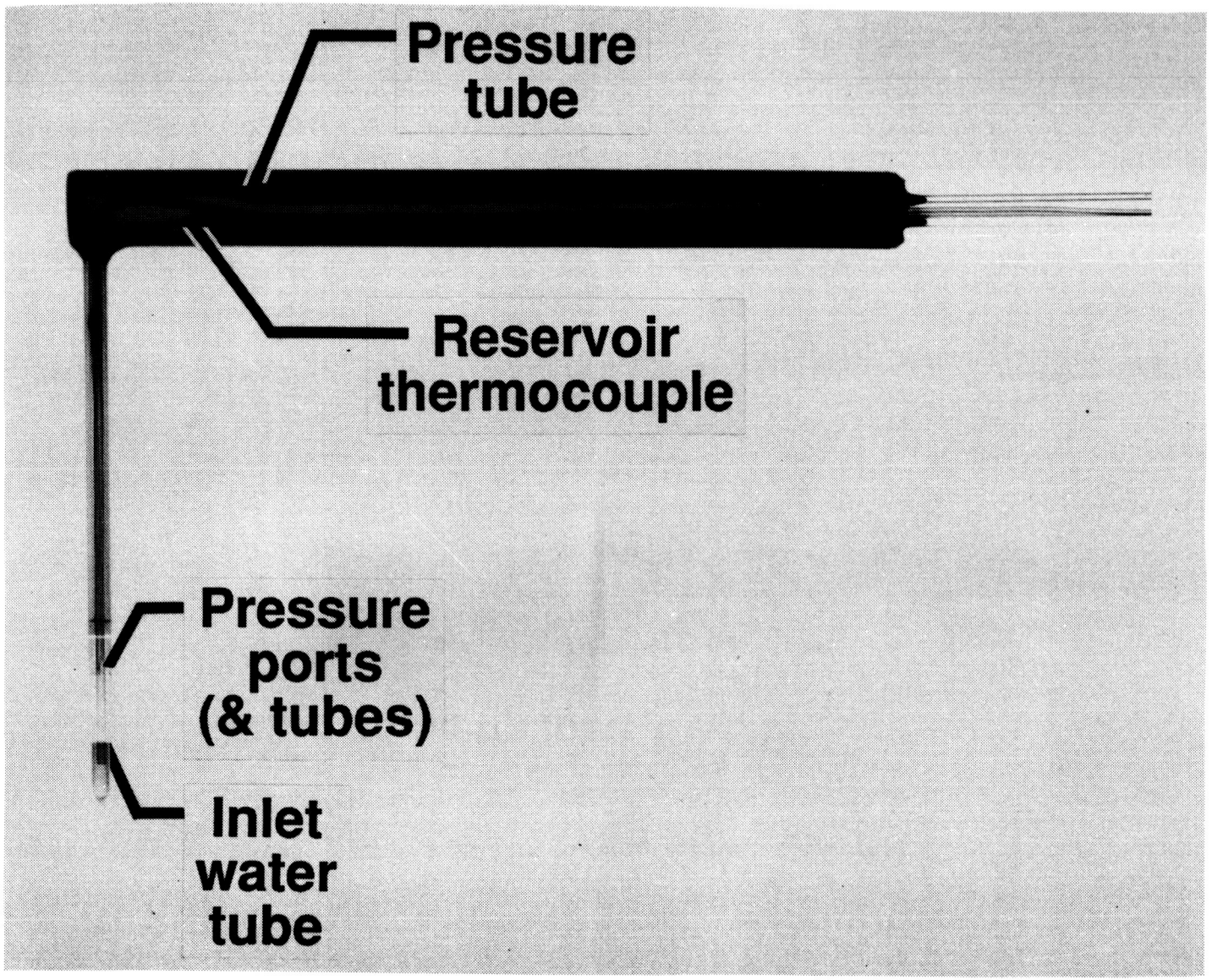

Figure 25. CSP2 X-ray.

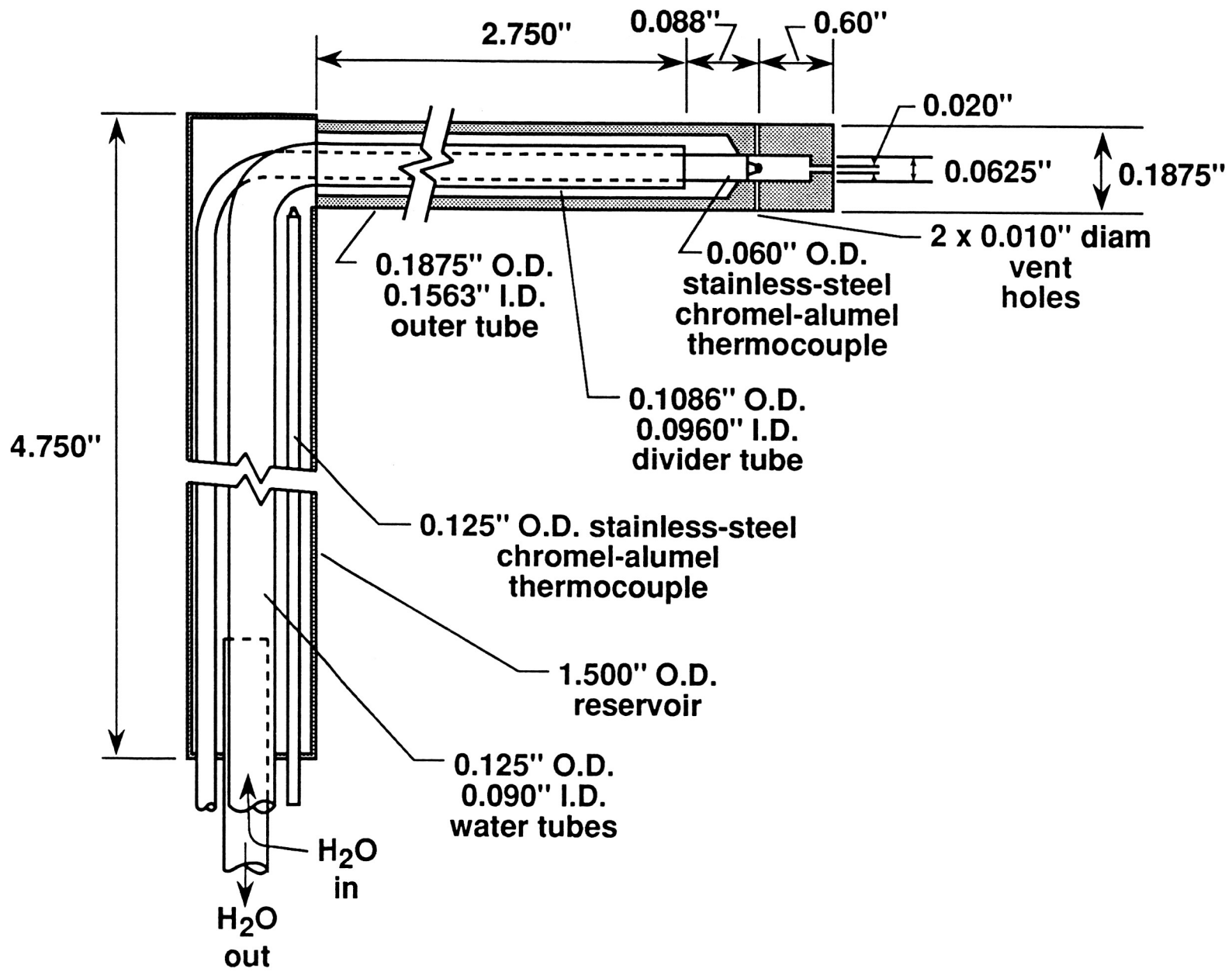

Figure 26. Water cooled total temperature probe.

Figure 27. CRT2 shown prior to assembly.

Figure 28. Overall experimental set-up highlighting the infrared system and traverse.

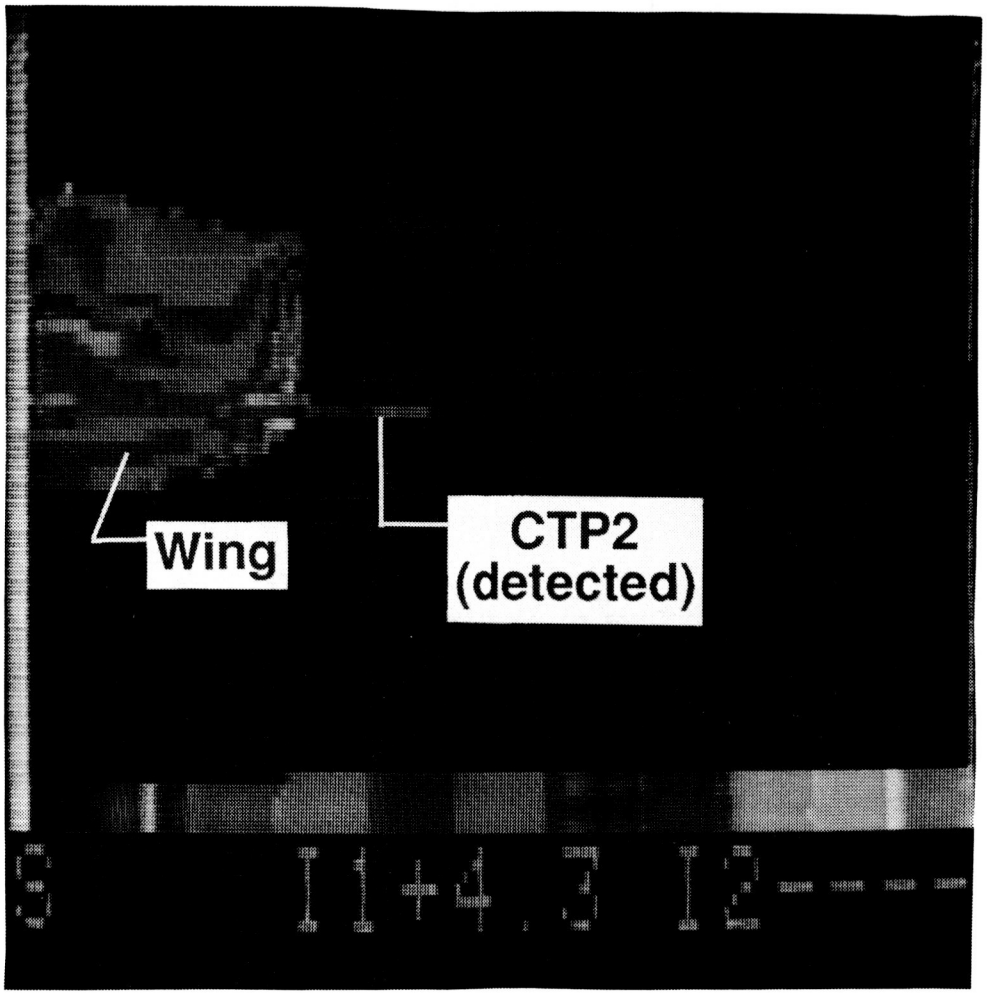

Figure 29. CTP2 infrared photo at 900 F.

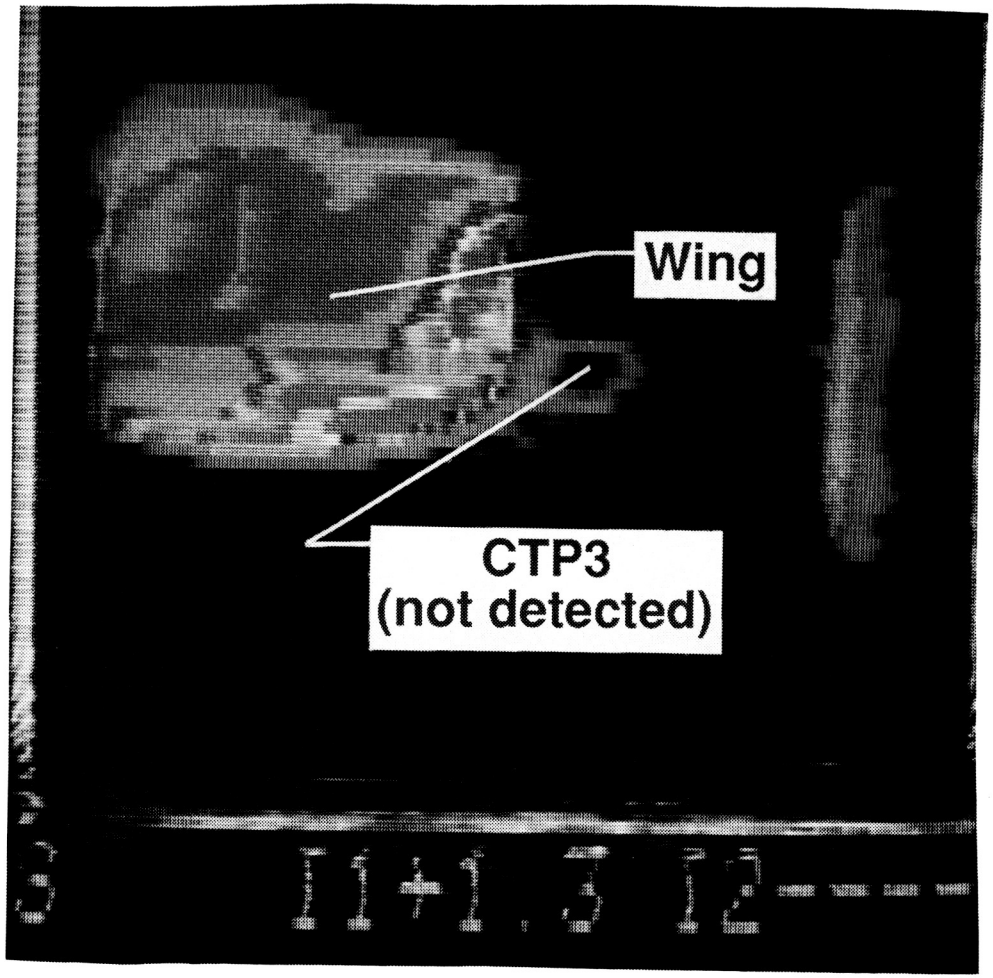

Figure 30. CTP3 infrared photo at 1600 F.

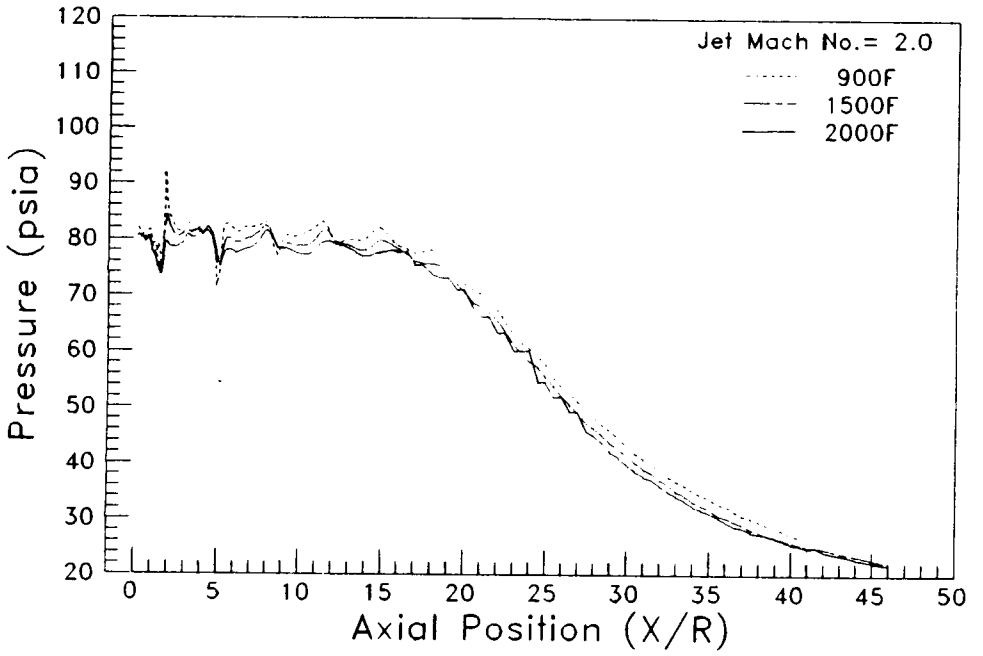

Figure 31. Measured jet centerline total pressures at 900 F, 1500 F, and 2000 F.

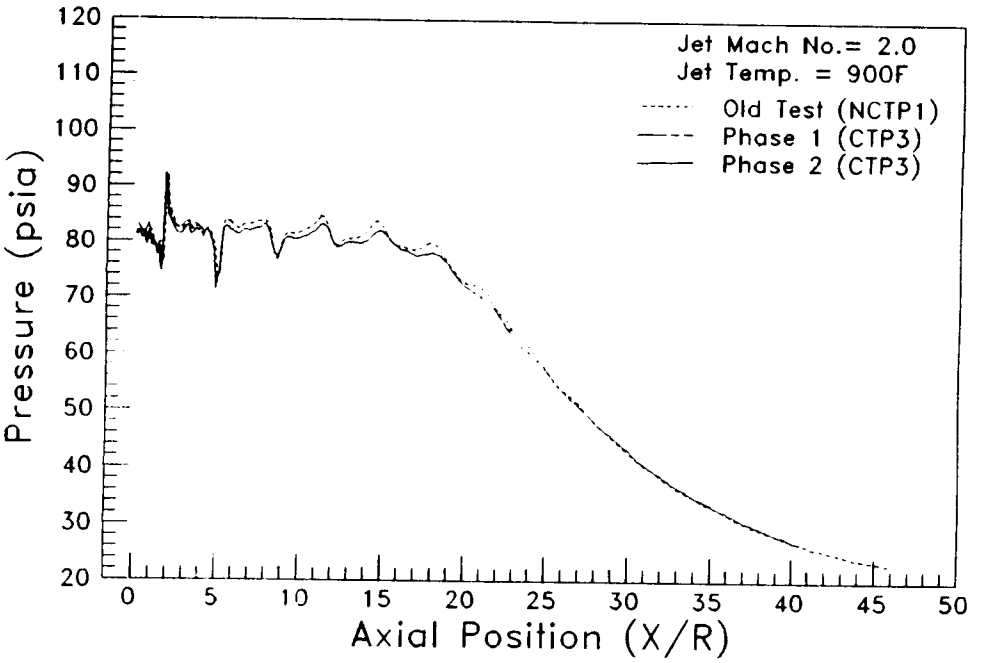

Figure 32. Measured jet centerline total pressure comparison at 900 F.

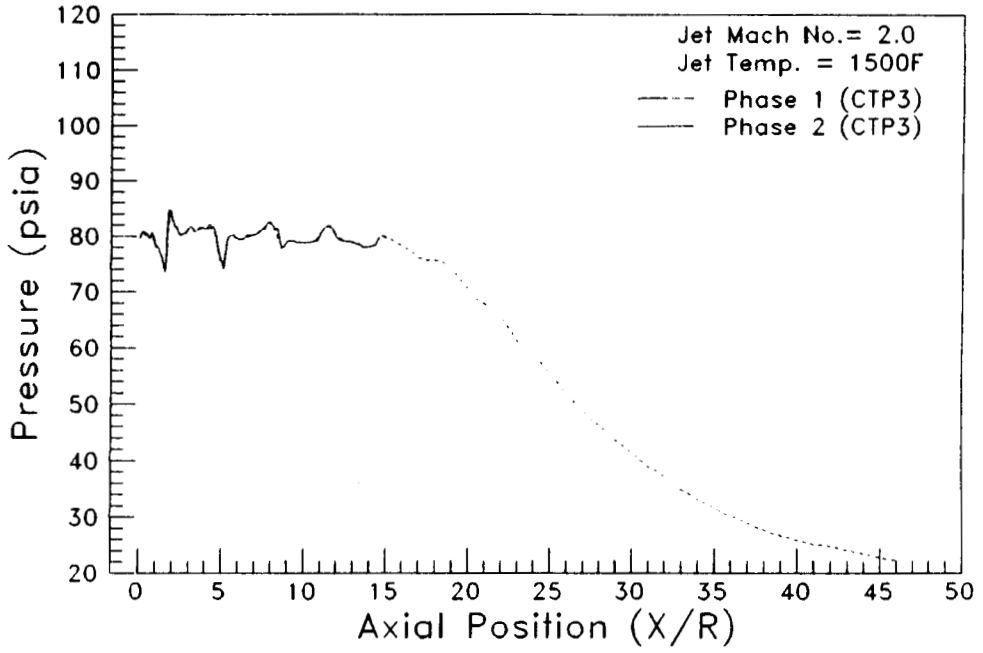

Figure 33. Measured jet centerline total pressure comparison at 1500 F.

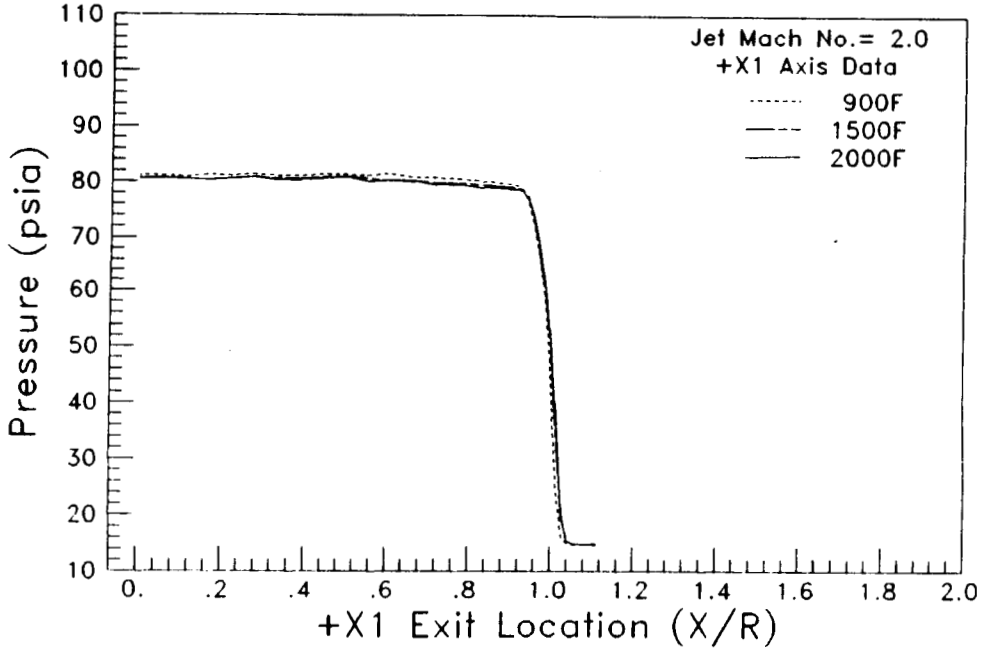

Figure 34. Measured +X1 axis total pressures at 900 F, 1500 F, and 2000 F.

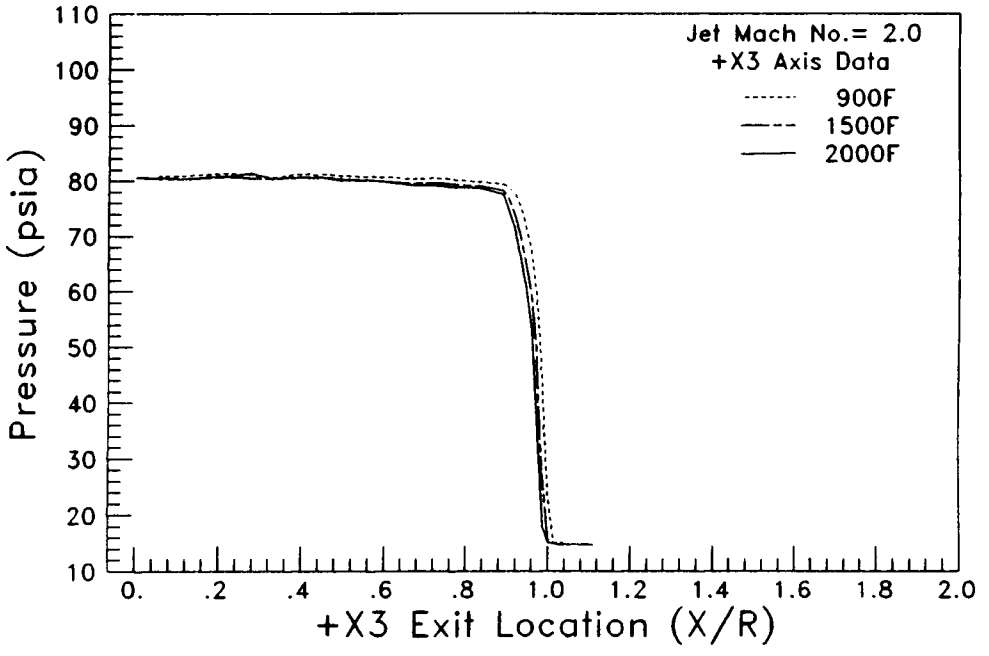

Figure 35. Measured +X3 axis total pressures at 900 F, 1500 F, and 2000 F.

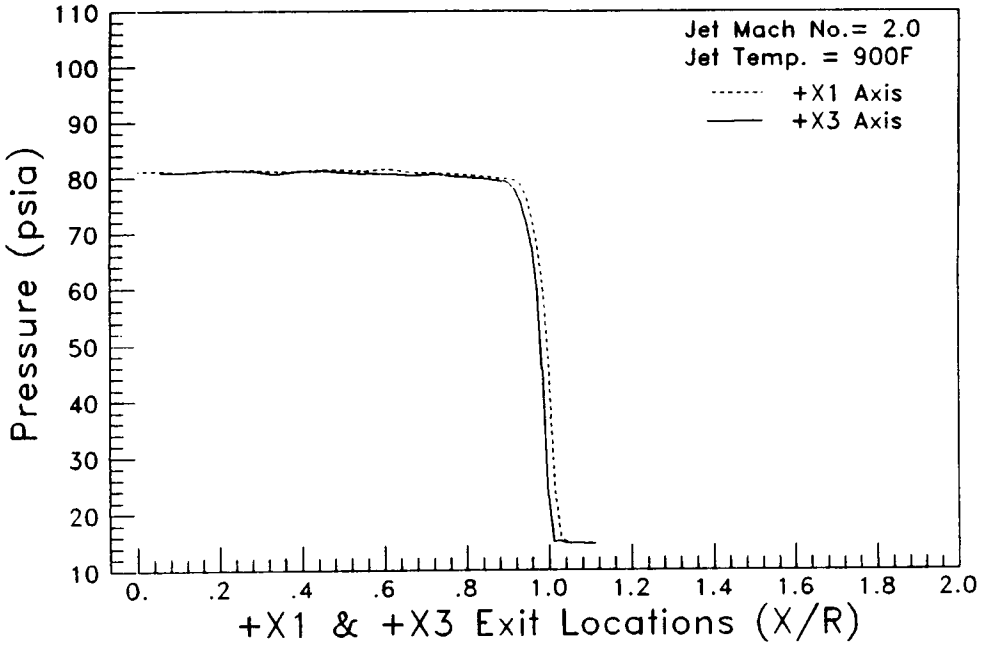

Figure 36. Measured +X1 and +X3 axes total pressure comparison at 900 F.

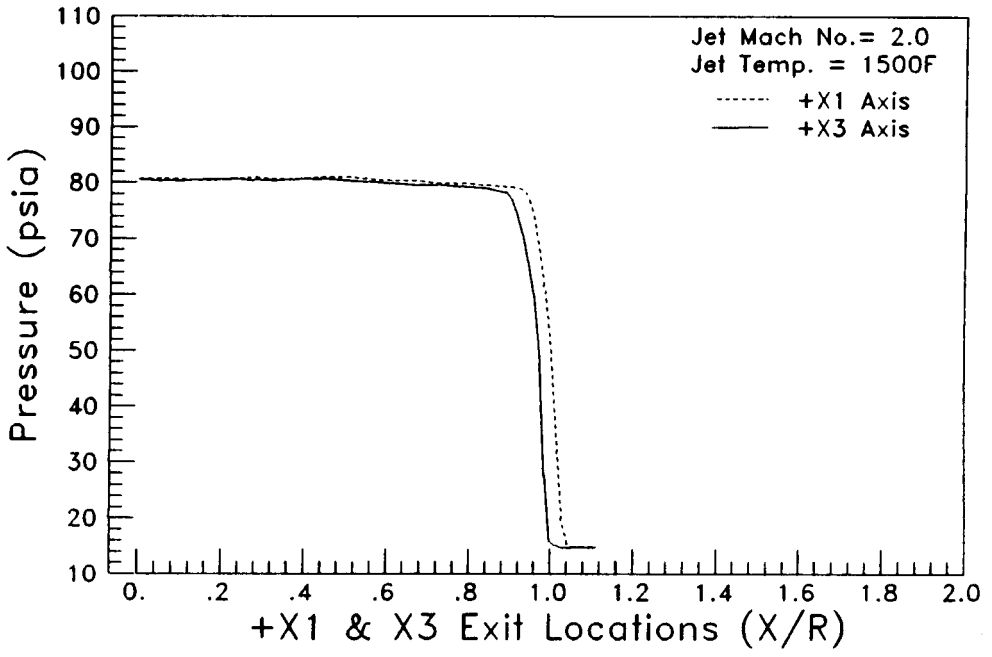

Figure 37. Measured +X1 and +X3 axes total pressure comparison at 1500 F.

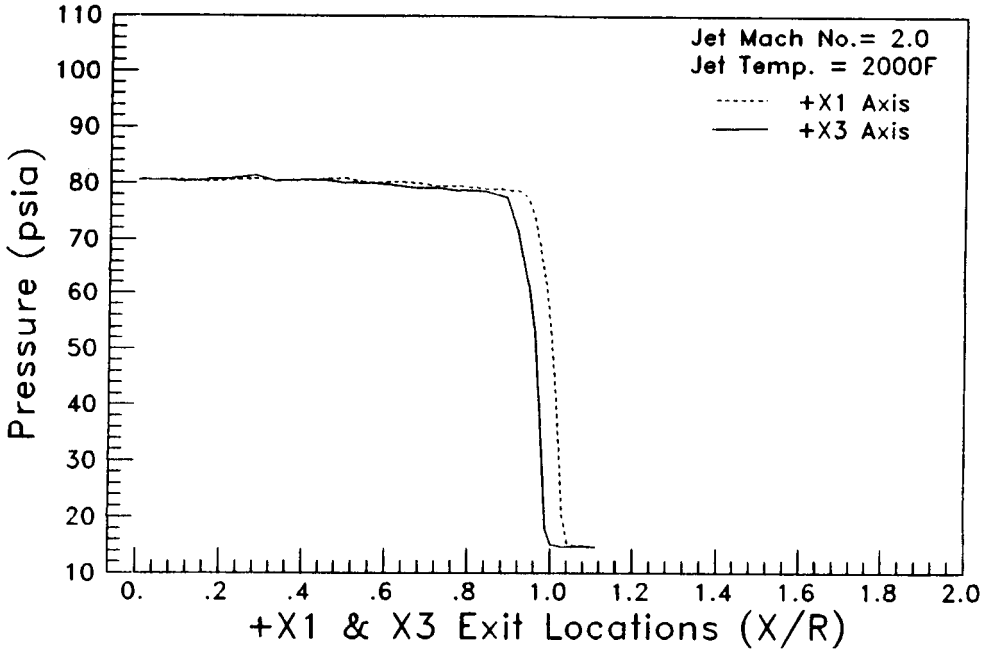

Figure 38. Measured +X1 and +X3 axes total pressure comparison at 2000 F.

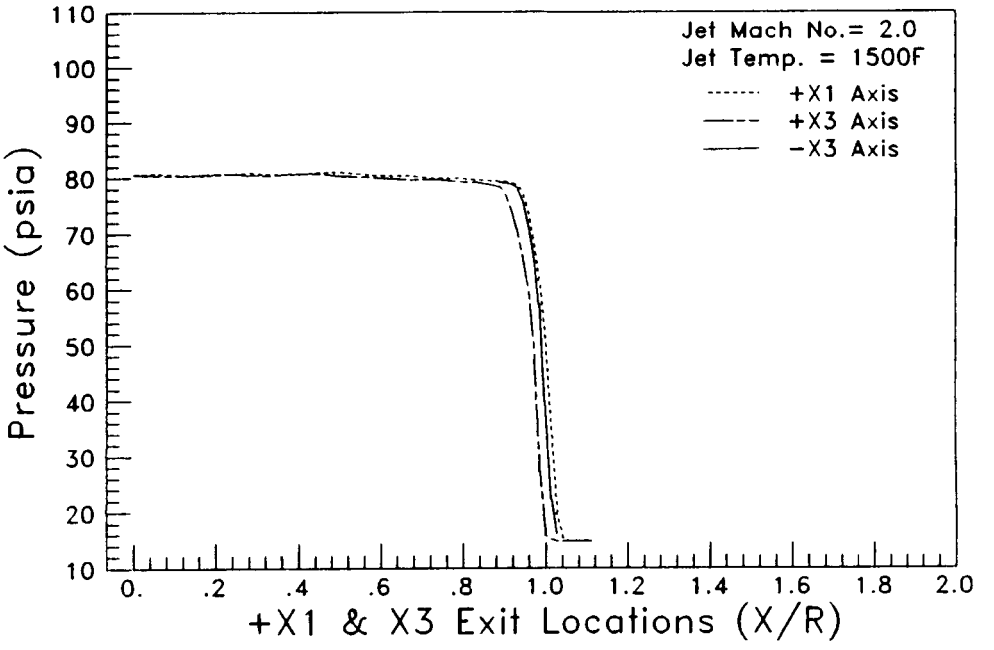

Figure 39. Measured +X1, +X3, and -X3 axes total pressure comparisons at 1500 F.

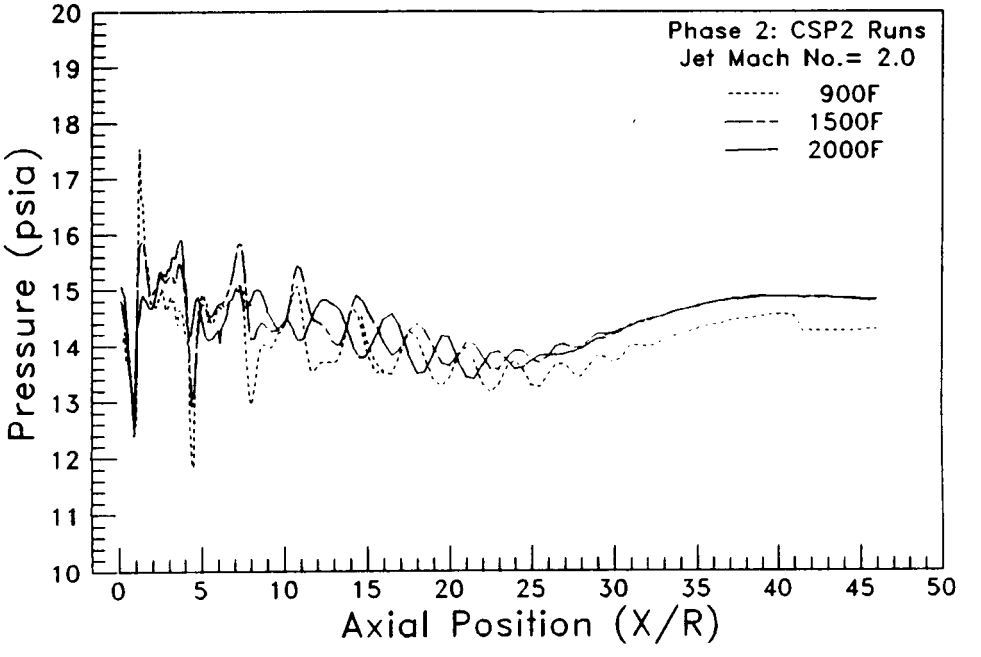

Figure 40. Measured jet centerline static pressures at 900 F, 1500 F, and 2000 F.

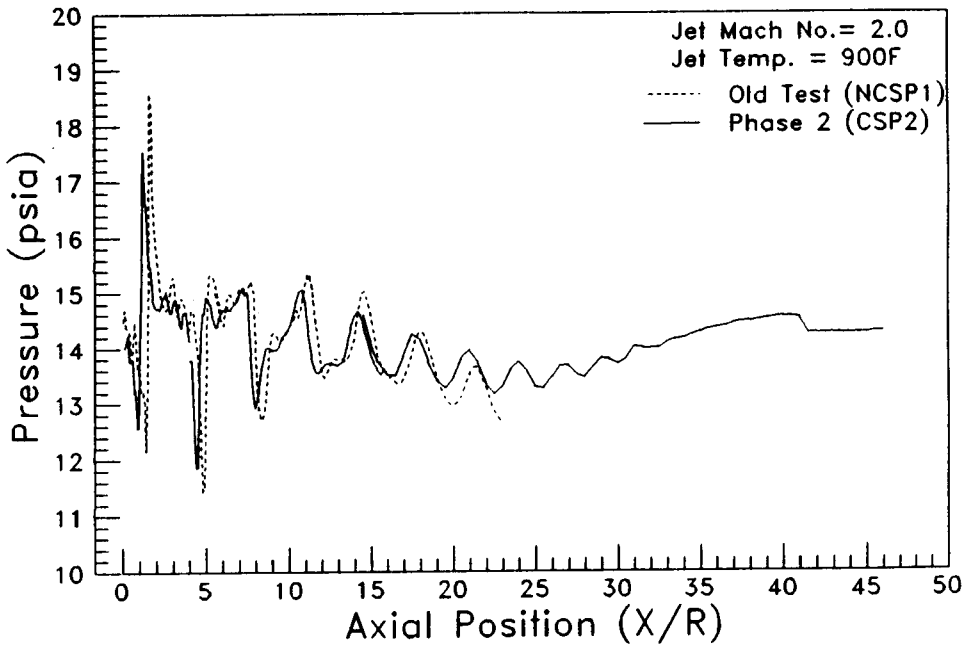

Figure 41. Measured jet centerline static pressure comparison at 900 F.

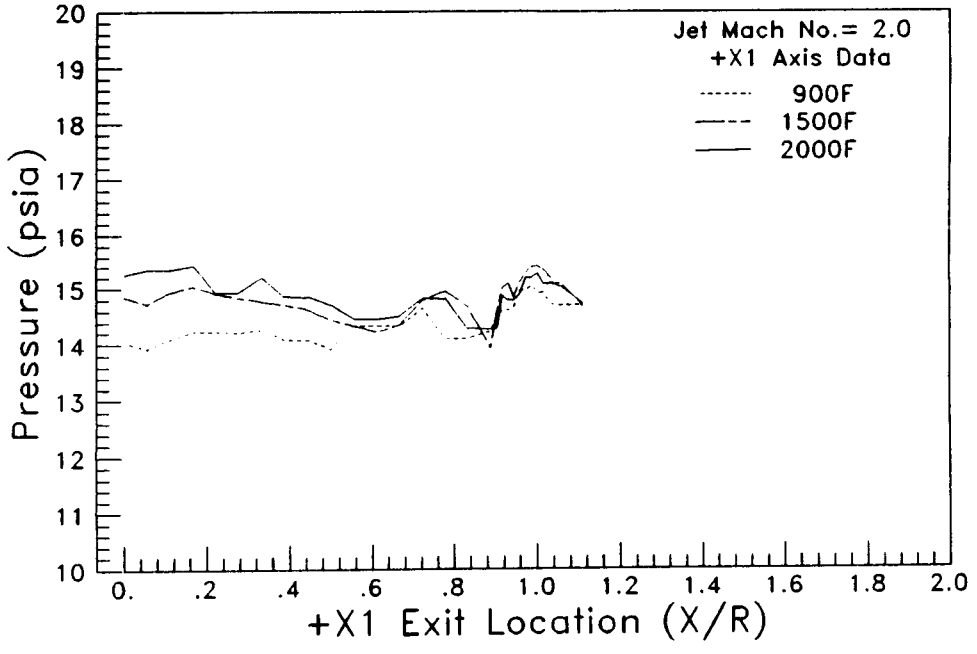

Figure 42. Measured +X1 axis static pressures at 900 F, 1500 F, and 2000 F.

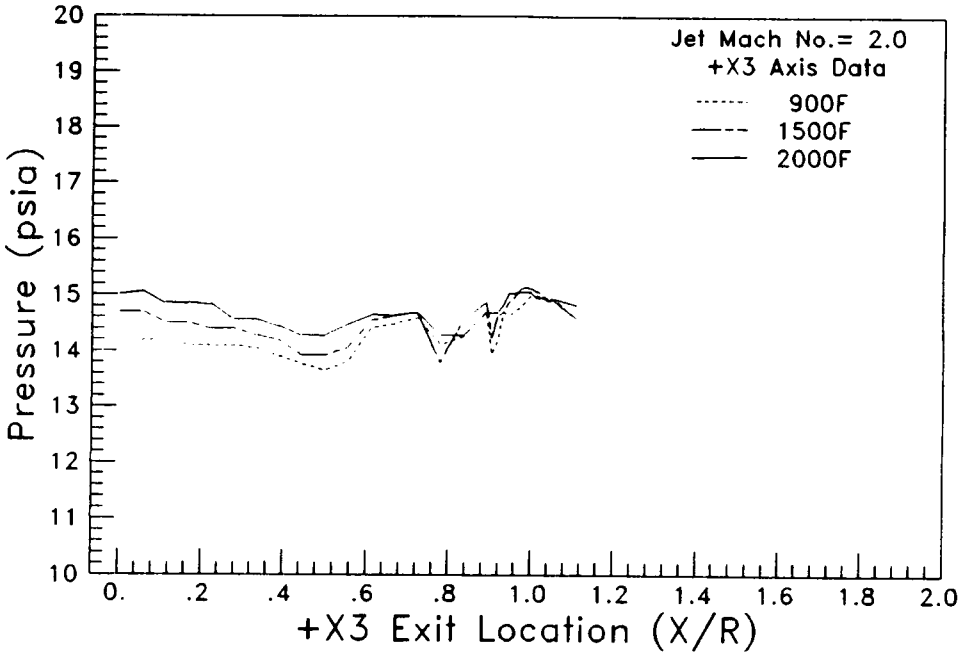

Figure 43. Measured +X3 axis static pressures at 900 F, 1500 F, and 2000 F.

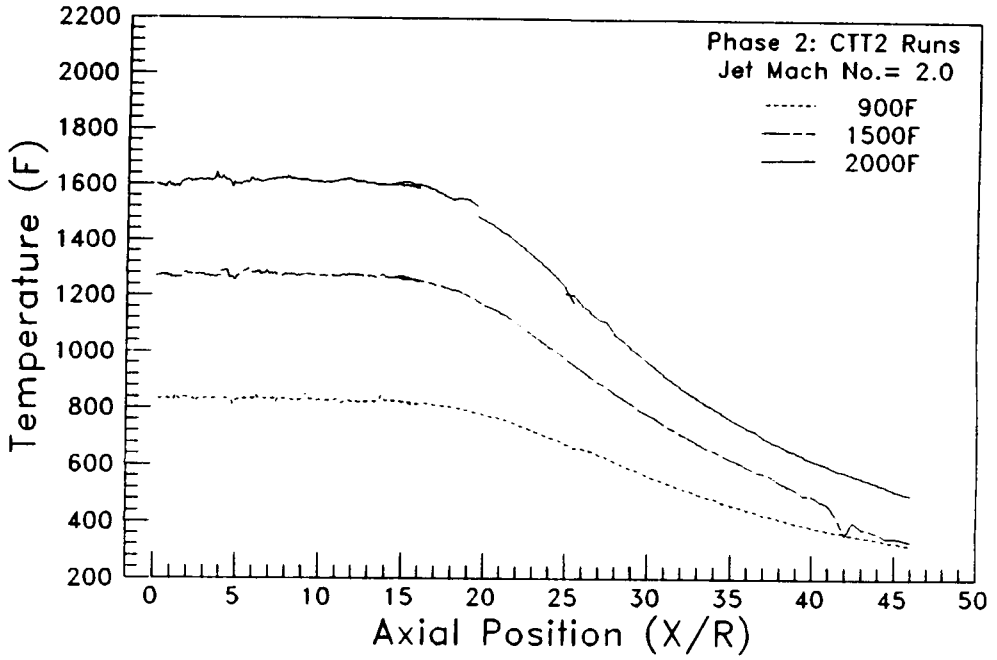

Figure 44. Measured jet centerline total temperatures at 900 F, 1500 F, and 2000 F.

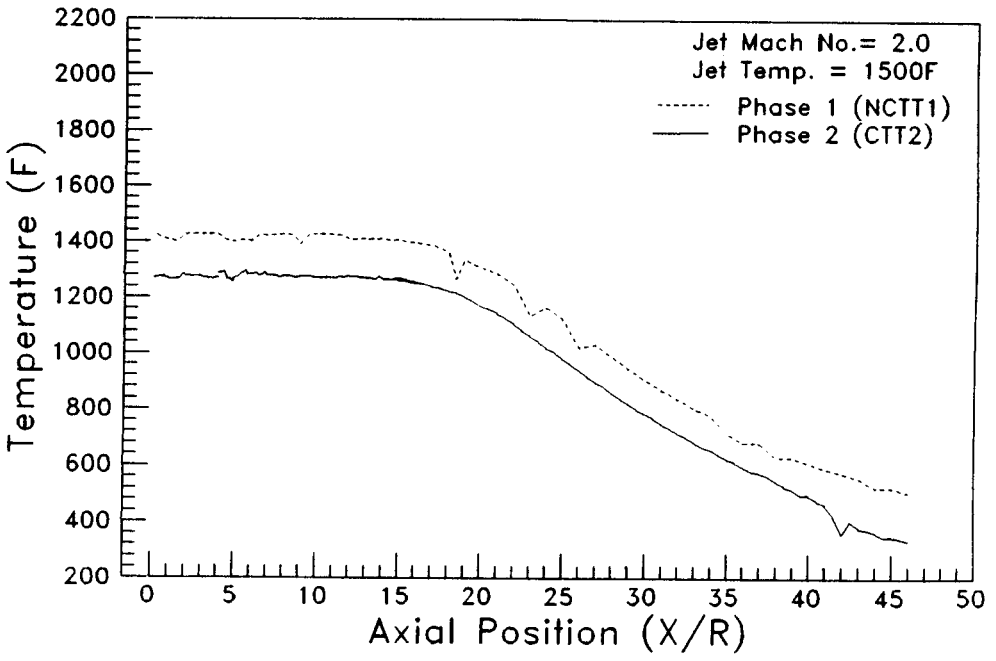

Figure 45. Measured jet centerline total temperature comparison at 1500 F.

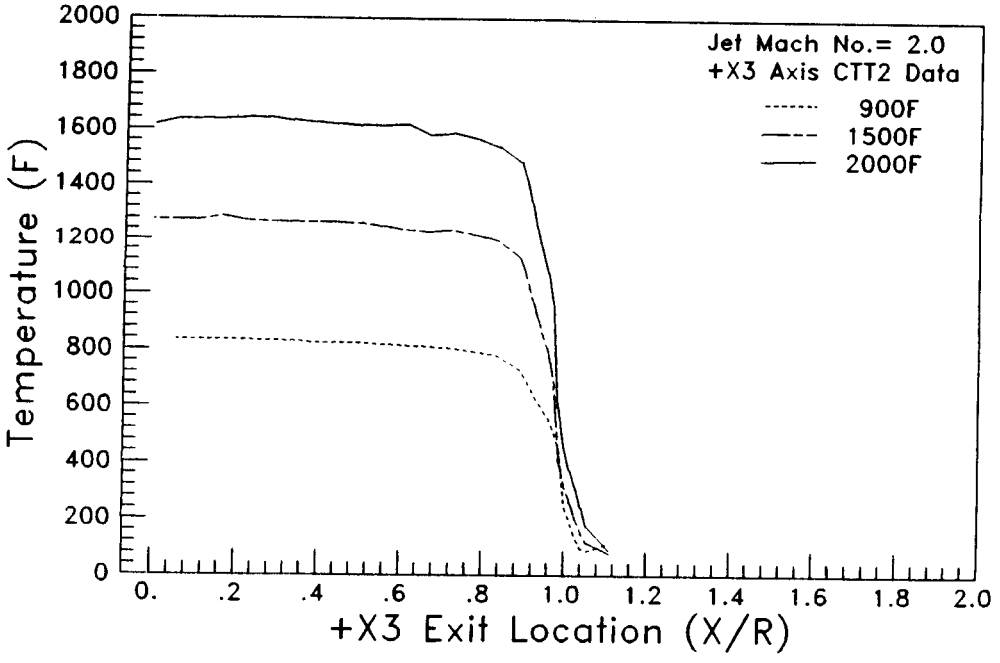

Figure 46. Measured +X3 axis total temperatures at 900 F, 1500 F, 2000 F.

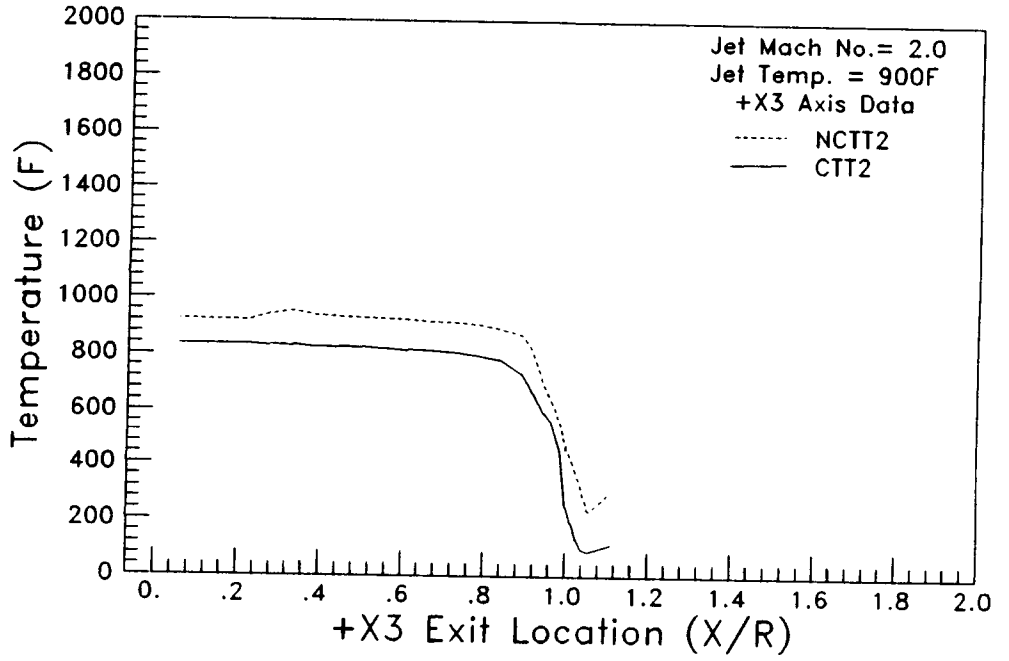

Figure 47. Measured +X3 axis total temperature comparison at 900 F.

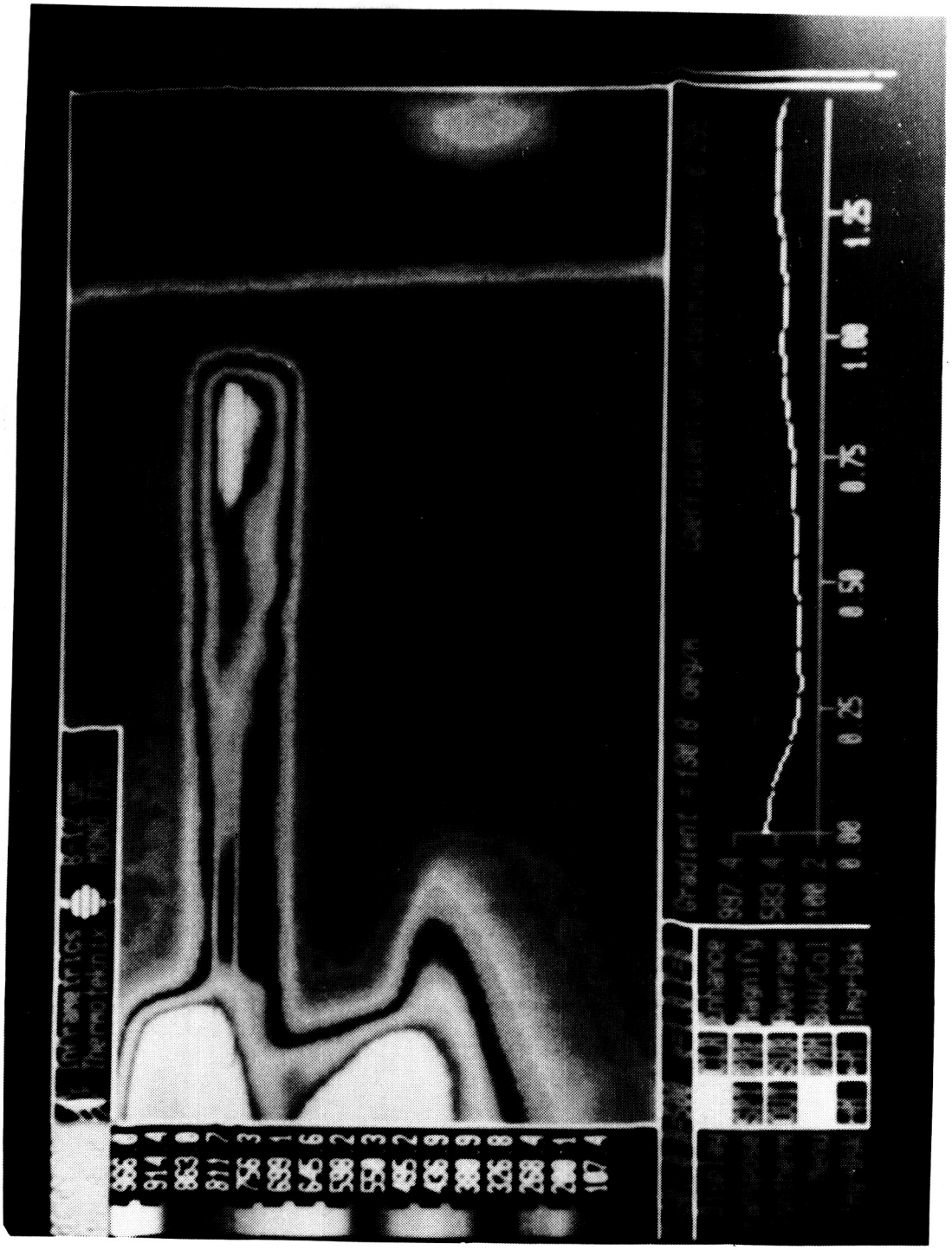

Figure 48. NCTT2 infrared photo at 900 F.

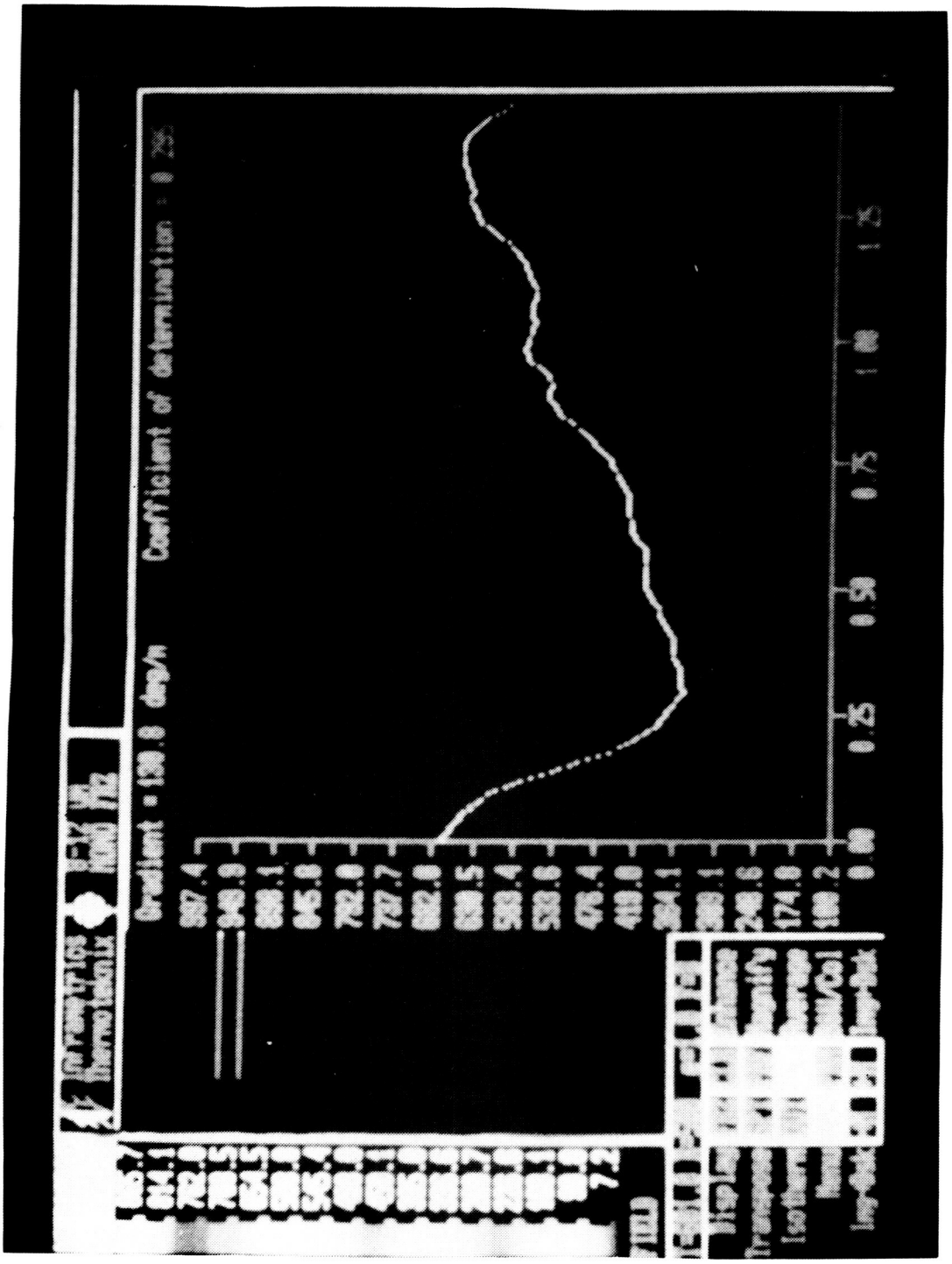

Figure 49. NCTT2 surface temperature distribution at 900 F.

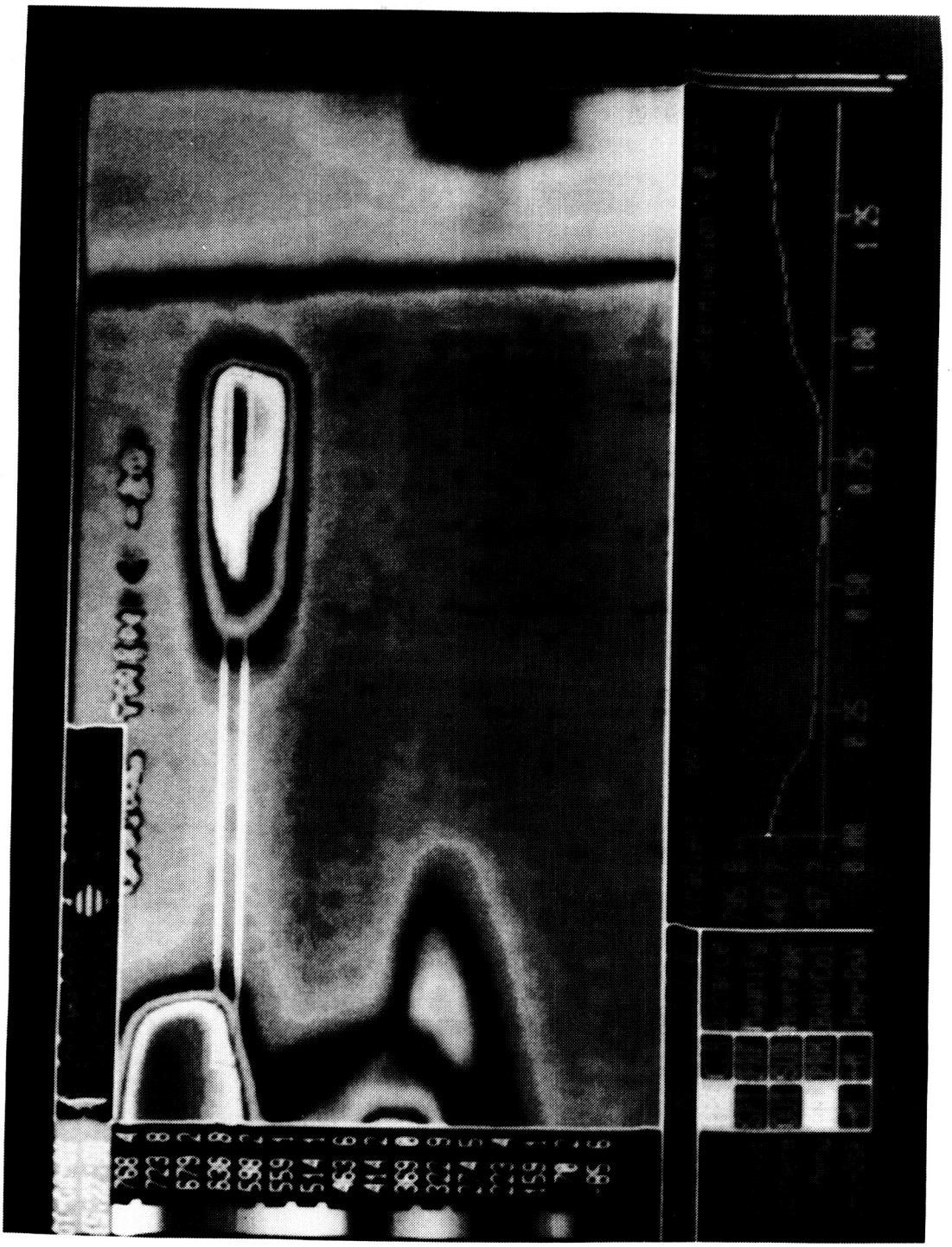

Figure 50. CTT2 infrared photo at 900 F.

Figure 51. CTT2 surface temperature distribution at 900 F.

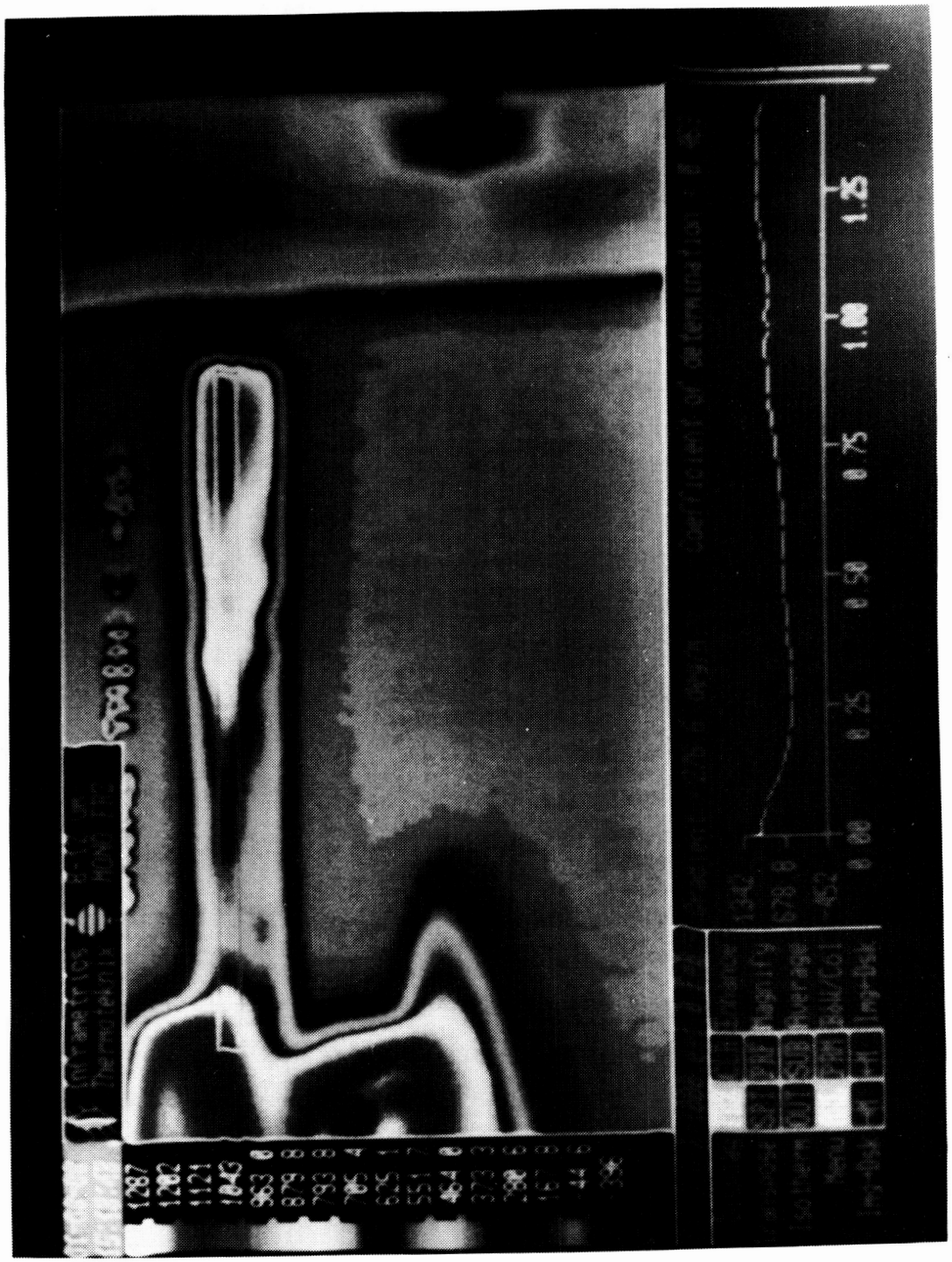

Figure 52. NCTT2 infrared photo at 1500 F.

Figure 53. NCTT2 surface temperature distribution at 1500 F.

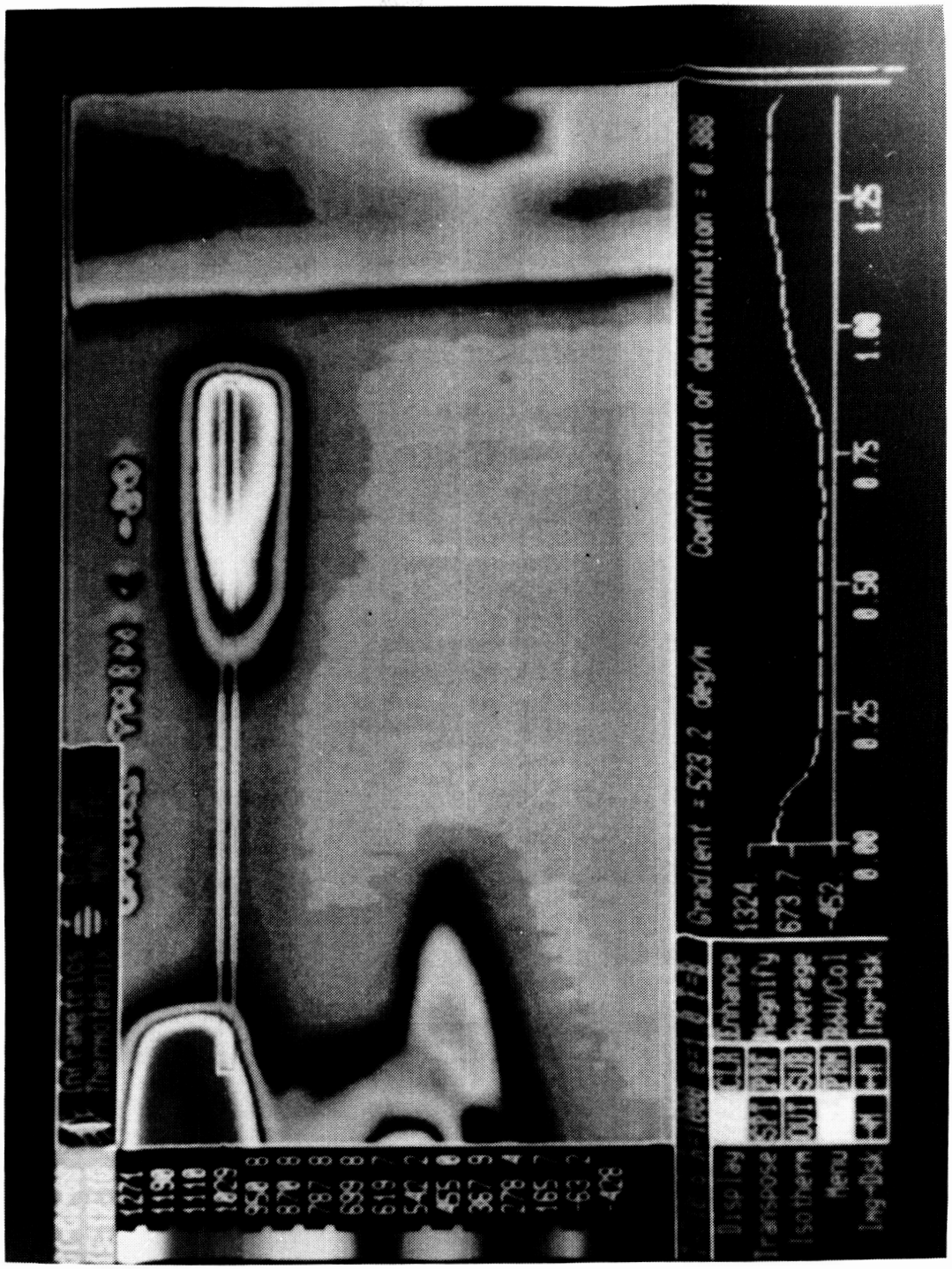

Figure 54. CTI2 infrared photo at 1500 F.

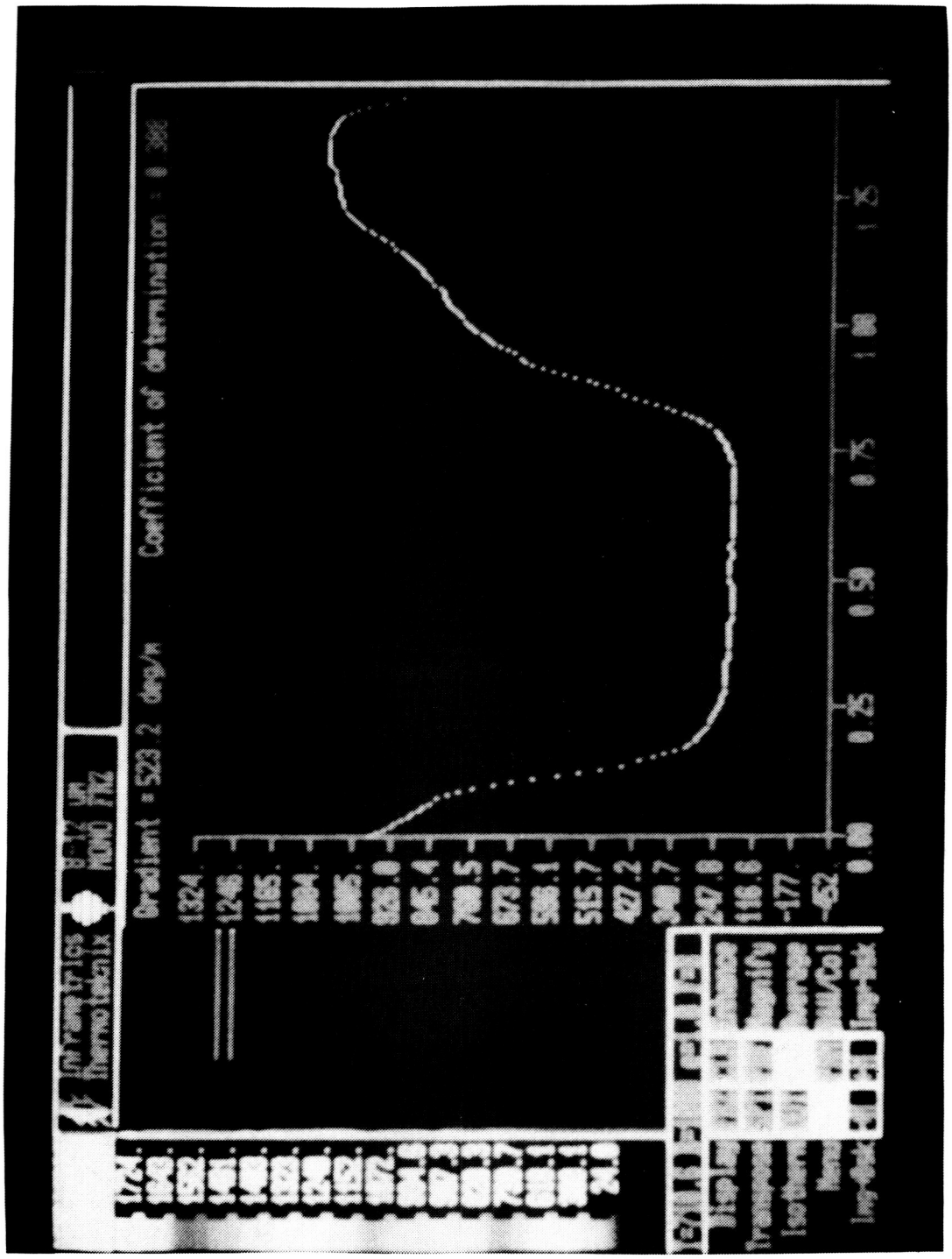

Figure 55. CTT2 surface temperature distribution at 1500 F.

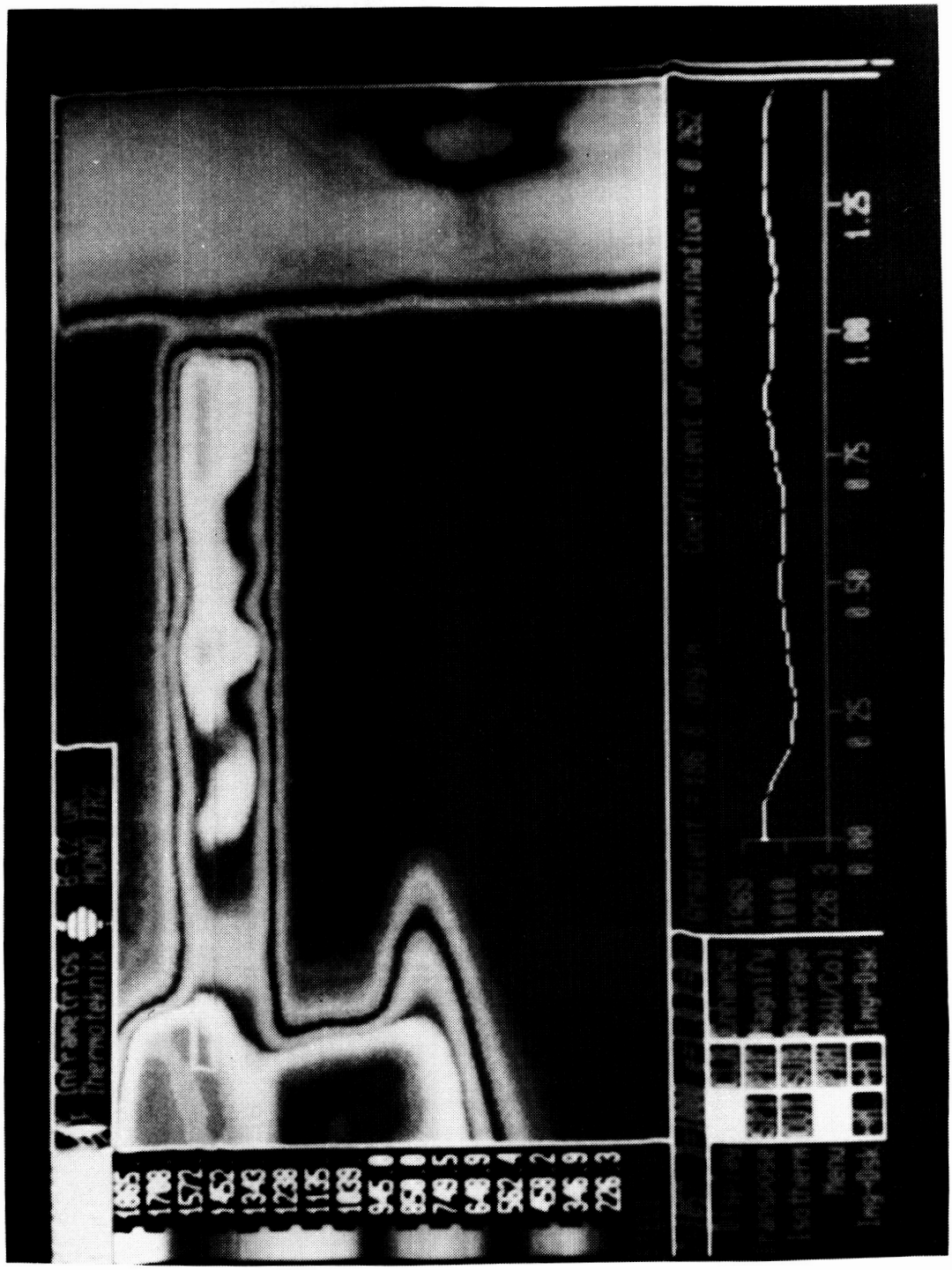

Figure 56. NCTT2 infrared photo at 2000 F.

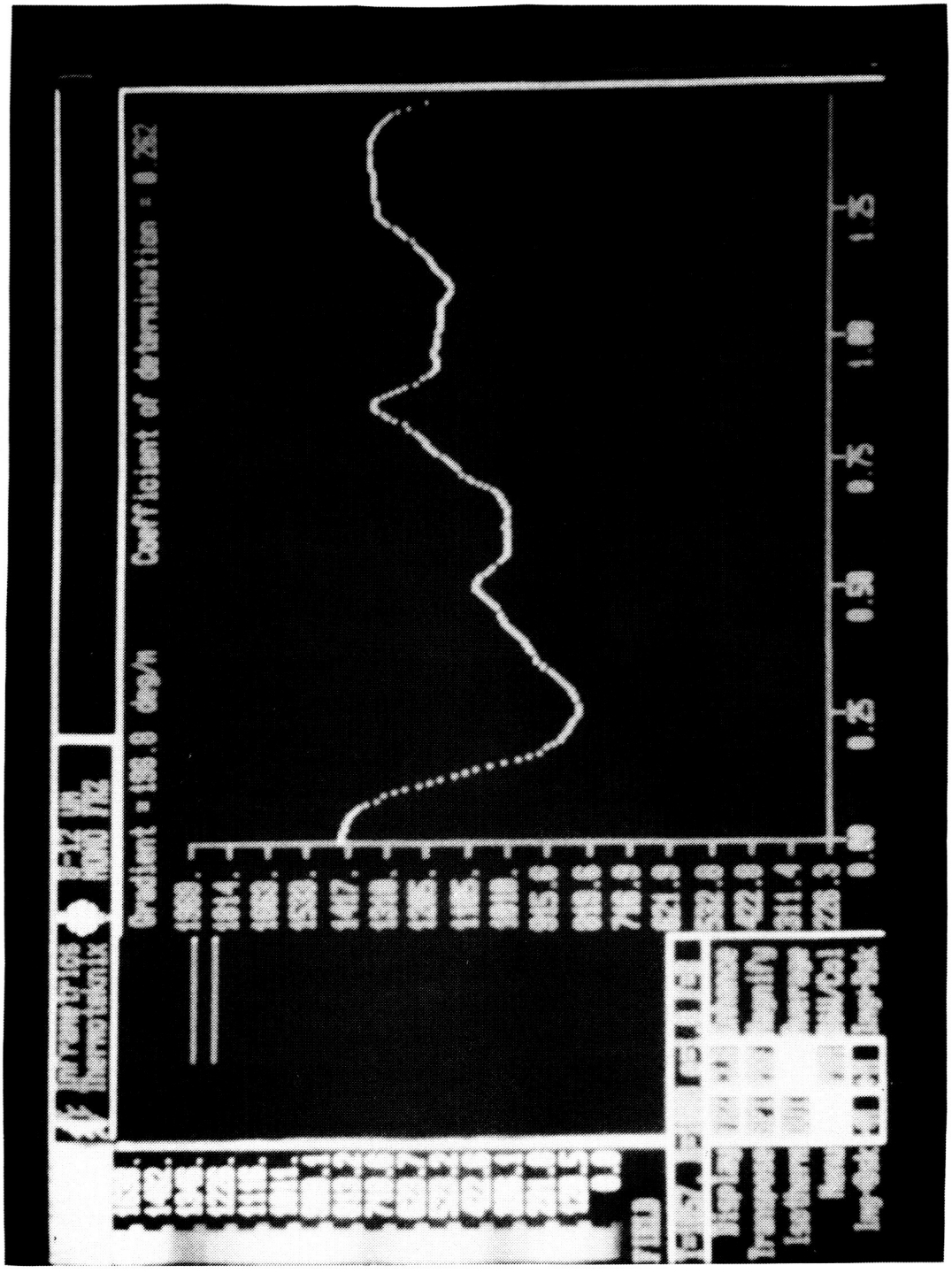

Figure 57. NCTT2 surface temperature distribution at 2000 F.

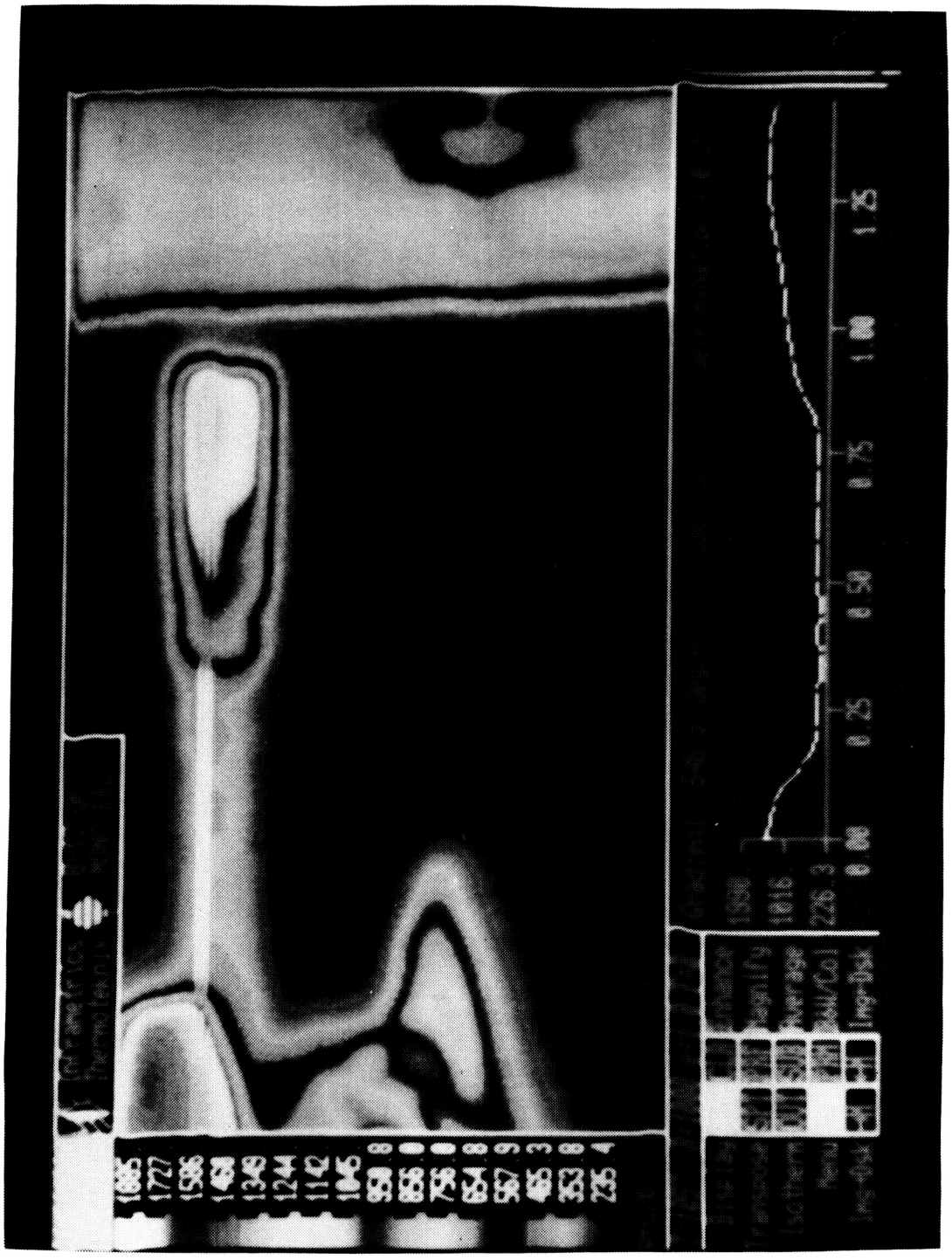

Figure 58. CTT2 infrared photo at 2000 F.

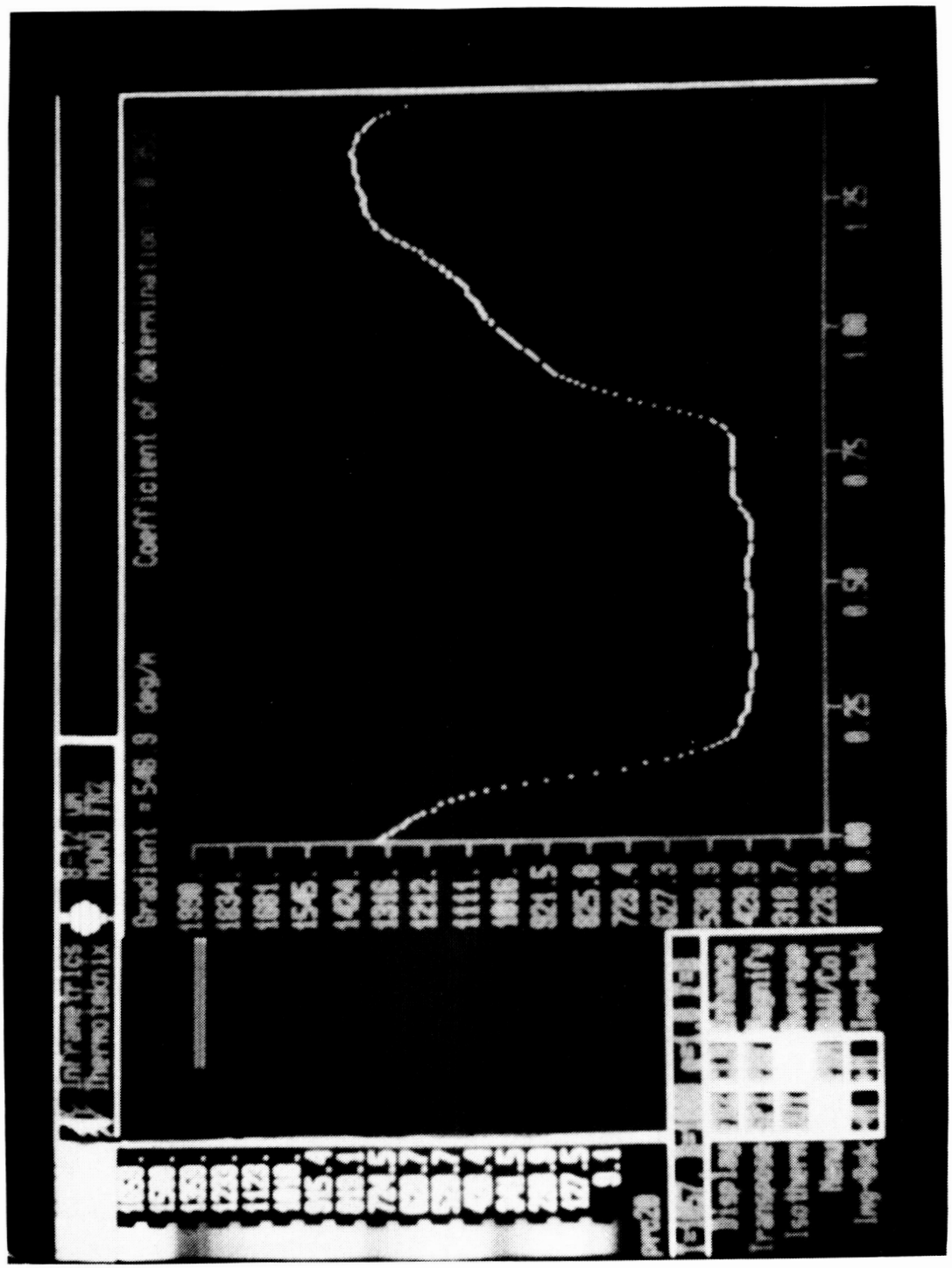

Figure 59. CTT2 surface temperature distribution at 2000 F.

Figure 60. Infrared system calibration with the blackbody.

Probe condition	Probe minimum temp (°F)	Cylindrical sidewall temp (°F)	Bead temp (°F)	Alumel conduction (BTU/h)	Chromel conduction (BTU/h)	Bead radiation (BTU/h)	Bead convection (BTU/h)	% bead temp error w/ jet temp
900F NOH20	350	600	851	0.171	0.259	0.123	0.553	5.4
900F H20	130	600	833	0.525	0.785	0.113	1.423	7.4
1500F NOH20	600	1005	1364	0.249	0.382	0.479	1.110	9.1
1500F H20	180	1005	1256	0.802	1.225	0.303	2.330	16.3
2000F NOH20	840	1350	1868	0.358	0.549	1.367	2.274	6.6
2000F H20	430	1350	1607	1.041	1.590	0.550	3.181	19.6

Table 2. Water cooled total temperature probe preliminary heat transfer analysis.

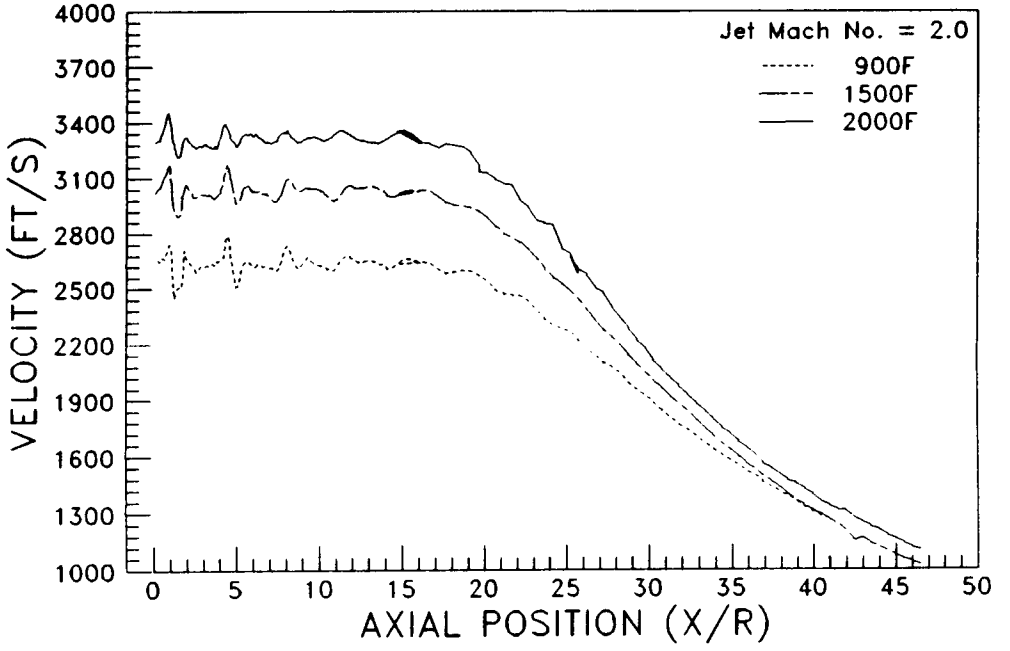

Figure 61. Calculated jet centerline velocities at 900 F, 1500 F, and 2000 F using the CTT2 data.

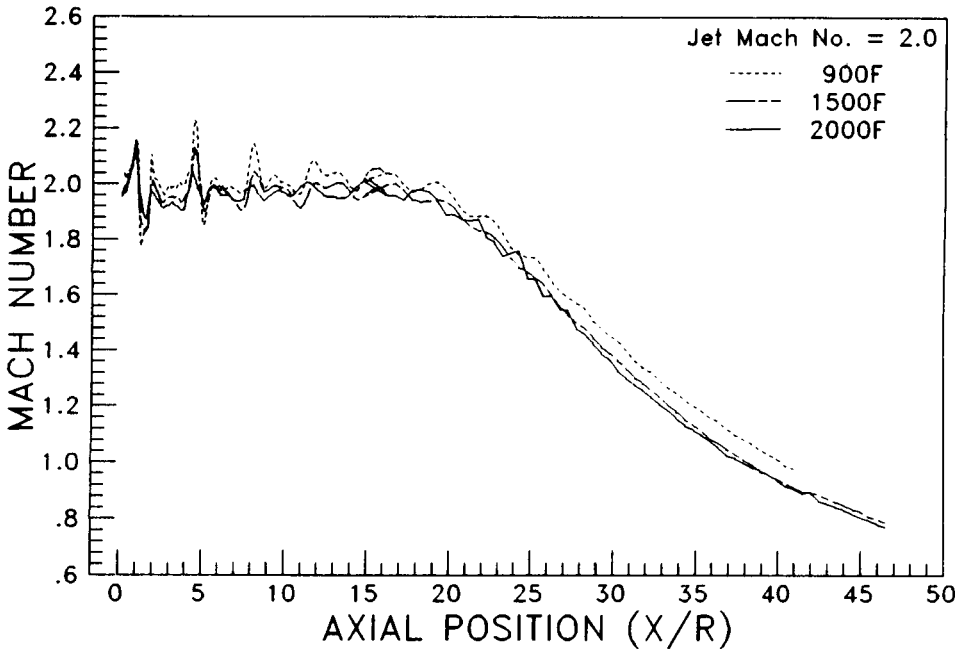

Figure 62. Calculated jet centerline Mach numbers at 900 F, 1500 F, and 2000 F using the CTT2 data.

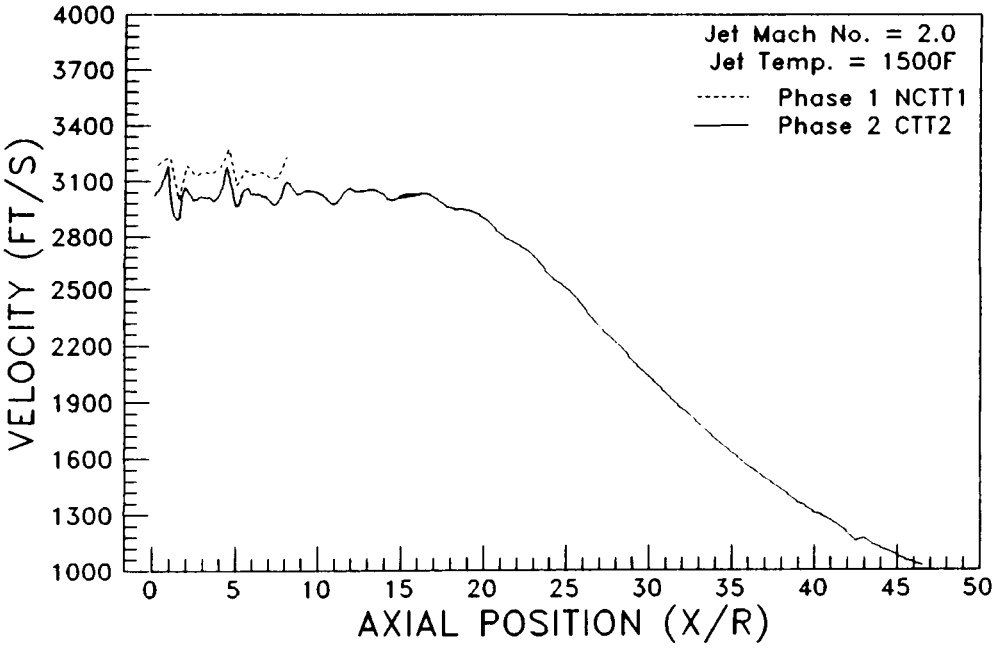

Figure 63. Calculated jet centerline velocity comparison at 1500 F.

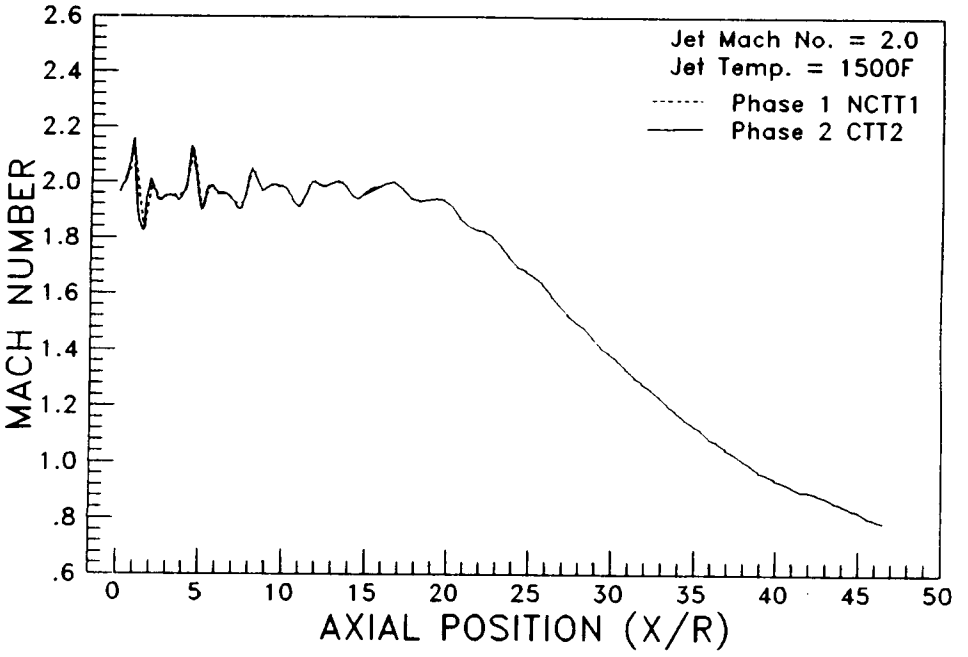

Figure 64. Calculated jet centerline Mach number comparison at 1500 F.

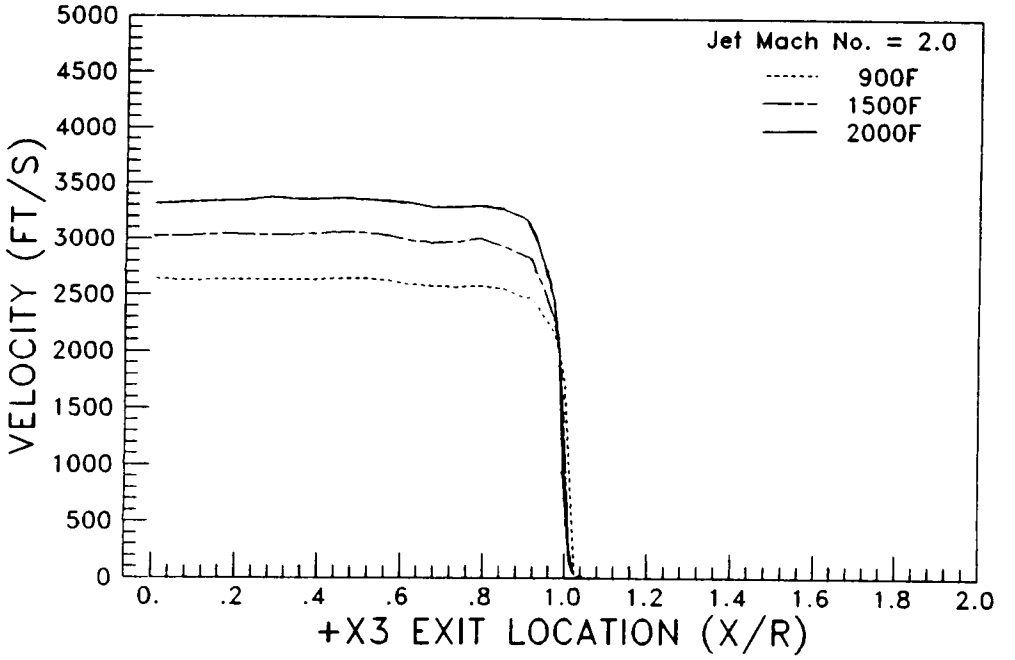

Figure 65. Calculated +X3 axis velocities at 900 F, 1500 F, and 2000F using the CTT2 data.

Jet total temp(°F)	Jet static temp(°F)	Ratio of specific heats,γ	Speed of sound (ft/s)	Theoretical velocity (ft/s)	Calculated velocity (ft/s)	% error
900	304	1.39	1349	2698	2650	1.2
1500	662	1.37	1624	3248	3050	6.1
2000	972	1.36	1828	3656	3350	8.4

Table 3. Calculated velocity error analysis.

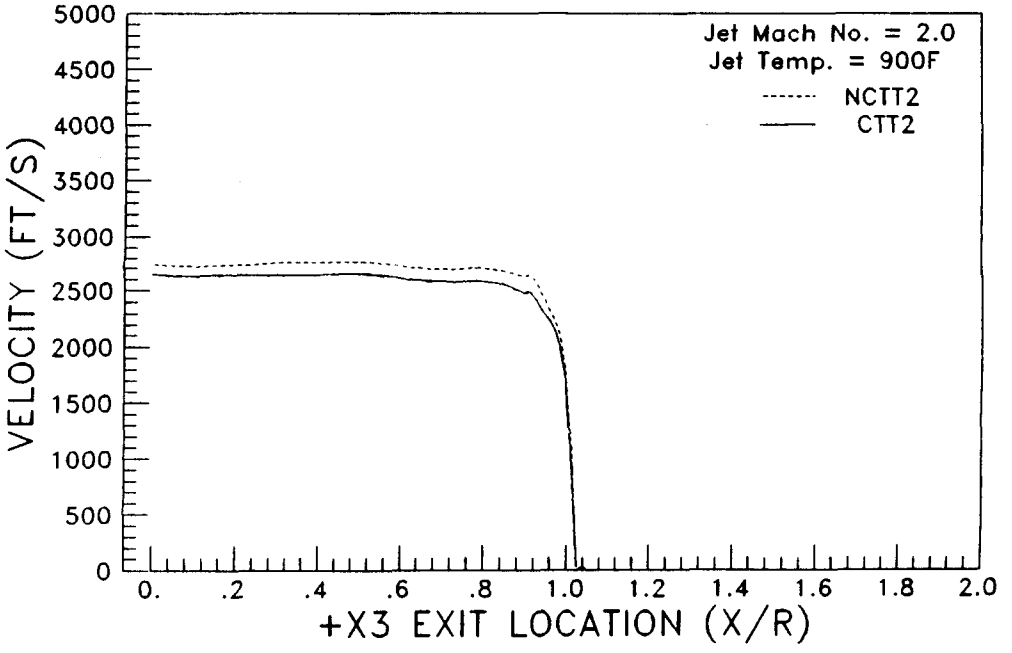

Figure 66. Calculated +X3 axis velocity comparison 900 F.

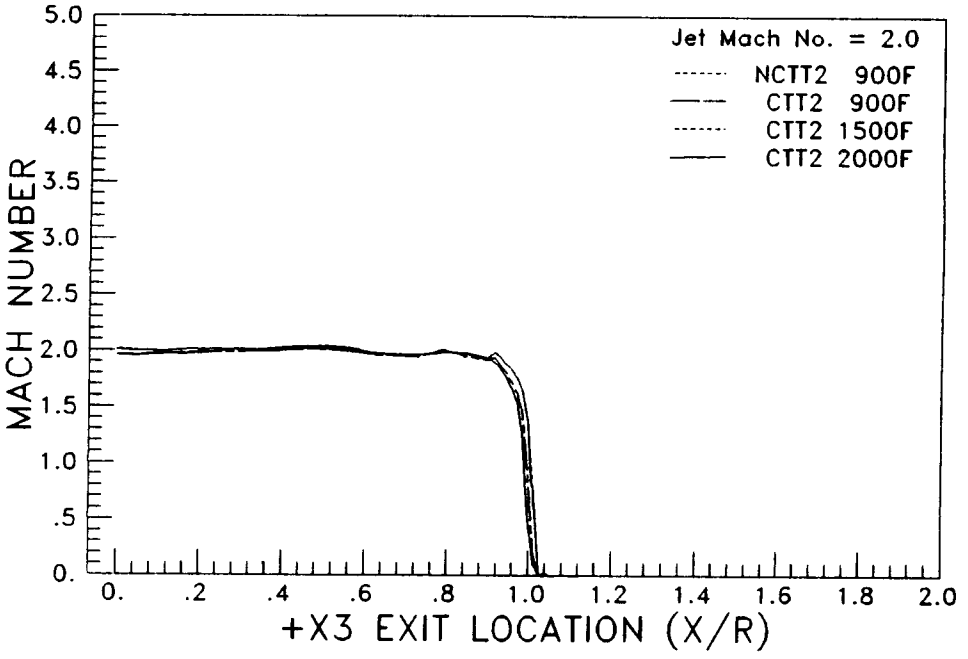

Figure 67. Calculated +X3 axis Mach number comparisons at 900 F, 1500 F, and 2000 F.

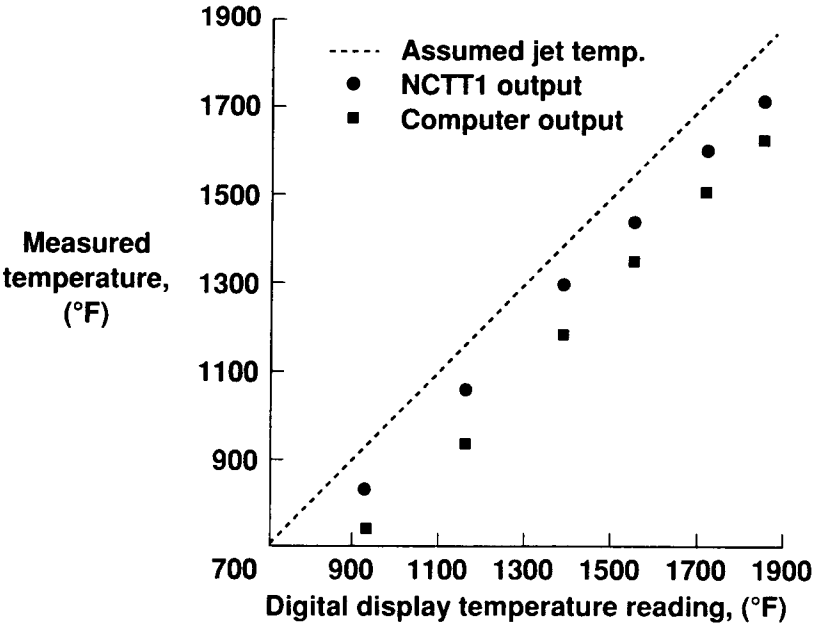

Figure 68. Burner (nozzle) total temperature calibration.

NASA

Report Documentation Page

1. Report No.	2. Government Accession No.	3. Recipient's Catalog No.
NASA TM-102612		

4. Title and Subtitle

Evaluation of Water Cooled Supersonic Temperature and Pressure Probes for Application to 2000°F Flows

5. Report Date

June 1990

6. Performing Organization Code

7. Author(s)

Nicholas T. Lagen
John M. Seiner

8. Performing Organization Report No.

10. Work Unit No.

505-63-91

9. Performing Organization Name and Address

NASA Langley Research Center
Hampton, Virginia, 23665-5225

11. Contract or Grant No.

13. Type of Report and Period Covered

Technical Memorandum

12. Sponsoring Agency Name and Address

National Aeronautics and Space Administration
Washington, DC 20546-0001

14. Sponsoring Agency Code

15. Supplementary Notes

Nicholas T. Lagen: George Washington University, Joint Institute for Advancement of Flight Sciences, Langley Research Center, Hampton, Virginia.
John M. Seiner: Langley Research Center, Hampton, Virginia.
NASA TM-102612 also presented as meeting paper at the 36th International Instrumentation Symposium, May 6-10, 1990, in Denver, Colorado.

16. Abstract This work addresses the development of water cooled supersonic probes used to study high temperature jet plumes. These probes are: total pressure, static pressure, and total temperature. The motivation for these experiments is the determination of high temperature supersonic jet mean flow properties.

A 3.54 in. exit diameter water cooled nozzle was used in the tests. It is designed for exit Mach 2 at 2000°F exit total temperature. Tests were conducted using water cooled probes capable of operating in Mach 2 flow, up to 2000°F total temperature. Of the two designs tested, an annular cooling method was chosen as superior.

Data at the jet exit planes, and along the jet centerline, were obtained for total temperatures of 900°F, 1500°F, and 2000°F, for each of the probes. The data obtained from the total and static pressure probes are consistent with prior low temperature results. However, the data obtained from the total temperature probe was affected by the water coolant. The total temperature probe was tested up to 2000°F with, and without, the cooling system turned on to better understand the heat transfer process at the thermocouple bead. The rate of heat transfer across the thermocouple bead was greater when the coolant was turned on than when the coolant was turned off. This accounted for the lower temperature measurement by the cooled probe. The analysis is presented in this paper. The velocity and Mach number at the exit plane and centerline locations were determined from the Rayleigh-Pitot Tube formula.

17. Key Words (Suggested by Author(s))	18. Distribution Statement
Static Pressure Probe Total Pressure Probe Total Temperature Probe High Temperature Jet Nozzle	Unclassified-Unlimited Subject Category 71

19. Security Classif. (of this report)	20. Security Classif. (of this page)	21. No. of pages	22. Price
Unclassified	Unclassified	81	A05